University of Washington
Department of Civil and Environmental Engineering

POTENTIAL EFFECTS OF CLIMATIC WARMING ON THE WATER RESOURCES OF THE COLUMBIA RIVER BASIN

Joan C. Sias
Dennis P. Lettenmaier

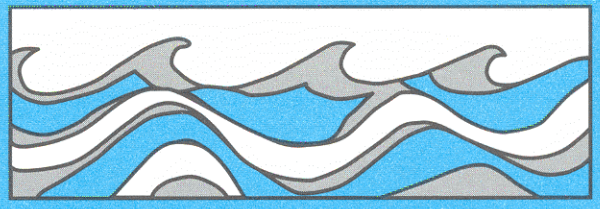

Water Resources Series
Technical Report No.142
October 1994

Seattle, Washington
98195

Department of Civil Engineering
University of Washington
Seattle, Washington 98195

POTENTIAL EFFECTS OF CLIMATIC WARMING ON THE WATER RESOURCES OF THE COLUMBIA RIVER BASIN

Joan C. Sias
Dennis P. Lettenmaier

Water Resources Series
Technical Report No. 142

October 1994

ABSTRACT

The sensitivity of the Columbia River basin reservoir system to two alternative climate scenarios (+2C and +4C warming) was assessed by using a sequence of deterministic and stochastic models. Thirty eight years of daily streamflow were simulated for three small index catchments, for each climate scenario. These sequences were then aggregated to a monthly time step, and subsequently disaggregated spatially using a space-time stochastic streamflow disaggregation model to produce monthly incremental streamflow for fourteen large subbasins, which comprise the total area of the Columbia River basin above the Dalles, OR (219,000 square miles, mean annual runoff of 190,000 cfs). The monthly stremflows were routed through a simple water resources system model, in which the existing system of storage reservoirs and run-of-the-river projects was represented as eighteen aggregate projects. The surrogate operating rule used by the water resources system model was to release from each of the aggregate projects historical average monthly outflow for the post 1974 period during which all major resources were in operation.

Most of the local inflows were moderately to highly sensitive to the +4C warming, and moderately sensitive to the +2C warming. Among the fourteen subbasins there were several different patterns of response to the alternative climate scenarios; the most typical effect was to cause a movement of the snowmelt peak to earlier in the year, and to decrease the magnitude of the snowmelt peak, on average par. In most cases runoff increased throughout the winter.

In general, the most important hydrologic effect of a warmer climate was to align the target releases of major reservoirs (inferred from post-development average reservoir releases) more closely with the unregulated streamflows. Therefore, with respect to the hydropower and flood control objectives that have dominated operation of the system until recently, performance of the reservoir system would be enhanced for the warmer climate scenarios. Specifically, the regulatory capacity of the system was sufficient that at most system nodes, the model was able to preserve the historical post-development monthly releases, on average, for both the +2C and +4C climate scenarios. The Upper and Middle Columbia basins in particular appear to be fairly robust to climate warming, with respect to hydropower and flood protection objectives. At John Day and the Dalles in the +4C scenario, regulated runoff was somewhat elevated in the winter, and depressed in the late spring. The +2C scenario had little impact on the regulated runoff at these nodes. Improved capacity for flood control was indicated by a decrease in the maximum mean monthly runoff for most subbasins, and by smaller excursions in reservoir contents. Notwithstanding the generally beneficial effect of the climate-altered hydrographs for flood control and hydropower, efforts to restore salmon runs in the Columbia River system may well be negatively impacted by hydrologic changes that would accompany a warmer climate.

Acknowledgments

The research described in this report is based on the Masters Thesis of the first author, and was funded in part by Pacific Northwest Laboratory. Pacific Northwest Laboratory is operated for the U.S. Department of Energy by Battelle Memorial Institute under contract DE-AC06-76RLO 1830. The insightful comments of Professors Stephen J. Burges and Richard R. Palmer, who served on the first author's advisory committee, are greatly appreciated.

Two other person have provided valuable assistance. Lance Vail of Pacific Northwest Laboratory contributed in a number if ways. Mr. Vail provided some of the data used in this study, including digital elevation models, and reconstructed historical flows for the Columbia River and its tributaries in digital form. He also provided basin and index catchment site locations, and assisted in the basin delineations and the development of the water resources model. Clayton Hanson of the Agricultural Research Service provided meteorological and streamflow data for the Reynolds Creek Experimental Watershed.

Table of Contents

List of Tables

List of Figures

Chapter 1 Background and Objectives

"That climate change is taking place is almost tautological, for climatic change has been a property of the earth's atmosphere as long as the earth has had an atmosphere..." (National Research Council, 1977).

1.1 Introduction

It has long been recognized that persistence in hydrologic time series occurs on time scales of years to decades. Failure to account for this non-stationarity can lead to undersizing of reservoirs or overestimation of firm yield. A well known example of the implications of long-term hydrologic persistence is the allocation of the Colorado River; estimates of the mean flow based on a period of persistent high flows led to over-allocation of the river (Dracup, 1977). The possibility of anthropogenic climate change compounds the problems that arise from non-stationarity of hydrologic time series.

This thesis describes a study undertaken to assess the potential implications of climate change for the Columbia River basin. The basic premises of the study described herein are (1) that changes in climate and/or climatic variability are likely on a decadal to century time scale; (2) that the possibility of anthropogenic warming enhances the likelihood that climate change could take place at a relatively rapid rate; and (3) that such changes will affect hydrologic processes and water resources system behavior. Climate change sensitivity studies for water resources systems can be useful for establishing (1) how water resources systems are likely to behave under different climatic conditions, and (2) what magnitude of climate change and over

what time scale climate change is likely to be of significance to water resources systems planning, development, and operation.

1.2 Natural and anthropogenic influences on climate

1.2.1 Characteristics of natural climatic variability

Natural climatic variability occurs on temporal scales ranging from decades to hundreds of thousands of years, and spatial scales ranging from local to global (Stockton, 1977). The possible natural causes of climate change include long term fluctuations in the earth's orbit; comet collisions, major volcanic eruptions (Henderson-Sellers and McGuffie, 1987), and changes in biogeochemical processes that affect atmospheric composition (Sellers, 1991). Transitions from one climate state to another can occur abruptly (Intergovernmental Panel on Climate Change, 1992), even on decadal time scales. A recent example of an abrupt climate change is the Little Ice Age (c. 1400 to c. 1700), where the global mean temperature was estimated to be about 1°C cooler than the preceding and subsequent periods.

There is an important distinction to be made between regional and global climate change. Global mean climate statistics mask the fact the regional climate variability and/or change can be much larger (Schneider *et al.*, 1990). Paleological climate indicators render a picture of climate change from the warmest period of interglacials to the coolest period of the great ice ages to be on the order of 5°-10°C globally (Emiliani, 1972); in contrast, at high latitudes, the range between the extremes may have been on the order of tens of degrees (Mathews, 1971).

1.2.2 Anthropologic influences on climate

Climatic variability is a fact of nature, and it also appears to be a fact of human existence as well. Perhaps since humans first became sedentary, they began to modify the landscape (Sagan *et al.*, 1979), and particularly since the Industrial Revolution, also the composition of the atmosphere. There is physical reasoning, and in some cases empirical evidence, to support the hypothesis that large scale modification of the earth's landscape, such as through deforestation (Shukla *et al.*,

1990), desertification (Balling, 1991) and macroengineering projects (Eagleson, 1986) can, or already has, influenced climate. Inadvertent modification of the composition of the atmosphere (e.g. as a result of the burning of fossil fuels) appears to be most potent way that humans influence global climate, according to the Intergovernmental Panel on Climate Change (IPCC, 1992). Although large scale modification of the earth's surface is a source of great concern, much of the debate about climate change has centered on the warming effect of greenhouse gases (Mitchell, 1989) and negative feedback mechanisms.

1.3 Evidence of recent climate change and the possible link to greenhouse gases

1.3.1 Historical climate

The earliest instrumental records suitable for describing climate date from the mid 1800's. Figure 1.1 shows the mean annual global and hemispheric temperature over the last 130 years, as constructed by Wigley *et al.* (1989). Apart from a slight cooling from 1930 to 1950, mean global temperature has shown an increasing trend; with the change in the mean global temperature over the twentieth century amounting to about 0.45°C (IPCC, 1992). Over the same period, glaciers and sea ice have been receding, sea level has risen, and alpine areas in the Northern Hemisphere have been experiencing reduced seasonal snow accumulation (IPCC, 1992).

1.3.2 Greenhouse gases and climate change

Some of the supporting evidence that alteration of the land surface and influx of greenhouse gases and aerosols could result in climate change comes from general circulation model (GCM) experiments. GCMs are self-consistent, three-dimensional representations of large scale atmospheric dynamics, including land-surface and in some cases ocean-atmosphere interactions (Henderson-Sellers and McGuffie, 1987). GCMs incorporate in their atmospheric energy budgets the effect of atmospheric radiative forcing constituents (such as greenhouse gases), so it is possible to use such models for experiments to determine the potential effects of altered concentrations of greenhouse gases on climate.

There is sound scientific evidence that atmospheric concentrations of greenhouse gases have been increasing since the Industrial Revolution. Atmospheric carbon dioxide, for instance, appears to have increased by about 25% since 1750 (IPCC, 1992). Notwithstanding the considerable range in the quality of GCM replications of current climate, GCMs predict that the observed increase in greenhouse gas concentrations should have caused a global mean temperature increase about twice that observed (Schneider *et al.*, 1990). The overprediction is attributed to several factors which either cannot or have not been accurately quantified to date: natural climatic variability, oceanic sequestering of CO_2, and uptake of heat by the oceans (Dickinson, 1989), as well as many uncertainties in model parameters, and an imperfect understanding of some physical processes which the GCM attempts to model, particularly land surface-atmosphere interactions (Wood, 1992), such as soil moisture state, and energy and mass fluxes. The representation of atmospheric dynamics in GCMs, is, in most respects, acceptable (Sellers, 1991); the greatest uncertainties have to do with clouds (Harshvardhan, 1991; Chahine, 1992) and snow-ice-albedo feedback (Dickinson, 1989). There is strong empirical evidence that aerosols and SO_2 (which, after oxidation to H_2SO_3 and hydration, behaves as an aerosol) can modify the radiative properties of clouds in such a way as to mitigate greenhouse gas radiative forcing (Harshvardhan, 1991; Charlson 1987), but this may only have a local effect (Henderson-Sellers and McGuffie, 1987). Another negative feedback that may be important is the depletion of stratospheric ozone (IPCC, 1992), which influences both long and short-wave atmospheric radiation fluxes.

1.3.3 Projections of anthropogenic warming over the next century.

The accumulation of atmospheric greenhouse gases is likely to continue. Based on doubled CO_2 experiments with many different GCMs, the IPCC (1992) concluded that the mean global temperature increase corresponding to a doubling of atmospheric CO_2 will be approximately 1.5°C to 4.5°C, and that greenhouse gas

radiative forcing would likely double by late in the next century. By 2040 the consensus approach used by the IPCC (1992) suggests that the greenhouse effect will increase the mean global temperature by about 0.5°C to 1.5°C relative to what it would be otherwise. These IPCC scenarios do not include consideration of all the recognized likely negative feedback mechanisms, including those due to aerosols and stratospheric ozone. The superposition of natural variability, feedback effects, and the greenhouse effect could lead to an absolute change in global temperature which lies outside the predicted ranges.

1.3.4 Anticipated regional climate change

For water resources planning, regional climate scenarios, not global warming scenarios, are pertinent, and these can be considerably more variable than the global climate scenarios. It is likely that warming will be greatest at the high latitudes, and the least near the equator (IPCC, 1990). In this respect, paleoclimatalogic studies that indicate that this has been the pattern in epochal scale climate change are consistent with the GCM simulations; the physical mechanisms that explain this spatial pattern are the ice-albedo feedback, and the greater atmospheric stability poleward.

On a global basis it can be expected that a general warming will lead to an intensification of the hydrologic cycle (Office of Technology Assessment, 1993; Schneider, 1991). The moisture carrying capacity of air increases as it warms. On average then, it is likely that evapotranspiration, and therefore also precipitation will increase. GCMs predict that the mid-continental areas of the North America and Eurasia will experience reduced summer soil moisture, particularly in the central regions of the continents (Dickinson, 1989).

One question into which GCM results provide only modest insight is the regional distribution of precipitation changes. Other than a general indication of globally increased average precipitation, there is little consensus as to the regional change in precipitation that would accompany global warming. This uncertainty in

even the direction of likely precipitation change increases greatly the difficulty of complete hydrological interpretations of climate change.

1.3.5 Anticipated regional runoff changes in a warmer climate

The state of validation of GCMs and lack of consistency of $2xCO_2$ GCM experiments is such that it is premature to draw any quantitative conclusions about the regional hydrologic consequences of warming. Miller and Russell (1992) used a GCM to simulate runoff for the large basins of the world under 1x and $2xCO_2$ scenarios; however the $1xCO_2$ simulations reproduce historical runoff poorly (Kuhl and Miller, 1992). At least it can be said that droughts will not necessarily increase, since the probability of droughts depends not only on temperature but also on the mean, variance, and persistence of precipitation, as well as its seasonality and the pattern of storms, and on evapotranspiration. No definite conclusions can be made at this point about the regional hydrologic consequences of a warmer climate; both average annual runoff and inter-annual and seasonal variability of runoff could either increase or decrease, as could the frequency of severe droughts and floods.

The consequences of climate change are more predictable in snowmelt-driven, as opposed to rainfall-driven systems. Snow accumulation and snowmelt sensitivity is mainly related to changes in temperature rather than changes in precipitation (Gleick, 1987; Lettenmaier and Gan, 1990). Therefore it appears likely that the Columbia River basin, which derives most of its runoff from snowmelt, would be hydrologically sensitive to climate change. Investigations of the sensitivity of snowmelt-dominated catchments are consistent in their results (Gleick, 1987; Lettenmaier and Gan, 1990, Lettenmaier *et al.*, 1993; Saelthun *et al.*, 1990; Kaczmarek and Krasuski, 1991; Bultot *et al.*, 1991; Shiklomanov and Lins, 1991). Ignoring certain complicating factors, the result of a general warming in snowmelt-dominated catchments is that average snow water equivalent decreases, the snowpack melts earlier, winter runoff increases (in some cases substantially), summer soil moisture decreases, and annual runoff may increase or decrease slightly. Dracup and

Kendall (1990) argue that a change in seasonality of runoff in snowmelt-affected watersheds is likely to decrease the magnitude of floods of a given return period.

1.4 Climate change and water resources

The possibility of anthropogenic climate change adds to the concern that warming could continue. The relevant point, though, is that on a regional scale, natural variability alone or in conjunction with anthropogenic climatic forcing could have serious implications for various sectors, not the least of which is water resources. For water resources, the implications of climate change for runoff characteristics, design, and management of a developed system, are three separate but related issues. The possible implications of climatic warming for runoff in the Columbia River were discussed in the previous section. Now the implications of climatic variability in general for design and planning will be considered.

1.4.1 Sizing of reservoirs and estimates of reliable yield

From the point of view of design, the issue of climatic variability is an important one. Long term persistence seems to be characteristic of hydrologic time series (Hurst, 1950), and this is often considered to be evidence of short term (i.e. decadal or shorter) climate change. There is no question that shorter and longer term "climate change" is a feature of hydrologic time series, and that it takes place on a temporal scale relevant to design of reservoirs and storage reliability (Lettenmaier and Burges, 1978) within certain limits (see Klemes, 1981), and that estimates of firm yield of reservoirs are also sensitive to long term hydrologic persistence (Wallis and O'Connell, 1973). It is less clear whether climatic variability is as relevant to the operation and long term management of existing water resources systems as it is to design. This question is particularly pertinent to highly developed basins such as the Columbia River basin, where adaptation to climate change is less likely to take the form of major structural additions (i.e. addition of new reservoirs) as changes in operational strategies.

1.4.2 Management of a developed system in the face of climate uncertainty

The ideal situation for a water resources system is a stable supply, and/or an ample supply to demand ratio. Climate change may affect both supply and demand. As storage increases relative to mean annual flow, water resources system become more robust with respect to variations in runoff (Lettenmaier *et al.*, 1993). Therefore developed basins are likely to be less sensitive to climate change than unregulated catchments (IPCC, 1992). As Rogers (1991) points out, there are many factors that affect water resources planning decisions, including demographics (especially population growth), economics, politics, and water rights. Therefore, one point of view is that climate change may not be an overriding issue or concern, except perhaps in the sizing of reservoirs (see also Stakhiv, 1993).

On the other hand, as was already pointed out, in snowmelt-dominated basins such as the Columbia, climate change is expected to result in a strong change in the seasonality of runoff, to which a system designed primarily to reshape the seasonal hydrograph (as opposed to storing water from one year to the next) may be quite sensitive. The results of Lettenmaier *et al.* (1993) for the snowmelt-dominated American River (a tributary to the Columbia River) with +2°C and +4°C alternative climate scenarios, showed that hydroelectric power revenues could be greatly enhanced in the winter, but that water supply demand often could not be met in the warmer climates.

There is a strong rationale for investigating the sensitivity of the Columbia River water resources system. Despite the many sources of uncertainty about future runoff, the hydrologic response to warmer climates is predictable in a general sense. The kind of changes expected in the Columbia River basin in a warmer climate will certainly alter the behavior of the system and influence operation, and there is unlikely to be any major additions to total storage. A sensitivity analysis is valuable in that it will help to characterize the thresholds of sensitivity, and place climate uncertainty and its potential consequences in the overall context of future stresses on

the system, including growth and increasing priority on environmental quality, as affected by system operation.

1.5 Study objectives

This thesis describes a study of the potential implications of climate change for the Columbia River basin. For the purposes of this study, the projects of the water resources system are aggregated to fourteen nodes (see Section 3.4.1). Accordingly, the basin is divided into fourteen subbasins, each of which corresponds to one of the water resources nodes. The incremental flow to each node is the runoff produced in the corresponding subbasin.

The objectives of this study are 1) to investigate how the hydrology of the two major hydrologic regimes of the basin (semi-humid and semi-arid) changes under alternative climate scenarios, and 2) to evaluate the sensitivity of the water resources of the Columbia River basin to climate change, with emphasis on hydroelectric power production. These objectives will be fulfilled by a combination of deterministic precipitation-runoff modeling of small index catchments, stochastic disaggregation of the index catchment flow to major tributaries of the Columbia and Snake Rivers, and routing through a simplified model of the reservoir system.

1.6 Summary

Chapter 1 laid out the prospect of climate change and climatic variability, and its relationship to water resources. Model based sensitivity studies for individual basins can provide some insight into the vulnerability of hydrologic systems to climatic change. On-line and off-line GCM-coupled modeling approaches have been used for hydrologic studies, but yet there is not a strong basis for believing that GCM-linked studies have any predictive ability. In Chapter Two, the most common non-GCM-based approaches for water resources studies are reviewed, as well as results for water resources system and catchment scale studies of sensitivity to climate change. Both developed water resources and catchment scale studies are

considered, with an emphasis in the latter case on snowmelt-dominated catchments, since most of the runoff generated in the Columbia River basin is due to spring snowmelt.

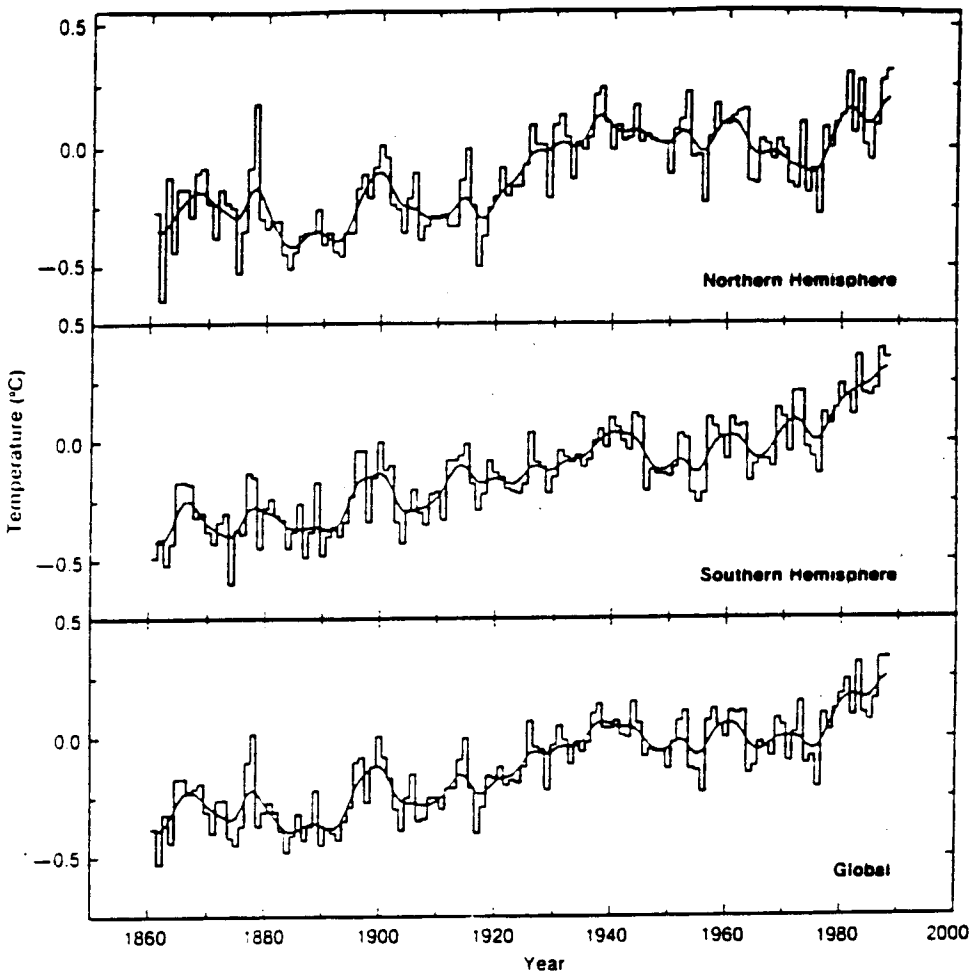

Figure 1.1 Mean annual global and hemispheric temperature, 1860 to 1988 (After Wigley, et al. 1989).

Chapter 2 Relevant Research

2.1 Approaches to climate impacts assessment in water resources

2.1.1 On-line general circulation model experiments

In principle, studies of the water resources effects of climate change can be performed by imbedding algorithms that simulate reservoir system performance within coupled land-atmosphere models, such as GCMs. A promising research direction is the use of finer scale nested mesoscale models (Giorgi and Mearns, 1991), which interact with the coarse scale GCM model, in one-way or two way fashion. Unfortunately, the hydrologic length scale of interest (on the order of tens to hundreds of kilometers for the subbasins of the Columbia River) is much smaller than the length scale of a GCM or even a mesoscale model.

It is due to this scale incompatibility that off-line approaches to climate assessment have been preferred. In off line assessments, GCMs provide meteorologic forcings to a hydrologic model, but no attempt is made to model surface energy fluxes (e.g. evaporation) to maintain consistency between the scale of the GCM and the hydrologic model. Another reason is the crude representation of land surface heterogeneities (especially topography) and consequently the space-time structure of precipitation and other surface meteorological variables in GCMs. These properties and processes are critical to accurate on-line simulation of runoff.

2.1.2 Off-line deterministic hydrologic modeling

For the reasons indicated, virtually all studies of water resources impacts of climate change have used off-line hydrologic modeling. Schwarz (1977) and others have used stochastic modeling and Monte Carlo analysis, but this kind of approach can not make direct use of regional climate scenarios. Deterministic hydrologic modeling for climate change studies is typically performed as follows. First, one or more regional climate change scenarios are formulated based on GCM results or other methods, such as direct specification of proportional or additive change (e.g. a given percentage change in precipitation, or a given shift in temperature). Second, the climate scenario is applied to a time series of meteorologic events. Third, the adjusted meteorological series are then used as forcing data for a hydrologic model, and runoff is simulated for each scenario. If water resources system performance is also being studied, then the simulated runoff is routed through a model of the water resources system, such as a reservoir simulation model.

The most common way to form the alternative climate scenario is to apply some prescribed change to the historical temperature and precipitation series. This has been called the ratio and difference method (Lettenmaier *et al.*, 1994). The ratio and difference method has also been used with GCM results (Lettenmaier and Gan, 1990; Kite, 1993). In this case, the normal procedure is to take the ratio (for precipitation) or the difference (for temperature) between the 1x and $2xCO_2$ runs, and apply this to the corresponding historical meteorological series. The result is taken as the $2xCO_2$ scenario, and the historical meteorological series as the reference case. The rationale behind this approach comes from the assumption that the model biases in the two GCM runs cancel out when the difference is computed. The disadvantage of the ratio and difference method is that it preserves the historical sequencing of storms and temperature anomalies (Lettenmaier *et al.*, 1994). The principal advantage over other most other methods (statistical procedures, on-line experiments) is the ease of implementation.

A major disadvantage of prescribed change scenarios is that such scenarios are not self-consistent. Given the uncertainty in GCM simulations, it is questionable whether the alternative, off-line decoupled incorporation of seasonal GCMs results into a hydrologic model by the ratio and difference method is justifiable. In a study of the hydrologic sensitivity to climate change of the Sacramento-San Joaquin, CA river basin, Gleick (1987) used both GCM-derived and prescribed change scenarios for precipitation (P) and temperature (T). He found that the results with the GCM and the prescribed change scenarios were consistent, despite the fact that the GCM scenarios incorporated seasonally varying changes. Given that GCMs cannot at present produce results that could be regarded as regional climate forecasts, it seems more justifiable to perform climate sensitivity studies in a sensitivity analysis framework, through use of prescribed change scenarios.

2.2 Hydrologic climate sensitivity in relation to climatic and regional factors

2.2.1 Previous research

A number of climate change studies have made use of Langbein's (1949) well-known isotherms for regression of annual runoff for 22 basins in the United States on precipitation (Stockton and Bogess, 1979; Revelle and Waggoner, 1983; Idso and Brazel, 1984; Wigley and Jones, 1985), and are frequently cited as empirical evidence that annual runoff in arid climates is more sensitive to precipitation changes than to changes in temperature or evaporation. These studies necessarily evaluate climate impacts on an annual basis. Idso and Brazel (1984) took into consideration evapotranspiration changes, and found only modest decreases in runoff for a given change in precipitation, in contrast to the results of Revelle and Waggoner (1983). It is questionable whether Langbien's (1949) empirical regressions should be applied to individual basins (Karl and Riebsame, 1989); these studies do not take into consideration seasonal and sub-seasonal variability in precipitation, soil moisture, and PET (Wigley and Jones, 1985), and are of limited usefulness in application to water resources studies (Nemec and Schaake, 1982).

One of the earliest water resources climate change impact assessments based on deterministic modeling was that of Nemec and Schaake (1982). They applied the Sacramento Model (Burnash *et al.*, 1973), a deterministic conceptual hydrologic model, on a daily time step to study the sensitivity of an arid catchment (Pease River at Vernon, Texas; 9034 km^2) and a humid catchment (Leaf River near Collins, MS; 1949 km^2) to changes in precipitation and runoff. In the humid basin, a 25 percent increase in precipitation and a +1C increase in temperature resulted in a 60 percent increase in runoff; the same change in precipitation and temperature in the arid catchment resulted in a 180 percent increase in runoff. In their study, runoff was more sensitive to changes in precipitation than to changes in evapotranspiration (temperature). As in the empirical studies mentioned, the model of runoff for the arid basin was more sensitive to changes in precipitation and ET than the humid basin. The Sacramento model was also used by Nash and Gleick (1991) to model the arid Colorado River basin response to climate change scenarios. The response of runoff to warming was significantly weaker than predicted by Revelle and Waggoner (1983).

Highland areas dominated by snowmelt or mixed rain-and-snow show a different pattern of sensitivity than that indicated for catchments in arid regions. In their study of the Colorado River basin, Nash and Gleick (1991) found that annual runoff in snow-affected subregions were less sensitive to changes in precipitation than were rainfall-dominated regions of that basin. On an annual basis, small increases in runoff in snow-affected areas appears to be a typical finding (Saelthun *et al.*, 1990; Lettenmaier and Gan, 1990; Lettenmaier *et al.*, 1993).

Croley (1990) evaluated the potential changes in the hydrology of the Great Lakes basin (770,000 km^2) for three GCM-derived climate scenarios (ratio and difference method) with a conceptual hydrologic model of basin groundwater and surface water inputs to the lakes, and overlake moisture flux (precipitation and evaporation). The precipitation changes for the three scenarios ranged from +1

percent to +6 percent. The overall effect of the scenarios was to reduce total annual net moisture supply (overlake precipitation plus surface runoff minus overlake evaporation) for all but one of the six Laurentian Great Lakes. Warming was also predicted to affect water temperature cycles and seasonal turnover of lake water. The seasonality of runoff was affected because snowmelt-associated runoff is important in this basin.

McCabe and Ayers (1989) used a water balance model to study the potential effects of climate change on soil moisture and runoff in the Delaware River basin. Two subbasins were studied, one of which is snowmelt affected. The snowmelt-dominated portion of the basin responded to warming as in other studies. They concluded that to offset the effect of a +2C and +4C warming, increases in precipitation of 5 percent and 15 percent, respectively, would be needed.

2.2.2 Studies of snowmelt-dominated watersheds

A number of studies have focused on the hydrologic response of snowmelt-dominated watersheds to global warming. Among these are four studies of mountainous watersheds of western North America: Gleick (1987), who studied the Sacramento-San Joaquin; Lettenmaier and Gan (1990), who also studied the Sacramento-San Joaquin; Lettenmaier *et al.* (1993), who studied the American River catchment; and Kite (1993), who studied the Kootenay River basin, BC. Gleick used a regional water balance model, while the other studies used conceptual soil moisture accounting models, but the results of all these studies are similar. The dominant influence was an increase in temperature, which resulted in movement of the seasonal peak runoff from spring or early summer toward early spring or winter. Other studies of changes in seasonality of runoff in snowmelt-affected watersheds give similar results (Saelthun *et al.*, 1990; Kaczmarek and Krasuski, 1991; Bultot *et al.*, 1991; Shiklomanov and Lins, 1991). Saelthun *et al.* (1990) performed hydrologic sensitivity studies for catchments in Norway, and noted increases in the frequency of floods in autumn and winter. Using a full-energy balance snowmelt model, Tsuang

and Dracup (1991) obtained a similar result in response to a multi-parameter climate change scenario, in a one year simulation for an alpine catchment in the Sierra Nevada Mountains in California. The scenario included warmer temperatures and assumptions about direct and indirect effects of CO_2 on the incoming all-wave radiation. The simulation also indicated winter flash flooding and a shorter duration snowmelt peak, in addition to earlier onset and cessation of ablation.

Lettenmaier and Gan (1990) modeled the responses of four different catchments within the snow-affected Sacramento-San Joaquin Basin to temperature and precipitation change scenarios. Warmer climate scenarios had the effect of reducing peak runoff in the most heavily snowmelt-dominated catchment, and increasing peak runoff in the others. Their results showed clearly that even within a region of relatively uniform climate, the responses of different catchments situated over different elevation ranges can be expected to differ, particularly if seasonal snow accumulation is characteristic of the hydrology. These results, which are explained by the dependence of temperature on elevation, and the strong orographic effects on precipitation in mountainous areas, indicate that the hydrologic response of a snowmelt-affected catchment to a change in mean seasonal temperature (and variability of temperature) depends on the current climate. In high elevation or continental watersheds, the hydrologic effect of warming may be somewhat modest, while in coastal catchments where winter precipitation presently occurs in a mixture of rain and snow, transition to a rainfall-dominated hydrology may occur for smaller incremental increases in temperature.

2.2.3 Incorporating climate sensitivity of model parameters

In most previous studies, hydrologic model parameters have been assumed to be invariant with climate change, an assumption that may not be justifiable. Among the four studies cited, only Kite (1993) varied model parameters to take into account changes in runoff dynamics that might accompany climate change. In particular, the model represents several classes of ground cover or vegetation type. Snowmelt rate

and potential evaporation were specified for each of three vegetation types: grassland, forest, and bare (alpine zone). The distribution of these vegetation classes was assumed to change as the climate warmed in a manner consistent with reported observed changes in the Alps. For example, in response to doubled CO_2, the grassland-forest transitional zone was assumed to migrate upward, such that basin-wide the distribution of vegetation was assumed to change from 98 percent forest (historical case) to 20 percent forest and 80 percent grassland. This assumption was based on other studies which suggested that vegetation zonal threshold elevations will migrate upward as mean atmospheric temperature increases. The evapotranspiration calculation explicitly took into consideration stomatal resistance, which was assumed to vary with the CO_2 scenario. (It is known that stomatal resistance increases when plants are exposed to increased atmospheric concentrations of CO_2 (Roger *et al.*, 1983). Stomatal resistance influences transpiration in plants, and therefore increased CO_2 may influence runoff response indirectly through its effect on stomatal resistance, in addition to effects on weather and climate.)

2.3 Water resources systems and modeled reservoir reliability under climate change

Relatively few water resources modeling studies have analyzed the impacts of climate change on water resources system behavior and management. Among these are studies by Lettenmaier and Sheer (1991), Lettenmaier *et al.* (1993); Miller and Brock (1989), Urbiztondo *et al.* (1991), and Fiering and Rogers (1989). Urbiztondo *et al.* (1991) modeled the hydrologic sensitivity of the Zambezi River of the Sahel, Africa, and the hydroelectric power production of a large dam on the Zambezi River, for $2xCO_2$ climate scenarios of four different GCMs, relative to the current climate. The four GCMs used projected both increases and decreases in runoff. However, hydropower was not significantly affected under any of the scenarios.

in evapotranspiration could have serious consequences for reliable yield, and that the relation between percent changes in precipitation and changes in storage required to reliably provide a given yield was highly non-linear.

Lettenmaier *et al.* (1993) found that warmer climates led to increased storage and release failures for two hypothetical reservoirs on the American River in Washington, which is snowmelt-dominated. The hypothetical reservoirs had capacities equal to 0.25 and 0.5 of the mean annual flow. Under the warmer climate scenarios (+2C and +4C, no change in precipitation) runoff was shifted to earlier in the year; water deliveries where degraded, but hydropower revenue increased. Their results suggest that hydropower revenue under warmer climate scenarios is more sensitive to reservoir capacity than to operating policy. Fiering and Rogers (1989) also modeled the operation of hypothetical reservoirs, and found that reliability was not very sensitive to changes in runoff if storage capacity exceed 50 percent of mean annual flow.

Lettenmaier and Sheer (1991) modeled the state and federal reservoir systems of the Sacramento-San Joaquin Basin, using synthetic monthly streamflow sequences for several climate scenarios (Lettenmaier and Gan, 1990). The water resources model simulated the actual system operating rules. Annual runoff increased in response to GCM-derived $2xCO_2$ - $1xCO_2$ difference scenarios (Lettenmaier and Gan, 1990); water supply deliveries were impaired in the state-operated but not in the federally-operated system. The reservoirs of the state-owned water resources system are small compared to annual runoff, and water demand exceeds supply, whereas in the federal system supply exceeds demand. The authors concluded that changes in demand would overshadow changes in reliability due to climate changes over the next century. Furthermore, it was concluded that increased winter flood risk would result in a greater need to operate reservoirs for flood control, rather than for conservation.

2.4 Climate impact assessment: From catchment scale to basin scale

GCMs, regional scale water balance models, and hydrologic models could all be applied to basin scale studies of water resources systems requiring multivariate streamflow sequences. All three approaches have significant shortcomings. The results of Kuhl and Miller (1992) reveal the shortcomings of GCM parameterizations with respect to streamflow prediction. They selected the 33 largest basins of the world, together comprising the total land surface of the globe. With an 8 degree latitude by 10 degree longitude resolution GCM, they performed on-line simulations of historical runoff ($1xCO_2$ scenario) for each basin. Although the model was calibrated to preserve the mean annual global runoff, mean annual runoff was overestimated for most basins. The model generated excessive precipitation and evapotranspiration. Modeled snowmelt runoff generally preceded the observed peak by about one month. The poor results were attributed to deficiencies in the GCM parameterization of atmospheric parameterization and/or representation of the land surface, rather than to scale incompatibility, since many of the basins in the study overlay multiple GCM grid cells.

One of the difficulties with using hydrologic simulation models is that they are difficult to apply to catchments at scales of thousands to tens of thousands of square kilometers. The complications at this scale are, first, the absence of streamflow data for calibration and validation that are free of water management effects; second, lack of accurate areal estimates of precipitation and snowpack; and third, questions as to whether the conceptualization and/or physical representations used in the models are appropriate at such large scales.

Gleick (1986, 1987) advocates the use of monthly water balance models on the basis that in most applications the available data do not support the use of finer scale models. This approach has the shortcoming that it precludes assessment of climate accompanied changes, such as increased rain-on-snow events and/or change in storm intensity, that are evidenced at shorter time scales. Gleick (1987) used a regional water balance model to study the hydrologic sensitivity to climate change

within the Sacramento-San Joaquin River Basin in California. In order to differentiate snowmelt and non-snowmelt-dominated regimes, the water balance model was calibrated independently for several large subbasins, and took into account orographic precipitation, and the dependence of temperature on elevation.

Lettenmaier and Gan (1990) described an approach for linking catchment scale hydrologic simulations to a large scale basin through the use of a stochastic transfer scheme, and applied the method to the Sacramento San Joaquin Valley. First, a conceptual hydrologic model (the Sacramento model) was used to simulate (for each climate scenario) daily runoff of a few small "index" catchments. The index catchment streamflows were then aggregated to a monthly time step, and a stochastic streamflow disaggregation model was used to disaggregate the index catchment streamflow to much larger subbasins. The same disaggregation model was used to generated synthetic streamflow for each subbasin and each climate scenario. Finally, as described in a related paper (Lettenmaier and Sheer, 1991), the subbasin sequences were routed through a water resources model to simulate reservoirs and diversions.

2.5 Summary

Hydrologic models have been used to assess the potential impacts of climate change on water resources, both on the catchment and the regional scale. Such studies typically use GCM-derived climate change scenarios or prescribed change scenarios. The climatic variables that are modified are usually limited to temperature and precipitation. Few studies have addressed the issue of the direct and indirect influence of transitional and long term climate change on model parameters. Regional scale studies present certain difficulties for hydrologic modeling. One way in which hydrologic models have been applied to large scale water resources modeling is through the use of a stochastic transfer scheme. With this method (Lettenmaier and Gan, 1990), runoff for multiple small scale catchments is simulated with a deterministic hydrologic model, and then stochastically disaggregated to

obtain subbasin flows. The generated subbasin flows are then routed through a water resources system model. This is the approach that will be used in the study of the Columbia River basin, described herein.

2.6 Description of the study area

The Columbia River basin is the second largest basin in the United States, after the Mississippi, encompassing 219,000 square miles above The Dalles, Oregon with a mean annual runoff of 190,860 cfs (1928-1977). The basin extends into Canada, and encompasses most of Washington and Idaho, and parts of Oregon, Montana, and Wyoming. The water resources system consists of more than 200 federal, state, and private reservoirs and run-of-the-river projects. Major reservoirs serve multipurpose functions, including irrigation, flood control, recreation, navigation, and fisheries.

The Canadian portion of the basin comprises about 20 percent of the total drainage area, and contributes about 30 percent of the mean annual runoff. Much of the southern basin is semi-arid lowland. Precipitation throughout the basin is highly seasonal, with most storms occurring in winter. Average annual precipitation ranges from 10 inches per year in the lowlands to over 100 inches on some west-facing mountain slopes where strong orographic lifting of moist air masses occurs as they pass over mountainous terrain. Most of the runoff is produced in the spring due to melting of the snowpack of the eastern slopes of the Cascades and the Rocky Mountains, west of the Continental Divide.

Chapter 3 Model Description

3.0 Model components and interaction

This chapter describes the functional elements of the chain of models used to assess possible implications of climate change on the Columbia River reservoir system. This study follows the general approach described by Lettenmaier and Gan (1990), in which detailed streamflow simulations at a small number of index catchments were coupled with a stochastic streamflow disaggregation model to produce streamflow simulations at the nodes of a water resources system model. The elements of the model chain, as shown in Figure 3.1, are 1) a hydrologic model, 2) a stochastic disaggregation model, and 3) a water resources screening model.

The hydrologic model is a deterministic representation of the runoff response of a catchment to meteorological inputs. Because the hydrologic model simulates streamflow as a function of meteorological time series, it provides the means for inferring the effects of altered surface meteorological conditions on streamflow. The hydrologic model used in this study consists of the National Weather Service snow accumulation and ablation model (Anderson, 1973), coupled with a Penman type potential evapotranspiration algorithm, and an elevation band version of TOPMODEL, a semi-distributed soil moisture accounting model (Beven and Kirkby, 1979). The hydrologic model was applied to five small index catchments with drainage areas ranging from 204 to 2925 sq. km.

A stochastic disaggregation model (Stedinger and Grygier, 1990) was used to extrapolate the results of the index catchment simulations to the scale of large subbasins of the Columbia River drainage (of sizes ranging from 2400 to 190,000 km^2) while preserving certain statistical properties and relationships (e.g. cross-

correlations between flows in different subbasins at the monthly time step) of the historical streamflow records for the large subbasins. In most applications of stochastic streamflow simulation, the objective is to generate many streamflow sequences (e.g. hundreds), each of which constitutes a realization of the underlying parent streamflow population, whose properties are estimated from the historical streamflow series. This approach is commonly referred to as a Monte Carlo analysis. In this study the application is somewhat different in the sense that the synthetic streamflows are conditioned on the index sequence simulated streamflow, which is taken to be a particular realization of the underlying streamflow generating process. Nonetheless, it will be shown that the stochastic disaggregation technique is still applicable.

Ease of implementation is the primary motivation for using the stochastic model to bridge the gap in scales between the index catchments and the water resources system nodes. In theory, the entire Columbia River basin could have been deterministically modeled. However, this would have been a prohibitively time consuming undertaking. The stochastic disaggregation model parameters are estimated using historical streamflow records at a monthly time step. Thus, the combined use of deterministic and stochastic modeling provides a means for evaluating the physical effects of climate change on the hydrologic system, without exhaustive deterministic modeling at the scale of a large basin such as the Columbia River.

The water resources screening model is a simple fill and spill representation of eighteen equivalent run-of-the-river and storage projects that represent conceptually the real system of over one hundred reservoirs. In practice, reservoir operation is based on firm and secondary demands for water and hydroelectric power, current state of the system (e.g. reservoir energy content and flood control storage reservation), historic streamflow statistics, and daily and seasonal runoff forecasts, which in turn are based primarily on observations of snowpack water storage. The

simple screening model used in this study has no forecasting algorithm, but instead uses a monthly target discharge (constant from year to year) which is a surrogate for the combined effects of all water demands. No attempt was made to optimize the operation under the alternative climate scenarios.

The target discharge was formed from observed streamflows in the period 1974 to 1989, which is subsequent to completion of Mica, the last major dam to be built in the Columbia River basin. A more realistic operating policy would seek to maximize some function of hydropower demand, subject to constraints on flood control storage reservation, minimum releases, and pool levels. The use of the target discharge approach was selected, however, because it incorporates the effects of actual system operations in the past, provides a simple way to approximate historical operation, and avoids the need to adapt or create a reservoir system model for the Columbia River basin which is beyond the scope of this research.

3.0.1 Index catchments

Five index catchments were selected to represent the climatic and hydrologic diversity of the basin. Their locations are shown in Figure 3.2. The catchments range in size from 204 km^2 to 2925 km^2. All have long-term stream gage records, and are minimally affected by upstream storage and regulation. The North Fork of the American River, WA (AR) represents the east slopes of the Cascades. The Salmo River, British Columbia (SR) represents the Canadian headwaters of the Columbia. The Middle Fork Flathead River, MT (MF) represents the western slopes of the Rocky Mountains. Reynolds Creek, ID (RC) was selected to represent the central and lower Snake River basin. Finally, Camas Creek, OR (CC) was selected to represent the south central portion of the basin.

The historical mean monthly runoff for each catchment is shown in Figure 3.3. For the American River, Middle Fork Flathead River, and Salmo River catchments, snowmelt runoff is concentrated in May and June, whereas peak runoff occurs in March and April at Camas Creek, and March through May at Reynolds Creek.

Salmo River and the Middle Fork Flathead River have less winter runoff than American River, with the Middle Fork Flathead River having the least runoff in that period, and the most strongly defined snowmelt peak. Table 3.1 summarizes the characteristics of the five index catchments. Apart from Reynolds Creek, the limiting simulation period was at the Middle Fork Flathead River (1951 - 1988). The Reynolds Creek climate record allowed simulation only for the years 1964 to 1988. The record extension procedure MOVE2 (Hirsch, 1982) was used to extend the simulated records at Reynolds Creek to the period 1951 to 1988 for which there were concurrent hydrologic and meteorological data at the other four sites.

3.0.2 Subbasins

The fourteen large subbasins are shown in Figure 3.4. A subbasin is defined as the local contributing area to a water resources model node, i.e. that area which produces the incremental flow to any given water resources model node. Table 3.2 identifies the correspondence between tributaries or river reaches shown in Figure 3.4, and names of the water resources model nodes. The model nodes will refer both to subbasin local inflows, as well as to the aggregation of storage and run-of-the-river projects associated with each water resources node.

Both simulated runoff for the index catchments (base case climate) and the naturalized streamflow for each subbasin are required for estimation of the stochastic model parameters. Naturalized streamflows, which are the runoff that would have occurred if the system projects had not been in place, have been prepared by the Depletions Task Force of the Columbia River Water Management Group (1983), for water years 1929 - 1977, by correcting observed streamflow for diversions, changes in storage at projects, and for estimated reservoir evaporation. Local inflows to each control point were computed by difference. It is these local inflows that the stochastic model simulates. (The adjective historical, where used in reference to the subbasins, will refer to these reconstructed natural local inflows.)

The drainage areas and the historical (reconstructed) local inflows for each water resources model node are given in Table 3.3. Most subbasin local inflows are strongly dominated by snowmelt, except for subbasins in the southern region, including John Day, Roundbutte, Long Lake, and Brownlee. These four sites together account for about 23% of the total runoff at The Dalles. Figure 3.5 shows that the total, unregulated runoff at The Dalles, obtained by summing the 14 mean monthly local inflows, is mostly due to snowmelt.

For the purpose of streamflow disaggregation, each subbasin was associated with the one index catchment to which the local inflow was most highly correlated on an annual basis. Presentation of the selected subbasin-index associations and the annual cross-correlations is deferred to Section 3.7.1.2.

3.1 The hydrologic model

3.1.1 Snowmelt model

The snowmelt model is the temperature index model of Anderson (1973). It is an approximate energy balance method, in which the form and temperature of precipitation and the components of the snowpack energy budget are indexed to surface air temperature. The model uses a 6-hourly computational time step to represent the diurnal cycle. The only data requirements are precipitation and surface air temperature. The model continuously accounts for the snowpack heat content, surface layer temperature, melt in the surface layer, and liquid water content. The rain-plus-melt output of the snowmelt model (sum of rain on bare ground and snowpack outflow) becomes the input to the soil moisture accounting model.

The model differentiates three conditions, as described in Table 3.4. The primary distinction is between rain and non-rain conditions, where snowfall constitutes a non-rain event. Under rainy conditions, change in the snowpack heat content is based on a simplified energy budget. In non-rain periods the snowpack heat flux is based on a linear function of the temperature difference $T_a - T_s$, where T_s

is the temperature of the surface snow layer. Different coefficients are used for melt and non-melt periods, and these vary with Julian day.

3.1.2 Soil moisture accounting model (TOPMODEL)

The soil moisture accounting model is TOPMODEL (Beven and Kirkby, 1979). A key assumption in the most common implementation of TOPMODEL is that precipitation, or, in this case, rain-plus-melt (RPM), is spatially uniform (see for example Ambroise, 1993). A major difference in this work is that the model is applied in an elevation band format, so that RPM is assumed uniform only within an elevation band. The model is otherwise similar to the version described by Brettmann (1991), who applied it to the American River, WA. The model will first be described as applied to a single basin. Section 3.1.3 describes the application in the elevation band mode. The model parameters and their upper and lower bounds are given in Table 3.5. The upper and lower bounds are those used by Brettmann (1991) for application to the American River.

TOPMODEL accounts for spatial variability in runoff generation, subsurface contribution to streamflow, and soil moisture on the basis of a topographic index, which is defined as $ln(a/\tan\beta)$, where a is the area of the catchment draining a given contour segment of length C orthogonal to the flow direction, and $\tan\beta$ is the local slope. In practice the topographic index is computed from digital elevation data; the pixel width along a contour and the local slope are computed for rectangular grid cells (pixels) of size Δx by Δy. Pixels with the same wetness index are assumed by TOPMODEL to be hydrologically similar.

Wolock (1988) showed that the topographic classes index distribution can be reasonably well fit by a gamma distribution. In some past applications of TOPMODEL, the parameters of the fitted topographic index distribution have been calibrated to improve simulated runoff error. In this application a gamma distribution is fit but the parameters are not calibrated. The fitted distribution is discretized into

15 classes (see Section 3.5), and the model is applied to each class of pixels, rather than to each pixel.

The assumptions on which the subsurface flow model of TOPMODEL is based, and a derivation of the model, may be found in Brettmann (1991). TOPMODEL was derived from Darcy's Law with the Boussinesq assumption (local hydraulic gradient equal to the local topographic slope) for steady state, spatially uniform vertical flux and steady-state horizontal flux conditions. The derivation of TOPMODEL provides two physically-based equations. One equation gives the basin-average base flow QB_t, at time t, as a function of the basin-average topographic index (Λ). The other equation gives the time-varying distributed saturation deficit $S_{i,t}$ as a function of the local topographic index TL_i at time t, where i could represent a particular pixel, but in this application represents a single topographic class. Both state variables are functions of S_t, the time varying basin average saturation deficit at time t. S_t is computed through a mass balance according to the following equation:

$$\bar{S}_t = \bar{S}_{t-1} + QB_t - \sum_{i=1}^{I} QUZ_{i,t} \tag{3.1}$$

where I=15 is the number of discrete classes of the topographic index distribution, and QUZ is the local drainage from the upper zone to the ground water store (S_t and QB_t. as previously defined). Baseflow increases, and upper zone drainage decreases, the basin average saturation deficit.

The equation for basin average baseflow, obtained by integrating the steady state local subsurface flow equation over all topographic classes is

$$QB_t = TMAX \; exp\left(\frac{-S_t}{SZM}\right) \left\{\frac{1}{A}\int_1^I exp\,(TL_i - \Lambda)\; dA\right\} \tag{3.2}$$

where TMAX is maximum transmissivity, SZM is the soil characteristic parameter, TL_i and Λ are the local and basin average topographic indices, respectively, and dA_i is the area in topographic class i. The local saturation deficit $S_{i,t}$ is computed for each topographic class i in each time step t according to the following equation:

$$S_{i,t} = \overline{S}_t + SZM \left(\Lambda - TL_i\right) \tag{3.3}$$

The variable contributing areas are associated with those classes for which $S_{i,t}$ is less than or equal to zero. Areas with large values of the topographic index - i.e. with large contributing areas and moderate local slopes - will become saturated first. The extent of the saturated area expands and contracts as the basin average saturation deficit increases and decreases. This modeled behavior has been found to be in accord with field observations in gentle grade, shallow soil catchments, where variable source area runoff production is observed (Beven and Kirkby, 1979; Beven *et al.*, 1984). Of perhaps greater relevance to the present study is the report by Hornberger *et al.* (1985), in which they describe an application of the model to a steep, subsurface flow-dominated forested catchment of 5.2 square kilometers in Virginia. The authors concluded that the model simulated runoff reasonably well, and believed it to describe adequately the runoff mechanism active in that catchment.

The version of TOPMODEL used here includes a lumped parameter conceptual model for saturation overland flow, infiltration, evapotranspirative losses, and routing through the vadose zone similar to that used by Wolock (1988). The conceptual model is shown schematically in Figure 3.6. The vadose zone is represented as a fixed capacity root zone and a variable capacity upper zone. The local saturation deficit determines the (variable) storage capacity of the upper zone. Precipitation is reduced by potential evapotranspiration (PET). If PET is not satisfied by precipitation, then the computed actual evapotranspiration (AET) is taken from the root zone. A fraction of the precipitation (RIP) falls on riparian area and is routed directly to the channel. The remaining precipitation either infiltrates, or if the soil column is saturated, is routed as overland flow (QOF). The root zone

must be filled to capacity before any drainage to the upper zone occurs, unless PMAC is greater than zero. The parameter PMAC, which is supposed to simulate the effect of macropores, gives the fraction of moisture in the root zone that drains within each time step to the upper zone. The remaining fraction of moisture in the upper zone (1-PMAC) drains at a rate equal to the saturated hydraulic conductivity (KSAT) times the fractional storage in the upper zone (ratio of moisture content to capacity).

At each time step, baseflow QB_t (Eq. 3.2) and groundwater recharge (i.e. drainage from the upper zone, QUZ_t) are calculated, and the basin-wide average saturation deficit is updated by mass balance (Eq. 3.1). To determine the amount of exfiltration, infiltration, or saturation overland flow occurring in each pixel, the local saturation deficit $S_{i,t}$, which is a function of the local topographic index and the time-varying basin average saturation deficit, is evaluated (Eq. 3.3). QB_t and S_t are computed for the basin as a whole. All other model fluxes and storages - including root and upper zone storage, AET, QOF, and QUZ - are computed for each time step on a distributed basis (for each topographic class, in this application). Input daily RPM_t (output of the snowmelt model) is treated as spatially uniform. The watersheds are small enough that routing time in the channel network is assumed to be less than the computational time step (one day), so no channel routing algorithm is included.

3.1.3 Application in elevation band mode

To account for the ambient temperature lapse rate and for orographic effects on precipitation, the snowmelt model is applied in an elevation band mode. Each catchment was subdivided into eight elevation bands of equal area. In effect each elevation band is modeled as a separate hydrologic unit; consequently a pseudo-precipitation sequence is produced for each elevation band. A different zonal factor ZPX for each elevation band scales the station precipitation data. ZPX is assumed to increase with elevation, but is taken to be about 1.0 at the elevation of the

meteorological station. The station temperature is adjusted according to the median zonal elevation and a specified lapse rate which is treated as a model parameter. An ambient lapse rate of -6.0°C degrees per vertical km was assumed; this is approximately the pseudo-adiabatic lapse rate at 0°C and at a pressure height of 850 millibars. All other snowmelt model parameters are invariant with elevation.

The TOPMODEL parameter PXADJ (precipitation adjustment factor) is applied uniformly to RPM from each elevation band. The effective zonal precipitation factor for each band k is equal to the product of the TOPMODEL parameter PXADJ and the snowmelt model ZPX_k. The mean areal precipitation depth (I_{basin}) given in Table 3.1 is based on the calibrated model parameters:

$$I_{basin} = I_{station} * PXADJ * \frac{1}{K} \sum_{k=1}^{K} ZPX_k$$

where K=8 is the number of elevation bands.

TOPMODEL is also applied in an elevation band mode. Discretization of the distributed wetness index (as described in Section 3.5) was performed separately for each elevation band, resulting in fifteen topographic classes for each band. The RPM input differs for each of the eight bands, but, within each band, is treated as spatially uniform. The simulated base flow and overland flow from each band is summed to obtain the simulated streamflow hydrograph for the entire catchment

$$Q_{sim} = \sum_{k=1}^{K} [QB_k + \sum_{i=1}^{I} QOF_{k,i}].$$

Model parameters are calibrated to minimize the objective function, and therefore all of the model parameters (except the topographic index) are uniform across the elevation bands.

3.1.4 Potential evapotranspiration

Potential evapotranspiration (PET) was estimated according to the Penman equation (Shuttleworth, 1993). Apart from dew point temperature (T_d), which is needed for computation of the vapor pressure deficit, most of the meteorological input data required for the Penman calculation can be computed from air temperature (T_a) (see for example Chapter 5 in Bras, 1990). To estimate T_d, the empirically-based method of Bristow and Campbell (1984) was used, whereby T_d, T_a, and atmospheric transmissivity are inferred from T_{min} and T_{max}. With this method PET is easily computed for the alternative climate scenarios.

3.1.5 Hydrologic model calibration

The calibration period at each site was five years. The parameters of the snowmelt model and the soil moisture model were adjusted to minimize the objective function for years two through five of the calibration period; the first year of the simulation was used to minimize the influence of the initial storage values. The objective function used was the sum of the squared difference between simulated and observed daily runoff (SSE_d). Snow-cover data were not used to calibrate the snowmelt model parameters. For each site a calibration period was selected for which the last four annual hydrographs displayed a range of characteristics, such the timing of the onset of the snowmelt season, the duration of the runoff period, flashiness of runoff response, and the occurrence of both high and low flow years, and which would therefore be most likely to exercise all aspects of the model.

The snowmelt model parameter values, other than the zonal precipitation factors, were based on ranges suggested by Anderson (1973). The zonal precipitation factors were selected such that rainfall as a function of elevation had a negative second derivative, and mean annual runoff could be preserved in the TOPMODEL simulation. For the snowmelt model parameters most likely to influence the timing of runoff, only the ZPX_k had a strong influence. Therefore the snowmelt model calibration consisted primarily of choosing the precipitation-

elevation relationship to improve the timing of the onset and cessation of ablation, and such that the rain-plus-melt input to TOPMODEL would require little further adjustment (i.e. corresponding to PXADJ of 1.0).

Following calibration of TOPMODEL to minimize the objective function, PXADJ was always adjusted such that the average annual runoff bias was close to zero. The best parameter set as indicated by the lowest objective function value was identified after this adjustment of PXADJ. This adjustment did not necessarily minimize the objective function, which was sometimes improved by allowing a modest bias in predicted mean annual runoff. The snow model precipitation factors were modified and the TOPMODEL parameters recalibrated if PXADJ deviated by more than about 0.15 from 1.0.

During manual calibration it was found that several of the parameters could be eliminated from the model without affecting the model behavior. Specifically, it was found that in the five index catchments, the upper zone always drained completely in each time step unless KSAT was less than about 0.01 m/day; however KSAT below this threshold resulted in inferior simulations. Apart from this, the parameters KSAT and F appear only once in the model, as the ratio KSAT/F, which is equal to maximum transmissivity TMAX (Brettmann, 1991). Rather than calibrating both KSAT and F, TMAX was introduced as a calibration parameter, thereby reducing the number of parameters by one. Another parameter was eliminated by replacing ZROOT and THFC with SROOT = ZROOT*THFC, since these two parameters appear only once as a product. Model performance was insensitive to PMAC and RIP, within physically reasonable ranges, so these two parameters were also eliminated. (Incidentally, this model is almost identical to the reduced parameter model described by Hornberger *et al.* (1985), except that the parameter RIP was retained, and their model included a channel routing parameter SUBV.)

The calibration is greatly simplified by reducing by four the number of parameters to be calibrated. Since PXADJ is adjusted mainly to eliminate bias

(rather than to minimize the objective function), the main parameters to be calibrated in the reduced set are SZM, TMAX, and SROOT. The abbreviated set of parameters is given in Table 3.6. The upper and lower bounds were derived from the parameter bounds given in Table 3.5, as per the relationship between the two parameter sets.

Two different approaches to calibration were taken. One approach consisted of a manual calibration followed by automatic optimization using the Nelder-Mead algorithm (1965). The second approach was a fully automated search procedure which utilized the Nelder-Mead algorithm, but which used a strategy that reflected the experience gained in the manual search procedure. Based on the observation that the dominant parameter appeared to be SZM, and secondarily ZROOT and TMAX, an automated search strategy was devised that subdivides the allowable range for SZM. For each sub-range of SZM, the three parameters (ZROOT, TMAX and SZM) are randomly initialized and then optimized, after which PXADJ is optimized. This is repeated several times for each sub-range, starting with new random initial values for SZM, TMAX, and ZROOT, but reverting to the original value specified for PXADJ. This procedure, which explores every sub-range of SZM, is repeated for several values of PXADJ over a narrow range (generally 0.85 to 1.15). It is not the purpose here to demonstrate that this is the most effective search strategy, but to indicate that this emerged as an effective approach based on the author's experience in calibrating the model for several catchments.

When the calibrated models were used to simulate runoff for the period of record, in every case there was a small bias in the mean annual runoff. Therefore the parameter PXADJ was adjusted to eliminate this bias. The stochastic model makes use of the streamflow at the index catchments as simulated with this adjustment to PXADJ.

3.2 Stochastic model of node and index runoff

A two stage approach of a spatial disaggregation followed by a temporal disaggregation similar to that performed by Tennessee Valley Authority (1993) was

used. First the index site annual runoff was spatially disaggregated to the large subbasins. Next the simulated annual runoff for each index catchment (IC) and the local inflow to each large subbasin (LSB) was temporally disaggregated to obtain seasonal runoff (in this case monthly). Rather than generating the index site sequences, as would be the case in a streamflow synthesis application, the simulations for the alternative and base case index site simulations were taken as known sequences in the generation step. In this way the generated sequences were conditioned on the index simulation sequences. Two realizations for each subbasin were generated.

The stochastic disaggregation model was performed using SPIGOT (Stedinger and Grygier, 1990), a FORTRAN implementation of the simplified space-time model of Stedinger *et al.* (1985). SPIGOT provides a choice of models that employ a contemporaneous disaggregation procedure and explicitly model only a limited number of correlation statistics. Specifically, the correlation between monthly and annual flows, the lag-1 monthly auto-correlations, and the lag-0 cross-correlations are preserved in the models used. In general the models operate on a transform of the raw data (e.g. lognormal) that is assumed to be normally distributed. Several of the models in SPIGOT also make use of an adjustment procedure to force the transformed monthly flows to sum to a specified (generated or otherwise) annual flow.

A key concern for this study, in addition to preserving the mean and variance of flows at each subbasin, is to model the cross-correlation of flows between all the subbasins at the monthly and annual level, and the persistence of annual and seasonal flows. Grygier and Stedinger (1988) showed that the condensed models and disaggregation schemes provided in SPIGOT were as successful as more complex models in preserving such statistics, and in forcing the generated monthly flows to sum to the specified annual flows.

SPIGOT was modified by Grygier (1992) to allow inclusion of "index" flows in the generation step (after estimation of the model). The first stage uses SPIGOT's spatial disaggregation (SPA) module and the second uses the annual-to-multivariate-monthly (AMM) module. This is the only practical model sequence that can be devised with the current version of SPIGOT and that permits the use of index flows, as required for this study. SPIGOT refers to the site flows which are disaggregated as basin flows, and the resulting flows as key flows. A basin (index catchment) and its dependent key sites (LSB) are referred to collectively as a group.

Both the SPA and AMM are applied as separate models for each group, allowing the inclusion of the simulated IC runoff sequences as index flows, as required in this application. Unfortunately this configuration does not explicitly preserve the inter-group cross-correlations. However, there remains the possibility that they could preserved implicitly because of the cross-correlated IC simulations.

With both models, each group is modeled separately. The matrix equation for the two models are as follows. The spatial disaggregation model is non-recursive, with each annual key site flow (Y_{nk}, year n and site k) being generated from the independent index site annual flow (Z_n). In year n, the model equation is

$$\mathbf{Y}_n = \mathbf{A} + \mathbf{B}\,Z_n + \Pi\,\mathbf{E}_n \qquad (3.4)$$

where

Y_n	Kx1	Vector of transformed flows for each key site, in year n, where K number of sites in the group.
A	Kx1	The kth element of this matrix is $[\mu_k \cdot (1-\beta_{k,k})]$ which preserves mean of the transformed flow μ_k for site k, and where $\beta_{k,k}$ is an element of **B**.
B	KxK	Diagonal matrix of Y_n and Z_n lag-0 correlations
Z_n	scalar	Transformed annual basin site (i.e. IC) flow in year n
Π	KxK	Upper diagonal coefficient matrix
$\mathbf{E}_n$	Kx1	Independent and normally distributed innovations with mean zer

The model preserves the mean, variance, and other parameters of the marginal distribution of transformed annual flows, as well as the covariances of the transformed flows between each basin and key and between each key within a group.

Given the basin annual flow for the basin, the AMM generates monthly flows at each key site and, unless monthly index flows are provided, also for the basin. The model preserves 1) the mean, variance, and other parameters of the monthly marginal distribution of transformed flows; 2) the lag-1 monthly and the monthly-annual autocorrelations for the transformed flows; 3) total flow in each year; and 4) the lag-0 seasonal cross-correlation. In year n, season 1, the model is

$$\mathbf{Y}_{n1} = \mathbf{A}_1 + \mathbf{C}_1 \mathbf{Z}_n + \mathbf{\Pi}_t \mathbf{E}_{n1} \tag{3.5}$$

and for seasons 2 through 12

$$\mathbf{Y}_{nt} = \mathbf{A}_t + \mathbf{B}_t \mathbf{Y}_{n,t-1} + \mathbf{C}_t \mathbf{Z}_n + \mathbf{D}_t \Delta_t + \mathbf{\Pi}_t \mathbf{E}_{nt} \tag{3.6}$$

where

$\mathbf{Y}_{nt}$	(K+1)x1	Vector of transformed flows for each basin (k=1)and key site (k=2,K+1), in year n, month t, where K+1 is the number of sites in the gro (including the IC).
$\mathbf{B}_t$	(K+1)x(K+1)	Diagonal matrix, preserves lag-1 monthly autocorrelations for r
$\mathbf{C}_t$	(K+1)x(K+1)	Diagonal matrix of $Y_{n,t}$ and $Z_{n,t}$ lag-0 cross correlations for r
$\mathbf{D}_t$	(K+1)x1	Diagonal coefficient matrix
Δ	(K+1)x1	Surrogate flow (weighted sum of year n flows from month 1 to 1 1)
$\mathbf{\Pi}_t$	(K+1)x(K+1)	Upper diagonal coefficient matrix, preserves the key-key lag-0 cross-correlations

Site-site cross-correlations are modeled through the Π matrix. $\mathbf{D}_t$ Δ_t forces the summed seasonal transformed flow (from season 1 to season t-1) to be approximately equal to the transformed annual flow in the same year. Any discrepancy after inverse transforming (e.g. exponentiating if a 2-parameter lognormal transformed flow) is corrected for by proportion.

When seasonal index flows are provided by the user (or generated in a previous step), then the consequence is that the innovation (the first element of the vector $\mathbf{E}_{n,t}$) for the basin (k=1) is known by difference. This forces the generated key site seasonal flows (k=2 to k=K+1) to be cross-correlated to the given basin sequence.

3.3 Adjustment procedure for alternative climate scenarios

The alternative climate scenarios are incorporated into the study through the deterministic model. The two scenarios considered are constant increases in temperature of two degrees and four degrees centigrade. The meteorological forcings for the hydrologic model (temperature and PET) are modified to form the alternative climate scenarios. The altered climate data are then used as inputs to the calibrated hydrologic model, in order to produce corresponding streamflow sequences at each index site. The stochastic model, the parameters of which are estimated using base-case climate IC simulations and historical LSB local inflows, is then used to generate synthetic LSB inflows, conditioned on the simulated streamflow for each climate scenario.

To implement the stochastic model for the alternative climate cases without violating the model assumption of stationarity, it was necessary to perform an external adjustment to the model inputs and outputs. The procedure used here is the same as that used in a study of the Tennessee Valley Authority (1993). The stationarity assumption is satisfied for the alternative climate scenario applications by adjusting the alternative climate scenario index catchment simulations in transform space such that the natural flows will have the same mean and variance as in the base case climate. For this adjustment, a lognormal distribution is assumed, so that the adjustment of the index catchment sequences is given by:

$$x^{\oplus} = exp\left[\left(y^{+} - \mu_{y}^{+}\right)\left(\frac{\sigma_{y}^{\circ}}{\sigma_{y}^{+}}\right) + \mu_{y}^{\circ}\right]$$

where y is the natural logarithm of the natural flow (x), and '⊕' indicates that the sequence has the base case statistics due to the adjustment. The mean and variance of the index site altered climate flows μ^+ and σ^+ are estimated by the method of moments (Equations A.1 and A.2). The adjusted (⊕) simulations are then included as index flows in the generation step. Consequently, the generated LSB sequences will have (at-site) base case climate statistics, regardless of the climate scenario; these are also denoted with the superscript ⊕, prior to adjustment.

The basic premise of the index catchment subbasin approach is that the simulated change in runoff for the index catchment is a guide to how the runoff of the large subbasins will change in response to warming. Specifically, it is assumed that the relative change in mean monthly runoff at the subbasin is equal to the simulated change in mean monthly runoff at the index catchment. One additional assumption is required regarding the coefficient of variation. The two conditions used here are 1) that it is invariant, or 2) that the relative change is the same as at the index catchment. These two assumptions were used, giving two adjustment procedures.

The two alternative adjustment procedures are both applied to the natural logarithms of the generated LSB (⊕) sequences, as a result of which the moments of the processed sequences will conform to assumptions about how the runoff of the LSB's respond to climate changes. The derivation for each adjustment procedure, and the equations used to adjust the natural logarithms of the generated flows are given in Appendix A. Figure 3.8 shows how the adjustment procedure is integrated into the chain of models.

3.4 Water resources model

3.4.1 Description of the aggregate nodes

Table 3.2 gives the local and total runoff at each project relative to mean annual flow (MAF) at The Dalles, which is 140 million acre feet (maf). Sixty eight percent of MAF at The Dalles passes Grand Coulee dam. The total model reservoir

storage capacity (39.2 maf) is 30 percent of MAF at The Dalles, 91 percent of which is located in the Columbia River basin above Grand Coulee Dam (including Franklin D. Roosevelt Lake active storage). Four reservoirs (three nodes) - Libby, Grand Coulee, Arrow, and Mica (4.9, 5.23, 7.15 and 12.0 maf, respectively) account for 60 percent of total storage. The model storage is less than the actual system storage because of the omission of non-federal projects, the most significant being those on the Snake River, upstream of Brownlee (Jackson Lake, Palisades, and American Falls). The Bonneville Power Administration does not have jurisdiction over the reservoirs upstream of Brownlee, which constitute 80 percent of Snake River storage. Therefore the Depletions Task Force did not make corrections for upstream changes in storage in the case of Brownlee, for which the local inflow represents the entire central and upper Snake River drainage.

Table 3.2 lists the major projects included in each aggregate node, storage capacities, and the percent of total system energy content (43.6 maf) and hydroelectric capacity (32,600 average megawatts) accounted for by the projects in each node. The most significant aggregate hydroelectric projects are Mica plus Revelstoke, Albeni Falls (eight projects including nodes 17 and 18), Lower Granite (4 projects), John Day (plus Bonneville and McNary), and Grand Coulee/Arrow (eight projects, including node 16). The first 3 each account for about 15 percent of total system capacity, John Day accounts for about 10 percent, and Grand Coulee/Arrow for 42 percent. As for percent generated power, the most important nodes are Grand Coulee/Arrow (34 percent), John Day (19 percent), and Mica/Revelstoke (18 percent).

3.4.2 Formulation of the water resources model

The water resources model consists of eighteen nodes; the four additional nodes represent run-of-the-river projects (one or more) with no local inflow but for which aggregation of power generation capacity with one of the other fourteen nodes was not feasible. The structure of the model is based on nineteen look up tables provided

by Dean (1992). Reservoir storage capacity, turbine discharge capacity, and power-storage-discharge relationships were determined from the information provided in these tables. (Two of the nineteen tables were combined, such that 18 nodes were modeled, rather than 19.)

Records of historical runoff were used to form the target discharge rule, and to validate the model. The sites selected for these purposes, referred to hereafter as reference sites, are listed in Table 3.7. Table 3.7 also indicates which reference site data are used to form target discharges that affect the model simulation of reservoir operation, and which data are used to validate the model. Reference sites are used for model validation only if located immediately downstream of a project node, and therefore not subject to significant incremental flow with respect to the node. In Section 3.7.3 it will be shown that the validation of the model is not compromised by lack of identification of a suitable reference site for every node.

Power production, computed by assuming the monthly discharge to be uniform over the time step, is interpolated from multi-linear approximations to lookup tables (Dean, 1992), which give power production as a function of storage and discharge, or, for run-of-the-river projects, as a function of discharge only. Two or three linear equations relating power to storage at constant discharge were formed from each look-up table, depending on the complexity of the surface suggested by the look-up table. These equations were then used by the model to calculate power, by interpolation. To show a typical example of how well the model equations fit the data, Figure 3.8 compares the model-generated data (lower panel) for the Grand Coulee/Arrow aggregate reservoir to look-up table data (upper panel); each data series corresponds to some value of constant storage. The monthly turbine discharge capacity was taken to be the discharge at which the power was maximized. Monthly outflow in excess of the monthly turbine discharge capacity as regarded as a spill.

Figure 3.9 shows a schematic of the 14 water supply nodes, and the four additional run-of-the-river (hydroelectric project) nodes (nodes 15 through 18). The model proceeds from headwater exterior nodes to the downstream interior node to solve the network. The solution sequence was as follows (by node): 14, 13, 12, 11, 10, 17, 9, 18, 7, 6, 16, 5, 4, 3, 2, 1, 15. At each time step the model adds the monthly synthetic (adjusted) local inflows and the modeled regulated outflows from each adjacent upstream node (if any) to obtain the total inflow to a node. The inflow is added to the water in storage at the end of the previous time step. Next, the model releases the lesser of available storage or the target discharge. Additional water is released, if needed, to bring end-of-month storage to not greater than storage capacity. The model steps through all of the nodes before advancing to the next time step.

If average discharge in any month exceeds turbine discharge capacity (discharge at which power is maximized), the excess is treated as a spill, and hydropower is calculated at the turbine capacity. Monthly power production and discharge at all projects, and various operational statistics for the storage projects are recorded, including end-of-month storage, storage failures, release failures (releases less than the required minimum release, Qmin), and spills. Q_{min} is taken to be the tenth percentile low flow at the same site from which the target discharge was formed. Storage failures occur when the end-of-month storage is zero, i.e. when the storage, after adding the inflow, was less than or equal to the target discharge.

3.5 Digital elevation data and calculation of the topographic index

Catchment boundaries were delineated from 3 arc second DEM (Digital Elevation Model) data using GRASS (Geographic Resources Analysis Support System) software, version 4.0 (US.Army Construction Engineering Research Laboratory, 1991), or (in the case of the Middle Fork Flathead River basin), a fast delineation program provided by J. Ferriera. Once the catchment boundaries were obtained, the accumulated drainage areas were computed using an algorithm

patterned after the 8 pointers method of O'Callaghan and Mark (1984). For the Middle Fork Flathead, the delineation was performed at 6 arc second resolution, and for the other four catchments, at 3 arc seconds. Each DEM was transformed to the Universal Trans-Mercator (UTM) coordinate system before computing the topographic index, so that every grid cell would be of equal area (about 6000 m^2).

For each of eight elevation bands of equal area, the value of the local topographic index was calculated for each cell in the delineated watershed. The local slope for each grid intersect (pixel) was calculated as the weighted average of the slope with respect to each downhill adjacent pixel, following the method of Quinn *et al.* (1991). For each elevation band, a three parameter gamma distribution was fit to the empirical distribution of the local topographic index, following Sivapalan *et al.* (1987). Fifteen percentiles were selected, and the corresponding quantiles of the fitted distribution were calculated for each elevation band. The discretization of the cumulative distribution function of the topographic index was performed so as to over-represent the upper tail slightly. This is important because cells with high values of the index (large contributing area, low slope), which are associated with variable source areas, contribute disproportionately to runoff. The upper threshold percentiles for each of the 15 classes are as follows: 0.10, 0.20, ..., 0.70, 0.80, 0.85, 0.90, 0.92, 0.94, 0.96, 0.98, and 1.00. Figure 3.10 gives empirical and fitted quantiles at each percentile for four of the eight bands of the Middle Fork Flathead catchment.

3.6 Meteorological data

The primary and secondary meteorological stations are given in Table 3.8, along with location and elevation. Missing precipitation depths in the primary station record were filled in by scaling the observed precipitation at the secondary station by the ratio of the monthly average precipitation at the two stations. Missing temperature observations were filled in according to the monthly average temperature difference at the two sites. In some cases a different station was used for different

months. When reasonably long records were available at several nearby sites, missing data in a particular month were filled in based on the site record which was most highly correlated for that month.

3.7 Model verification

3.7.1 Calibration and validation of the hydrologic model

3.7.1.1 Simulated runoff error

The model was first calibrated manually for all of the index catchments. The automated procedure described in Section 3.1.5 was then applied to American River, Salmo River, and the Middle Fork Flathead River. A lower objective function was found for the Middle Fork Flathead River through manual calibration (followed by automatic optimization) than through the automatic search procedure, apparently because the automated procedure converged to a local minimum. The improvement in the objective function for the American River and Salmo River through automatic optimization did not correspond to much noticeable improvement in the visual appearance of the (daily time step) hydrograph.

Final calibrated parameter values for each index catchment appear in Table 3.9. Typical simulations for each index catchment are presented in Figure 3.11. The observed mean monthly runoff (Q_{obs}), bias and absolute errors for the calibration and validation periods are presented in Figures 3.12 and 3.13. Table 3.10 gives several measures of averaged daily, monthly, and annual model errors for the calibration (4 years) and validation periods (14 to 35 years). To facilitate comparison between catchments, the mean monthly absolute error (MMAE) is given as a fraction of the observed mean monthly runoff; the objective function, SSE_d, was normalized by the number of years in the validation period, and by the square of the observed mean annual runoff.

Generally, the simulations for the two semi-arid catchments (Reynolds Creek and Camas Creek) were most time consuming and least successful. For these catchments, there was a tendency for the model to be overfitted (larger errors in the

validation than in the calibration period). By every measure, except for the bias in the validation period, the Salmo River simulation is most successful. The validation period simulation was especially poor for Camas Creek, relative to the calibration period simulation. The bias in mean monthly runoff for Reynolds Creek was small, but the mean monthly absolute error was quite high in both the calibration and validation periods. It appears that the less successful application of the model to the semi-arid catchments is related to the difficulty of estimating AET. The next section addresses this issue further.

Use of the stochastic MOVE2 procedure (Hirsch, 1982) to extend the Reynolds Creek simulation from 17 years to 38 years resulted in an extended record that had the correct mean and variance, but which was more weakly correlated to the simulated runoff at the other index catchments than was the base 17 year period simulation. It was found that the cross-correlations between the Reynolds Creek associated sites and other subbasins also suffered as a result of record elongation.

Due to the poor simulations for Camas Creek and Reynolds Creek, and the fact that the simulation period for Reynolds Creek was limited to the period 1964 to 1988, it was decided to eliminate these two sites from the model. Although it would be desirable to include Camas Creek and Reynolds Creek from the standpoint of geographic representativeness, I concluded that the poor quality of the simulation for these sites would degrade the overall model performance.

3.7.1.2 Cross-correlation of simulated and historical runoff

Ideally, the index catchment simulations should preserve the observed cross-correlation of runoff between the index catchments. In fact, this is unlikely to occur, since simulated streamflow includes model errors, which are likely to be independent from site to site, and therefore "dilute" the cross-correlations of simulated relative to observed flows. The results for the index catchments are presented in Table 3.11 (items 1 and 5). As expected, the cross-correlations for the simulated flows are lower than those of the observations. The difference between the observed and

simulated annual cross-correlations for SR-MF was only 0.21 (from 0.648 to 0.442), whereas for AR-SR, it was 0.54 (from 0.835 to 0.286). The AR-MF cross-correlation was well-preserved, dropping only 0.07 units (from 0.743 to 0.674). The generally poor preservation of the index catchment runoff cross-correlations involving Salmo River means that the inter-group cross-correlations (cross-correlation of synthetic runoff for subbasins keyed to different index catchments) will not be well preserved by the stochastic model.

Although the most successful simulation overall is that of Salmo River, this pattern in cross-correlation of simulated runoff suggested that among the three sites (American River, Middle Fork Flathead River, Salmo River) efforts to improve the Salmo River simulation should lead to improvement in the AR-SR and MF-SR correlations, and should be given higher priority than the model performance for the American River or the Middle Fork Flathead River.

After reviewing the cross-correlations of precipitation, historical runoff and simulated runoff, however, it became clear that further calibration would probably yield little improvement. The various correlations are presented in Table 3.11 (items 2-4). For all three sites simulated runoff (Q_{sim}) and observed precipitation (item 3, Table 3.11) were strongly correlated (ranging from 0.880 for the Middle Fork Flathead River to 0.967 for the American River), and, in fact, more highly correlated than precipitation and observed runoff, which stands to reason, since precipitation is the model driving variable. This result suggests that the cross-correlation of simulated runoff cannot be much higher than the cross-correlation of precipitation. Indeed, this is the case for these three catchments, as seen by comparing items 4 and 5, Table 3.11. Thus, the inability to preserve the cross-correlation between American River and Salmo River runoff is explained by the weak cross-correlation between the precipitation records. It is concluded that the limitations of the model to approximate soil moisture conditions and evapotranspiration are to blame, rather than the relative quality of the calibrations.

The tendency of the model to produce streamflow that is highly correlated to precipitation is particularly problematic for the semi-arid catchments because the historical correlation between precipitation and runoff tends to be considerably lower for catchments with lower runoff ratios. The semi-arid catchments are likely far more sensitive than more humid catchments to misrepresentations of soil moisture and AET. By this argument, there is little reason to expect that the model would be any more successful with other catchments in the southern region of the basin.

3.7.1.3 Selection of index-subbasin groups

The determination of the IC-LSB groups was based on the monthly and annual runoff cross-correlations. All monthly and annual cross correlations for every index catchment - subbasin pair is provided in Appendix B. The historical annual cross-correlations are given in Figure 3.14. The cross-correlation of runoff in the months of peak flow was generally consistent with the annual cross-correlations, so only the latter data are presented.

Among the fourteen local inflow sequences, only those of the Brownlee and Roundbutte Creek subbasins are more highly correlated on an annual basis with the observed runoff of either of the semi-arid catchments than with one of the other three index catchments. Following elimination of Camas Creek and Reynolds Creek from the study, Roundbutte was indexed to the American River, and Brownlee to the Middle Fork Flathead. Fortunately this is a small compromise, as the Brownlee and Roundbutte subbasins are relatively minor components of the overall system with respect to storage and regulation of peak flows, power production, and volume of runoff. The selected IC - LSB pairings to be used in the stochastic model are listed in Table 3.12, along with the index-subbasin annual cross-correlations. Five subbasins are keyed to the American River and to the M.F. Flathead River, and the remaining four to the Salmo River.

3.7.2 Stochastic model validation

The historical and simulated monthly and annual standard deviations and cross-correlations for all sites are presented in Appendix B. The disaggregation model preserved the mean and standard deviation of monthly and annual runoff for individual subbasins. The sum of the generated local inflow, which corresponds to the total mean annual total runoff at The Dalles, is 3.6 percent less than the historical mean annual runoff for the basin (142,609 kaf).

Table 3.13 gives the observed and synthetic local inflow annual cross-correlations (third and second columns from right, respectively) for selected subbasin pairs (consideration was given to magnitude of local inflow and physical distance in selecting data for presentation). The table is arranged according to whether the pairs of sites are indexed to the same index catchment (within-group) or to different index catchments (between-group cross-correlations). (The structure of the stochastic model is such that only within-group subbasin cross-correlations are explicitly modeled.) The observed within-group cross-correlations were fairly well preserved by the stochastic model. The exceptions to this are the John Day-Roundbutte and the Lower Granite-Brownlee cross-correlations, and the within-group cross-correlations involving Mica (Salmo River group). The cross-correlations involving Mica are overestimated by the model, while the other two are underestimated.

The between-group correlations were not well-preserved. This is attributed to the poor preservation of index site cross-correlations by the hydrologic model, as well as to limitations inherent in the stochastic model itself. Table 3.13 shows that if the model were to be estimated using historical flows (and then used to generate LSB flows conditioned on historical index catchment flows), it still would not be able to preserve most of the inter-subbasin cross-correlations in most cases (last column of Table 3.13). This suggests that even if the simulation were perfect, the selected stochastic disaggregation model would still significantly underestimate most between-group correlations.

On each tributary (i.e. at Albeni Falls and Lower Granite) and at Grand Coulee, the reservoir simulation model results will not be affected much by the weak inter-group cross-correlations. This is because subbasins on each tributary are mostly keyed to the same index. However, it is expected that the variability in the modeled total annual hydroelectric power production and annual runoff for the whole basin (at John Day) will be somewhat lower than observed historically. Therefore, the variability in the modeled total system hydroelectric production under the two ACS's should be compared to the base case climate simulation, and not to historical patterns. Otherwise the stochastic model is considered satisfactory.

Whether the model accurately simulates the historical runoff and hydroelectric power generation is not a fundamental concern, however, since the alternative climate scenario results will be compared to the base case simulation results, and not to the historical results. The assumption is that bias in the modeled results will be filtered out by evaluating differences between simulations.

3.7.3 Water resources screening model validation

The target discharges are a surrogate for the actual operation of the system after the date of full development (1974). The target discharge was formed by multiplying the mean annual flow at the node by the ratio of the mean monthly to mean annual flow at the corresponding reference site (Table 3.7). This procedure accounts for any difference in mean annual flow at the project node and the reference site, which is substantial in the case of Dworshak, Hungry Horse, and Kerr. The model is not expected to be able to simulate actual historical reservoir storage and power production on a year by year or month by month basis. However, provided that the model is able to reproduce the historical releases from major reservoirs on average, then it should be possible to draw general conclusions about the vulnerability of system performance to climate change. Following these considerations, it was decided that validation would consist only of demonstrating how well the model is able to reproduce on average certain project monthly

discharges. Storage and power production was not validated directly, but is assumed to be reasonably well represented provided that the model is validated for the historical discharge.

The validation depends only on those target discharges which are accurately representative of historical operation (Table 3.7). These include six sites: Mica, Libby, Grand Coulee, Albeni Falls, Lower Granite, and John Day. Of these, for only Mica, Libby, Grand Coulee, and Albeni Falls does the target discharge affect the model operation (the other two are run-of-the-river projects). This list includes the five most important measurement points for water supply - accounting for total discharge for the basins at Mid- and Lower Columbia, Snake River, and Pend Oreille, the three most important nodes for hydroelectric power (Grand Coulee/Arrow, John Day, and Mica), and the three most important nodes for reservoir operation (Mica, Grand Coulee/Arrow, and Libby).

Figure 3.15 shows the historical runoff at the reference site corrected for incremental flow ("A"), the discharge as obtained by routing the base case synthetic local inflow ("M"), and the predevelopment total discharge ("U") - which is simply the sum of the at-site and upstream node local inflows. The reason for including the predevelopment discharge (Q_U) is simply to indicate to what extent simulated changes in storage moderate the discharge, since this affects the interpretation of the results. Results are shown for the five validation nodes.

Except for Grand Coulee/Arrow, the modeled and observed outflows (Q_M and Q_A) are in good agreement, and the model seems to perform reasonably well. Because storage historically has very little impact on runoff on the Snake River (Q_U and Q_A are similar), the historical discharge at Lower Granite is easily preserved. Storage on the Pend Oreille (Kerr, Hungry Horse) is great enough that it could potentially influence the hydrograph at Albeni Falls. Although the model preserves the target discharge for Hungry Horse and Kerr reasonably well, the model fails partially in May and June at Albeni Falls, probably due to use of a non-ideal

reference site for Hungry Horse and Kerr. The discharge from Grand Coulee/Arrow accounts for 68 percent of the runoff on the lower Columbia, so the under-regulation at Grand Coulee largely explains the discrepancy between observed and modeled runoff at John Day.

Because of the model's inability to simulate the historical mean monthly outflow accurately at Grand Coulee, it was of interest to compare historical and simulated combined Grand Coulee/Arrow reservoir storage fluctuations (Figure 3.16). The historical data shown are the combined storage of Arrow Reservoir (Upper and Lower Arrow Lakes) and Franklin D. Roosevelt Lake (storage behind Grand Coulee dam) storage) . Two years of data within this period were not published. The Arrow record was incomplete in calendar year 1981; the Franklin D. Roosevelt Lake record was not available for water year 1974. (The simulated time series of storage, obtained by routing synthetic base-case local inflows through the water resources model, is not expected to correspond closely to the historical data on a month-by-month basis.) Over the period shown, the historical amplitude of the annual cycle is about 70% of the active storage capacity, on average, while the amplitude of the simulated fluctuations is nearly 100% of capacity.

The ability to model system-wide power generation was not validated, on the assumption that if the historical discharge is preserved, then the power generation is also preserved. Except for the spring, during which historically discharge exceeds the turbine discharge capacity at most projects, the plot of average power generation per month closely resembles the hydrograph. There are two reasons for this. First, power generation is only weakly dependent on storage, but strongly dependent on discharge; secondly, a large fraction of the system-wide power production is produced at run-of-the-river projects (Dean, 1991).

The aggregate projects of primary importance (Table 3.2) are Grand Coulee/Arrow, John Day, and Mica (61% generation), and of secondary importance are Kerr, Albeni Falls, and Lower Granite (23% generation, about 7.5% each); no

other project accounts for more than 4% of the 34,700 average megawatt capacity. The total average annual power generated by the system in the base case climate simulation is 16,140 MW annually. At Mica, the mean monthly outflow hydrograph matches the observed outflow at Revelstoke (i.e. the target discharge). The implication is that modeled power generation at the Mica-Revelstoke aggregate node should be similar to the historical mean power production. At other nodes there is some difference between the target discharge and the modeled outflow, and therefore power generation is probably under- or over-simulated in some months accordingly. At John Day and Grand Coulee/Arrow it is certain that the model underestimates power generation somewhat in February and March (since the simulated discharge in these months at these sites is on average below the target discharge, and the discharge is less than turbine capacity).

3.7.4 Summary

The greatest shortcoming of the model is in the simulation of regulated discharge at Grand Coulee which has some repercussions downstream at John Day. The use of a regulated local inflow for the Brownlee subbasin (as opposed to a naturalized flow) has less consequence for modeling the Lower Columbia than does the deficiency of the model at Grand Coulee. However, the use of the regulated flow at Brownlee as a basis for generating alternative climate scenario inflows through the stochastic transfer scheme could change the model results somewhat for both the Snake River, but is not a serious problem since it is only 9 percent of the total runoff at The Dalles. Another feature of the model is the use of a simple operating rule in the form of a target discharge, rather than an optimization scheme to determine releases. The target discharge rule is a surrogate for the actual operating rules of the Columbia River projects. Nevertheless, the model should provide some insights into the potential sensitivity of power production, storage behavior, and mean monthly peak flows in the Columbia River basin.

Table 3.1 Index catchment characteristics

Characteristic	American River	M.F. Flathead River	Salmo River	Camas Creek	Reynolds Creek
Area (km^2)	204	2925	476	314	232
Elevation Range (m)	838-2096	959-3037	618-2372	1097-2010	1099-2238
Median Elevation (m)	1486	1744	1498	1504	1402
Gage Location	46:59N 121:10W	48:30N 114:00W	49:04N 117:17W	45:09N 118:49W	43:16N 116:45W
Streamflow Period of Record (Continuous)	1909-1990	1948 - 1988	1950-1988	1941-1989	1964-1980
Mean Annual Runoff (mm/yr)	1061	898	793	264	79
Mean Precipitation[a] (mm)	1553	1922	1524	945	553
Runoff Ratio	0.68	0.47	0.52	0.28	0.14
Mean Temperature (°C)					
January	-4.2	-5.9	-5.4	-3.9	-4.6
July	13.7	17.9	18.3	17.0	18.4

[a]Areal precipitation estimated from station precipitation through calibration of hydrologic model (as expained in Section 3.1.3)

Table 3.2 Description of aggregate projects in the water resources model [a]

Subbasin	Measurement Point for Local Inflow	Storage and Run-of-River Projects	WRM node [b]	Pmax [c]	Qmax [d]	Reservoirs	Aggregate Project Statistics	
							Percent Generation	Percent Stored Energy
Lower Columbia	John Day	John Day	1	2484	48.3	John Day	19.4	0.2
		Bonneville, The Dalles, McNary	15[e]	4324	22.6			
Deschutes River	Roundbutte	Roundbutte, Pelton Reregulation, Pelton	2	421	0.7	Roundbutte	0.8	0.3
Lower Snake	Lower Granite	Ice Harbor, Lower Monumental, Little Goose, Lower Granite	3	3482	6.0	None	6.7	0
N.F. Clearwater River	Dworshak	Dworshak	4	460	3.6	Dworshak	1.4	4.5
Middle/Upper Snake	Brownlee	Brownlee, Oxbow, Hells Canyon	5	1345	2.0	Brownlee	4.3	1.1
Middle Columbia	Grand Coulee	Arrow, Grand Coulee, Chief Joseph, Wells	6	9410	15.7	Grand Coulee, Arrow	33.8	23.2
		Rocky Reach, Rock Island, Wanupum, Priest Rapids	16[f]	3645	8.5			
Lake Chelan	Lake Chelan	Chelan	7	54	0.1	Lake Chelan	0.3	1.1
Spokane River	Long Lake	Post Falls, Upper Falls, MST, Nine Mile, Long Lake, Lower Falls	8	143	0.3			
Pend Oreille River-Clark Fork	Albeni Falls	Thompson Falls, Noxon, Cabinet George	17[g]	812	3.9			
		Albeni Falls, Box Canyon, Boundary	9	1000	3.2	Albeni Falls, Priest Lake, Noxon	8.3	4.8
		Seven Mile, Waneta	18[g]	946	3.9	None		
Flathead Lake	Kerr	Kerr	10	160	0.3	Kerr	8.3	4.9
S.F. Flathead River	Hungry Horse	Hungry Horse	11	295	0.6	Hungry Horse	0.7	14.8
Lower Kootenay	Duncan	Cora Linn	12	829	1.6	Duncun	3.9	3.9
		Kootenay Canal, Upper and Lower Bonnington, South Slocum, Brilliant						
Upper Kootenay	Libby	Libby	13	604	5.4	Libby	1.1	14.9
Columbia Headwaters	Mica	Mica, Revelstoke	14	3540	3.2	Mica	18.0	25.5

[a] L. Vail, personal communication (1992), Dean (1992), Scott, *et al.* (1993)

[b] Water resources model (WRM) node numbers; these correspond to nodes shown in Figure 3.9

[c] Maximum power generating capacity (MW). The summed system capacity is 33954 MW.

[d] Discharge (in kaf/month) at which power generation capacity is maximum (may be less than turbine discharge capacity).

[e] Node 15 is within subbasin 1 (John Day - Lower Columbia)

[f] Node 16 is within subbasin 6 (Grand Coulee - Middle Columbia)

[g] Nodes 17 and 18 are within subbasin 9 (Albeni Falls -Pend Orielle River)

Table 3.3 Subbasin drainage area and mean annual runoff

Subbasin measurement point		Drainage Area[a]	Local Inflow[b]	Total Runoff	Discharge at TDA: Local Inflow[c]	Discharge at TDA: Total Runoff[c]
The Dalles[d]	TDA	---[d]	0	134,093	---[d]	100.0
Roundbutte	RBT	7,820	3,269	3,269	2.1	2.4
John Day	JDA	18,580	11,103	130,824	7.5	97.6
Lower Granite	LWG	32,760	19,486	37,417	13.6	27.9
Dworshak	DWR	2,440	4,405	4,405	3.0	3.3
Brownlee	BRL	73,300	13,526	13,526	9.0	10.1
Grand Coulee	GCL	57,464	33,339	90,831	27.9	67.7
Lake Chelan	CHL	924	1,468	1,468	1.1	1.1
Long Lake	LLK	6,283	5,725	5,725	4.0	4.3
Albeni Falls	ALF	18,714	10,605	15,139	7.5	11.3
Kerr	KER	5,432	1,931	4,534	4.2	3.4
Hungry Horse	HHR	1,654	2,603	2,603	1.8	1.9
Duncan	DUN	942	2,658	2,658	1.8	2.0
Libby	LIB	8,985	8,924	8,924	5.9	6.7
Mica	MIC	8,290	15,051	15,051	10.7	11.2

[a] mi^2

[b] kaf

[c] Local and total runoff at the subbasin measurement point expressed as a percentage of the mean annual flow at The Dalles (TDA)

[d] The Dalles is the study area outlet node, but is not associated with a subbasin. Total runoff at The Dalles is equal to the sum of the total runoff at John Day and Roundbutte.

Table 3.3 Computation of snow accumulation or ablation under three different meteorological conditions.

	Air Temperature < TBASE[a]	Air Temperature > TBASE[a]
Precipitation > 0.01 inches	III. Snow	I Rain-on-snow and/or Rain-on-bare ground
Precipitation < 0.01 inches	III. Non-Melt	II. Non-Rain, Melt

Meteorological Condition	Snowpack Surface Temperature (T_s)	Change in Snowpack Heat Content (ΔH)
I. Rain or Rain+Melt	0°C	Simplified energy budget for rain-on-snow events
II. Non-rain, Melt	0°C	$\Delta H = MF * T_a$[b] where MF = Melt Factor[c]
III. Non-Rain, Non-Melt	f (Snowpack Antecedent Temperature Index)	$\Delta H = NMF * (T_a - T_s)$ where NMF = Negative Melt Factor[c]

[a] TBASE is the temperature below which precipitation is assumed to occur as snow

[b] T_a: air temperature; Ts: snowpack surface temperature

[c] MF and NMF vary according to Julian Day

Table 3.5 TOPMODEL parameters and upper and lower bounds

Name	Description	Units	Bounds	
			Lower	Upper
KSAT	Saturated Hydraulic Conductivity	m/day	0.100	15.0
F	Transmissivity-Depth Function	1/m	0.070	4.00
SZM	Soil Characteristic	m	0.010	4.00
THFC	Field Moisture Capacity	(m^3/m^3)	0.100	0.700
ZROOT	Depth of Root Zone	m	0.050	0.300
PXADJ	Precipitation Adjustment	dimensionless	0.70	1.30
PMAC	Fraction Marcropores	dimensionless	0.0001	0.500
RIP	Fraction Riparian Area	dimensionless	0.0001	0.100

Table 3.6 Abbreviated TOPMODEL parameter set

Name	Replaces	Units	Bounds	
			Lower	Upper
TMAX[a]	KSAT/F	m^2/day	1.500	4.00
SZM[b]		m	0.010	4.00
SROOT[c]	THFC*ZROOT	m	0.005	0.200
PXADJ[d]			0.70	1.30

[a]Maximum transmissivity

[b]Soil characteristic

[c]Root zone storage capacity

[d]Precipitation adjustment

Table 3.7 Reference sites

Node	Reference Site	Target Discharge[a]	Validation[b] (Tributary or basin)
Reference site required for forming target discharge, but not suitable for validation[a]:			
Roundbutte	Col. R. at The Dalles, OR	√	
Dworshak	Snake R. at Ice Harbor, WA	√	
Brownlee	Snake R. at Buhl, ID	√	
Lake Chelan	Priest Rapids,WA	√	
Long Lake	NA		
Kerr	Flathead R. at Col. Falls, MT	√	
Hungry Horse	Flathead R. at Col Falls, MT	√	
Duncan	Columbia R. at IB[c]	√	
Reference site suitable for validation[b]:			
John Day	Columbia R. at The Dalles, OR		Col. R. at The Dalles, OR
Lower Granite	Snake R. at Ice Harbor, WA		Snake River
Grand Coulee	Col. R. at Bridgeport, WA	√	Col. R. at Grand Coulee
Albeni Falls	P. Oreille at Box Canyon,WA		Pend Oreille
Libby	Kootenay R. at Libby, MT	√	Upper Kootenay
Mica	Columbia R. at Revelstoke, BC	√	Upper Columbia

[a] Any node with variable reservoir contents requires a target discharge. Streamflow record used to form the target discharge is indicated (insignificant storage in John Day, Lower Granite, and Long Lake subbasins)

[b]The reference site is only suitable for validation if not subject to significant incremental flow with respect to the subbasin measurement point

[c]Columbia River at International Boundary, Washington

Table 3.8 Meteorological stations

Catchment (location of streamgage)	Station[a]	Location	Period	Elevation[b]
American River, WA (46:58:39N. 121:10:05W)	Stampede Pass, WA[c]	47:17N 121:20W	'44-'88	1207
M.F. Flathead River, MT (48:29:42N 114:00:32)	West Glacier, MT	48:30N 113:59W	'50-'89	960
	Kalispell, MT	48:18N 114:16W	'00-'89	904
Salmo River, BC (49:04:07N 117:16:36W)	Salmo, BC	49:11N 117:18W	'72-'80	685
	Waneta, BC	49:01N 117:35W	'29-'77	558
	Warfield, BC	49:06N 117:45W	'48-'88	606
Camas Creek, OR (45:09:40N 119:18:25W)	Ukiah, OR	45:05N 118:56W	'50-'89	1024
	Pilot Rock 1 SE, OR	45:29N 118:49W	'49-'89	2022
	Meacham Amos, OR	45:30N 118:24W	'49-'75	1234
Reynolds Creek, ID (43:16:12N 116:45:00W)	Lower Sheep Cr., ID[d]	43:08N 116:43W	'63-'88	1648
	Reynolds, ID[e]	43:12N 116:45W	'61-'89	1198
	Deer Flat, ID[e]	43:35N 116:45W	'16-'89	765
	Caldwell, ID[e]	43:40W 116:41W	'04-'89	722

[a] First station listed is primary record, additional stations were used to estimate missing data.

[b] meters

[c] Filled-in record provided by K.Brettmann

[d] Agricultural Research Service shielded precipitation gage, processed record (no missing data), located within catchment

[d] Temperature data from the National Weather Service (Earthinfo CDROM)

Table 3.9 Calibrated model parameters

	American River	M.F. Flathead River	Salmo River	Camas Creek	Reynolds Creek
Calibration Period:	1974-1977	1969-1972	1968-1971	1986-1989	1968-1971
Parameter[a]	**Calibrated Parameter Value**				
SZM	0.0724	0.0940	0.0380	0.034	0.010
SROOT	0.0502	0.117	0.0280	0.162	0.0696
TMAX	94.33	34.3	5.000	20.0	10.00
PXADJ	1.000	1.08	0.8300	1.00	0.95

[a] Parameters and their upper and lower bounds are defined in Table 3.6

Table 3.10 Model error - calibration and validation periods

Index Catchment[a]	Period	Number years	Q_{obs}[b] (mm)	Q_{sim}[b] /Q_{obs}	SSE_d[c] (normalized)	MMAE[d] /MMR_{obs}[b]	MRAAE[e]
AR	Cal.	4	1128	0.980	0.572	0.300	0.208
	Val.	36	1070	0.853	0.548	0.288	0.171
MF	Cal.	4	1008	1.050	0.692	0.288	0.080
	Val.	33	891	0.880	0.757	0.264	0.167
SR	Cal.	4	774	1.004	0.027	0.300	0.143
	Val.	34	785	0.827	0.029	0.288	0.202
RC	Cal.	4	76	0.970	3.46	0.504	0.358
	Val.	14	78	0.974	9.22	0.660	0.480
CC	Cal.	4	237	1.013	0.8	0.516	0.113
	Val.	36	268	0.955	1.2	0.648	0.273

[a]AR - American River; MF - Middle Fork Flathead River; SR- Salmo River; RC - Reynolds Creek; CC - Camas Creek.

[b]Q_{sim} - simulated mean annual runoff; Q_{obs} - observed mean annual runoff; MMR_{obs} - observed mean monthly runoff

[c]Sum of Squared Errors (Daily) = $\sum_{i=1}^{n*365} (Qsim_i - Qobs_i)^2$

[d] Mean Monthly Absolute Error = $\frac{1}{n} * \sum_{k=1}^{n} \sum_{j=1}^{12} |Qsim_{j,k} - Qobs_{j,k}|$

[e] Mean Relative Annual Absolute Error = $\frac{1}{n} \sum_{k=1}^{n} \left| \frac{Qsim_k}{Qobs_k} - 1 \right|$ where n is the number of years in the calibration period.

Table 3.11 Annual correlations of observed and simulated data for index catchments

Site 1	Series 1	Site 2	Series 2	Correlation
1. Cross-Correlation of Qobs				
AR	Qobs	MF	Qobs	0.743
AR	Qobs	SR	Qobs	0.835
SR	Qobs	MF	Qobs	0.648
2. Correlation of Prcp and Qobs				
AR	Prcp	AR	Qobs	0.665
MF	Prcp	AR	Qobs	0.757
SR	Prcp	AR	Qobs	0.814
3. Correlation of Prcp and Qsim				
AR	Prcp	AR	Qsim	0.967
MF	Prcp	MF	Qsim	0.880
SR	Prcp	SR	Qsim	0.915
4. Cross-Correlation of Prcp				
AR	Prcp	MF	Prcp	0.527
AR	Prcp	SR	Prcp	0.460
SR	Prcp	MF	Prcp	0.454
5. Cross-Correlation of Qsim				
AR	Qsim	MF	Qsim	0.674
AR	Qsim	SR	Qsim	0.286
SR	Qsim	MF	Qsim	0.442

Table 3.12 Index Catchment and subbasin groupings for the stochastic streamflow disaggregation model

Index Catchment	Subbasin	Local Inflow[a]	Correlation[b]
American River	John Day	11,103	0.829
	Long Lake	5,725	0.890
	Dworshak	4,405	0.893
	Roundbutte	3,269	0.500
	Lake Chelan	1,468	0.919
M. F. Flathead River	Lower Granite	19,486	0.775
	Bronwlee	13,526	0.486
	Albeni Falls	10,605	0.862
	Kerr	1,931	0.962
	Hungry Horse	2,603	0.953
Salmo River	Grand Coulee	33,339	0.960
	Mica	15,051	0.595
	Libby	8,924	0.881
	Duncan	2,658	0.660

[a] kaf (historical)

[b] annual correlation of historical runoff

Table 3.13 Selected annual cross-correlations of local inflow

Group [a]	Subbasins [b]		Cross-Correlations			
			Historical Local Inflows	Generated Local Inflows		
				Type of index flow in model:	Simulated Base-Case [c]	Historical [d]
			Within-Group Cross-Correlations:			
AR	JDA	CHL	0.846		0.742	0.779
	CHL	LLK	0.875		0.736	0.766
	JDA	RBT	0.487		0.260	0.542
MF	LWG	BRL	0.800		0.552	0.645
	LWG	ALF	0.907		0.960	0.953
	KER	ALF	0.912		0.924	0.943
	KER	HHR	0.958		0.881	0.966
SR	GCL	MIC	0.533		0.703	0.862
	GCL	LIB	0.766		0.884	0.944
	LIB	MIC	0.355		0.754	0.907
	DUN	MIC	0.640		0.873	0.918
			Between-Group Cross-Correlations:			
AR-MF	JDA	LWG	0.736		0.353	0.512
	DWR	LWG	0.866		0.384	0.340
	LLK	ALF	0.927		0.485	0.408
AR-SR	LLK	GCL	0.807		0.117	0.631
	JDA	GCL	0.690		0.279	0.702
MF-SR	BRL	GCL	0.480		0.415	0.330
	LWG	GCL	0.804		0.881	0.547
	KER	GCL	0.702		0.235	0.406
	KER	LIB	0.889		0.181	0.569

[a] AR - American River; MF - Middle Fork Flathead River; SR - Salmo River.

[b] See Table 3.2 for explanation of 3-letter subbasin codes.

[c] Model parameters were estimated with simulated index catchment and historical subbasin data; generated flows were conditioned on simulated index catchment runoff.

[d] Model parameters were estimated with historical index catchment and historical subbasin data; generated flows were conditioned on historical index catchment runoff.

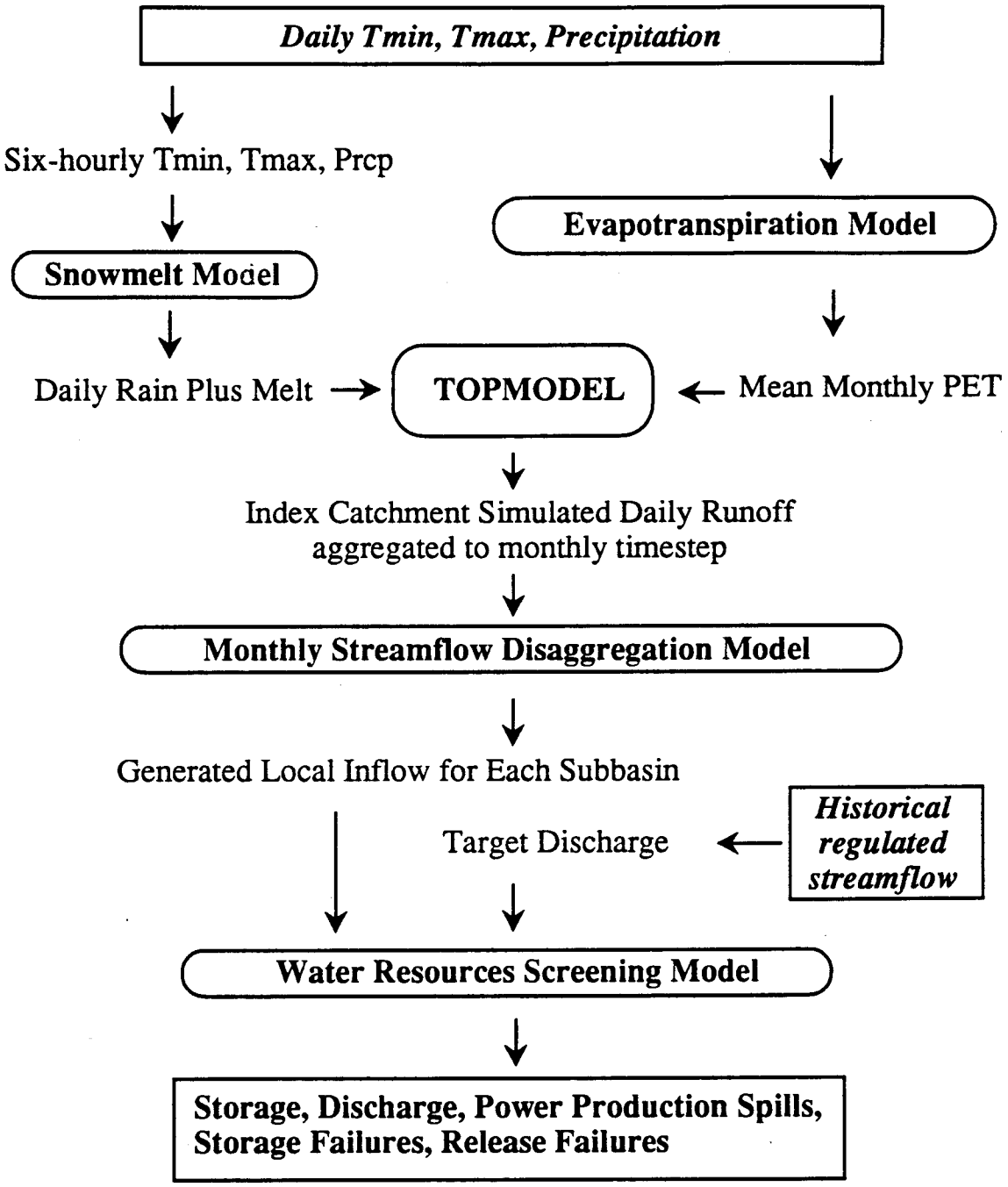

Figure 3.1 Models used in the study

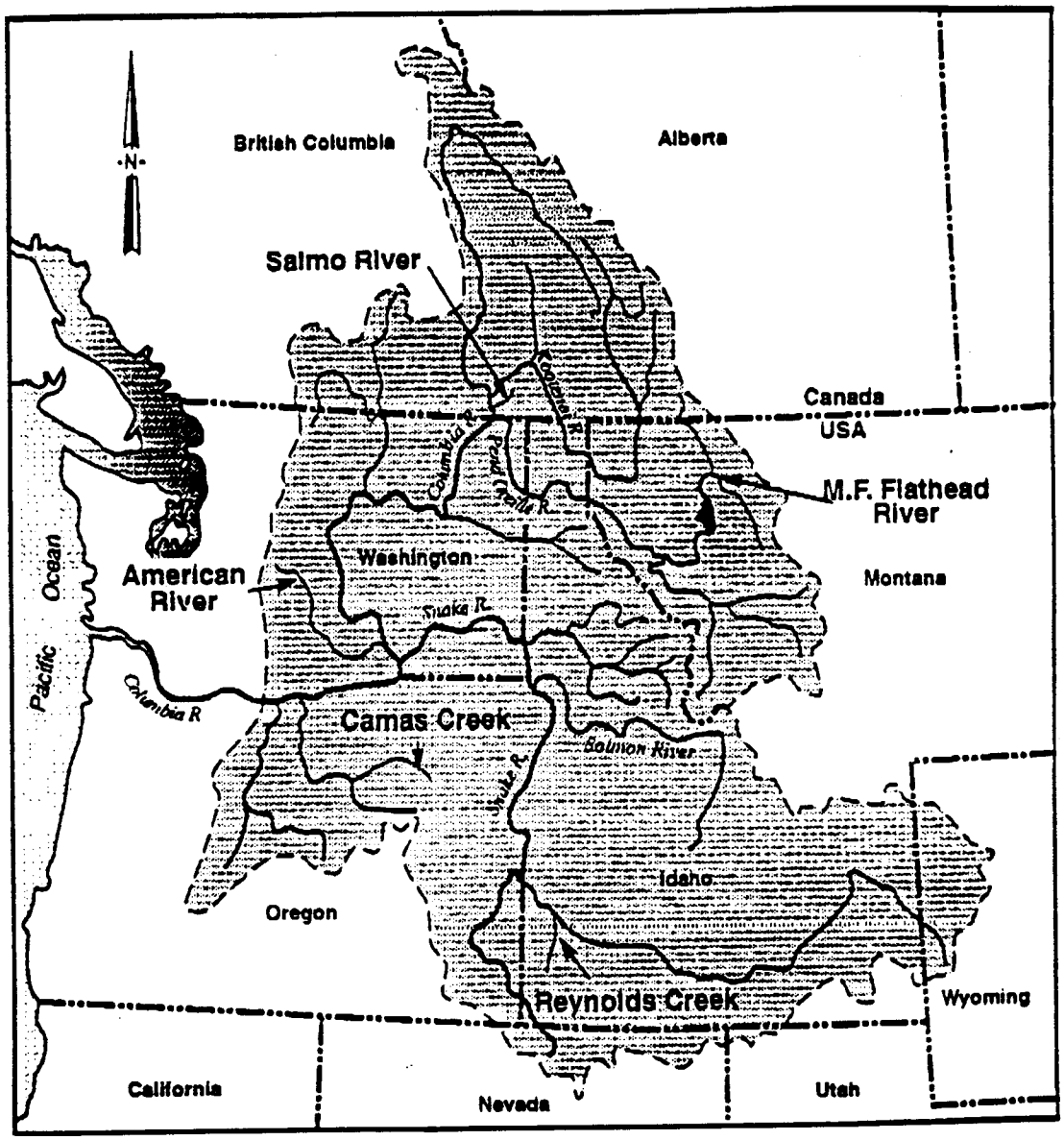

Figure 3.2 Location of index catchments

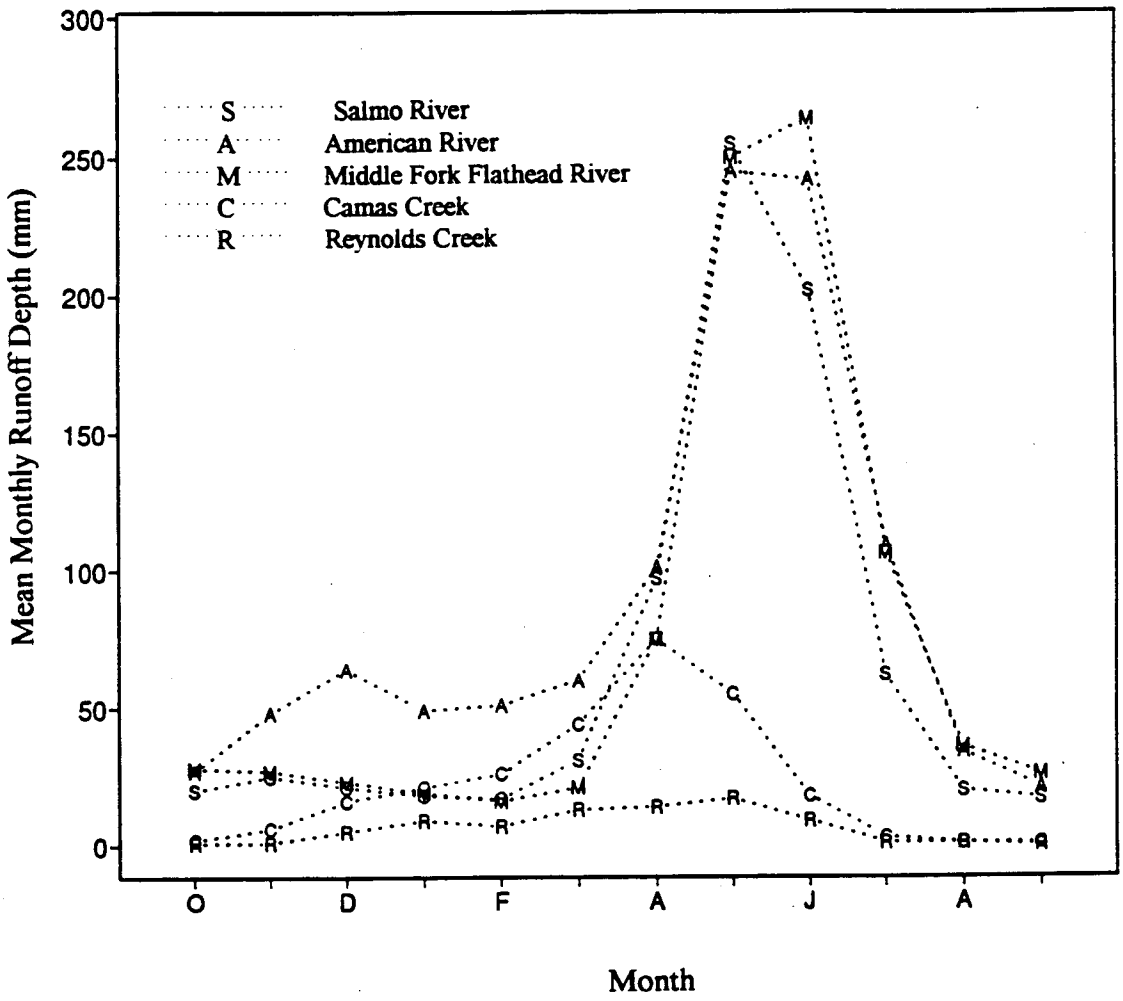

Figure 3.3 Historical mean monthly runoff for index catchments

(for periods of record see Table 3.1)

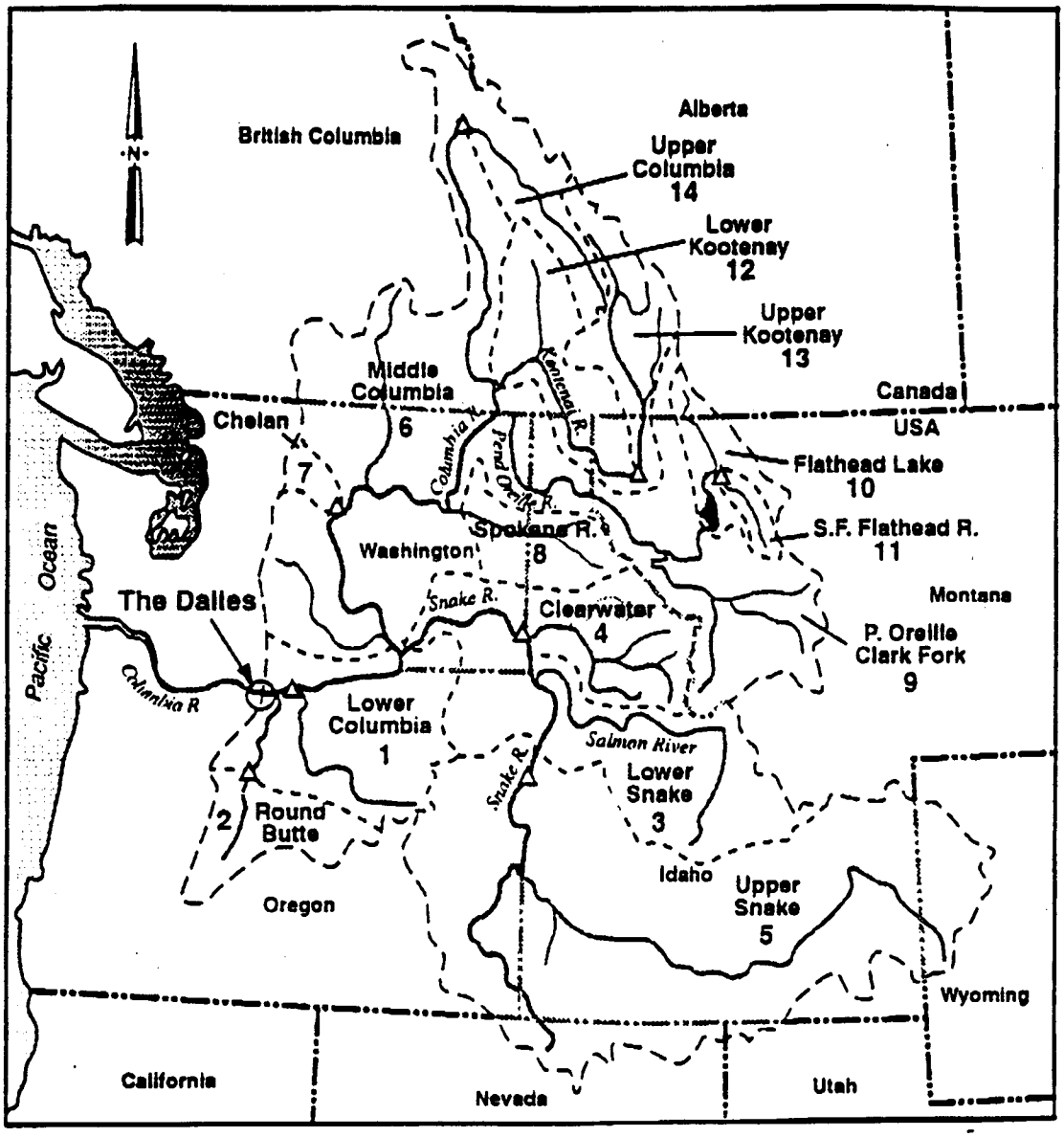

Figure 3.4 Indentification of subbasins

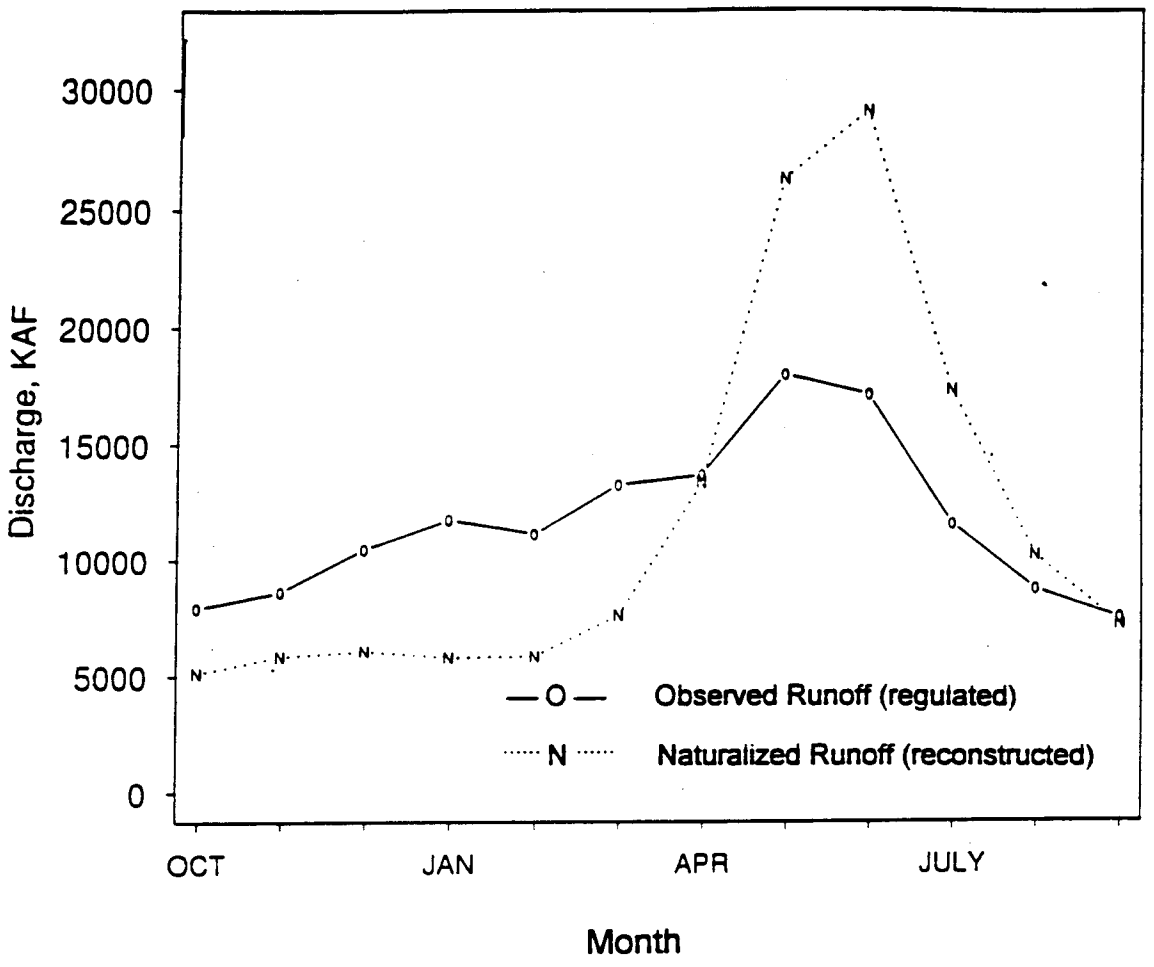

Figure 3.5 Columbia River basin mean monthly discharge: Reconstructed natural hydrograph (at John Day, 1928-1977) and observed (regulated) runoff (at The Dalles, 1974-1988)

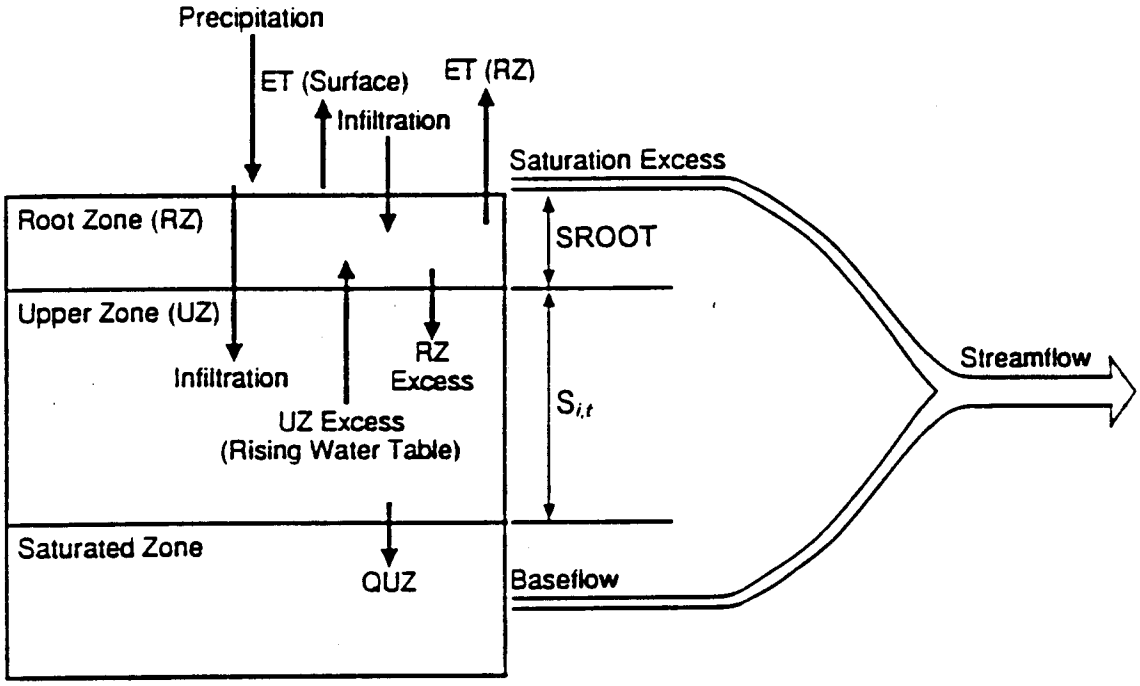

Figure 3.6 Schematic representation of TOPMODEL (after Brettmann, 1991).

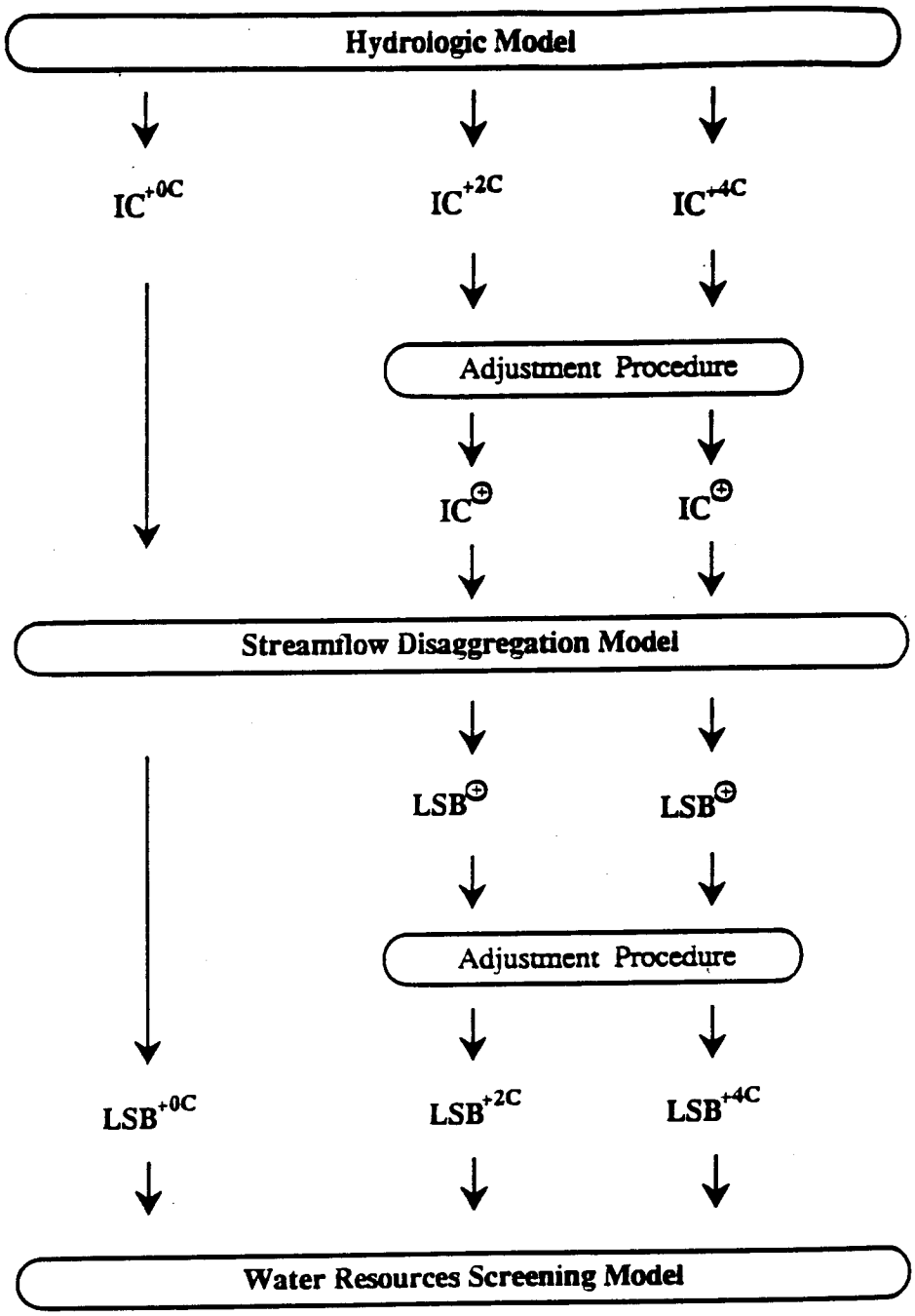

Figure 3.7 Implementation of the adjustment procedure. IC^k : index catchment simulated runoff; LSB^k : large subbasin synthetic local inflow sequence; superscript indicates a specific climate case. In the case of IC sequences, the symbol "⊕" indicates that a +2C or +4C sequence has been adjusted to have the base case climate (+0C) mean and variance. In the case of LSB sequences, "⊕" indicates that, prior to adjustment, the generated sequence has the same mean and variance as the LSB^{+0C} sequence.

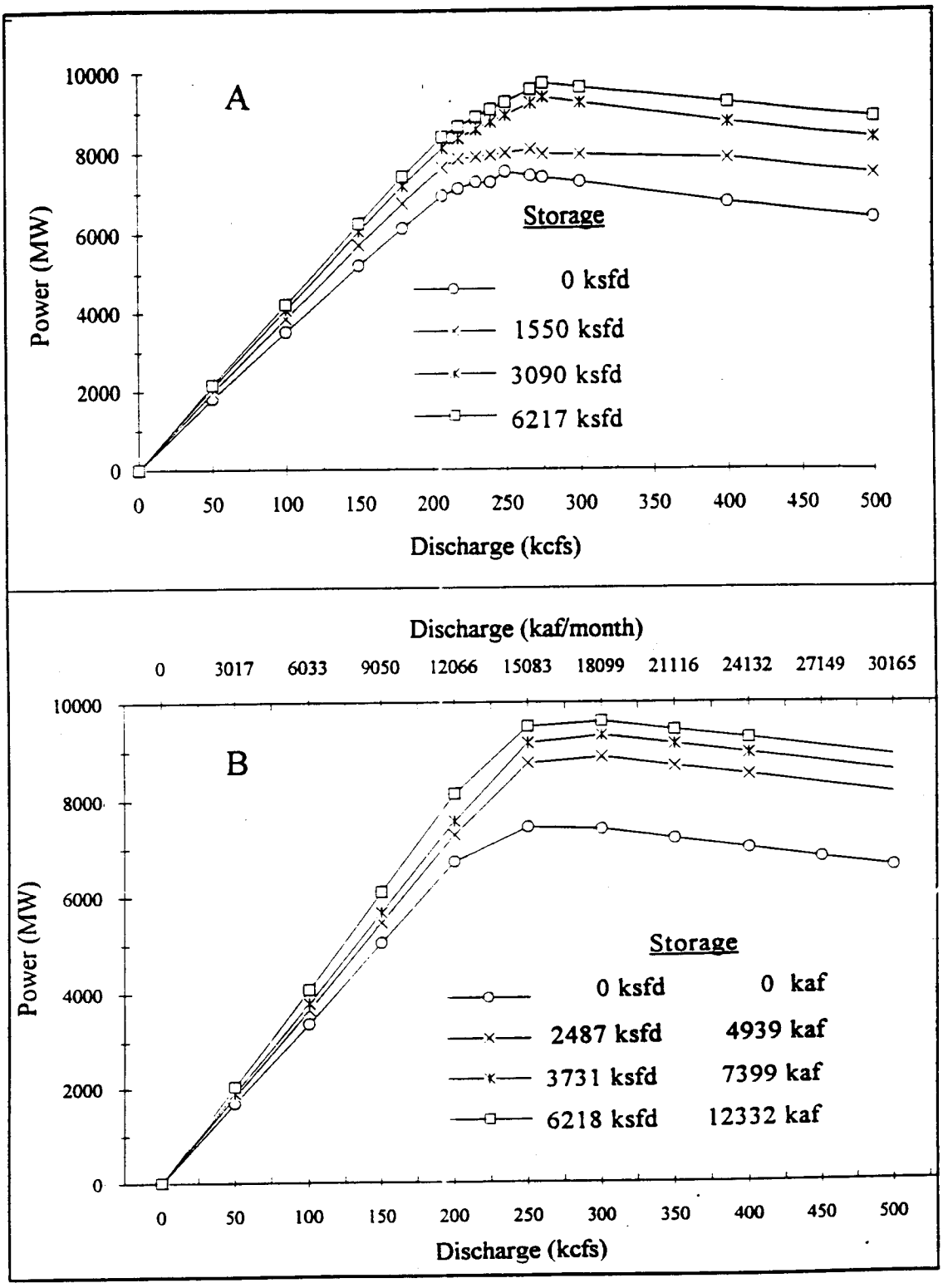

Figure 3.8 Power-storage-discharge relationships for Grand Coulee/Arrow aggregate node. (A) Linearly interpolated look-up tables, with storage in ksfd. (B) Fitted data, with storage given in kaf and ksfd (ksfd is thousand square feet days; 1 ksfd = 0.5019 kaf).

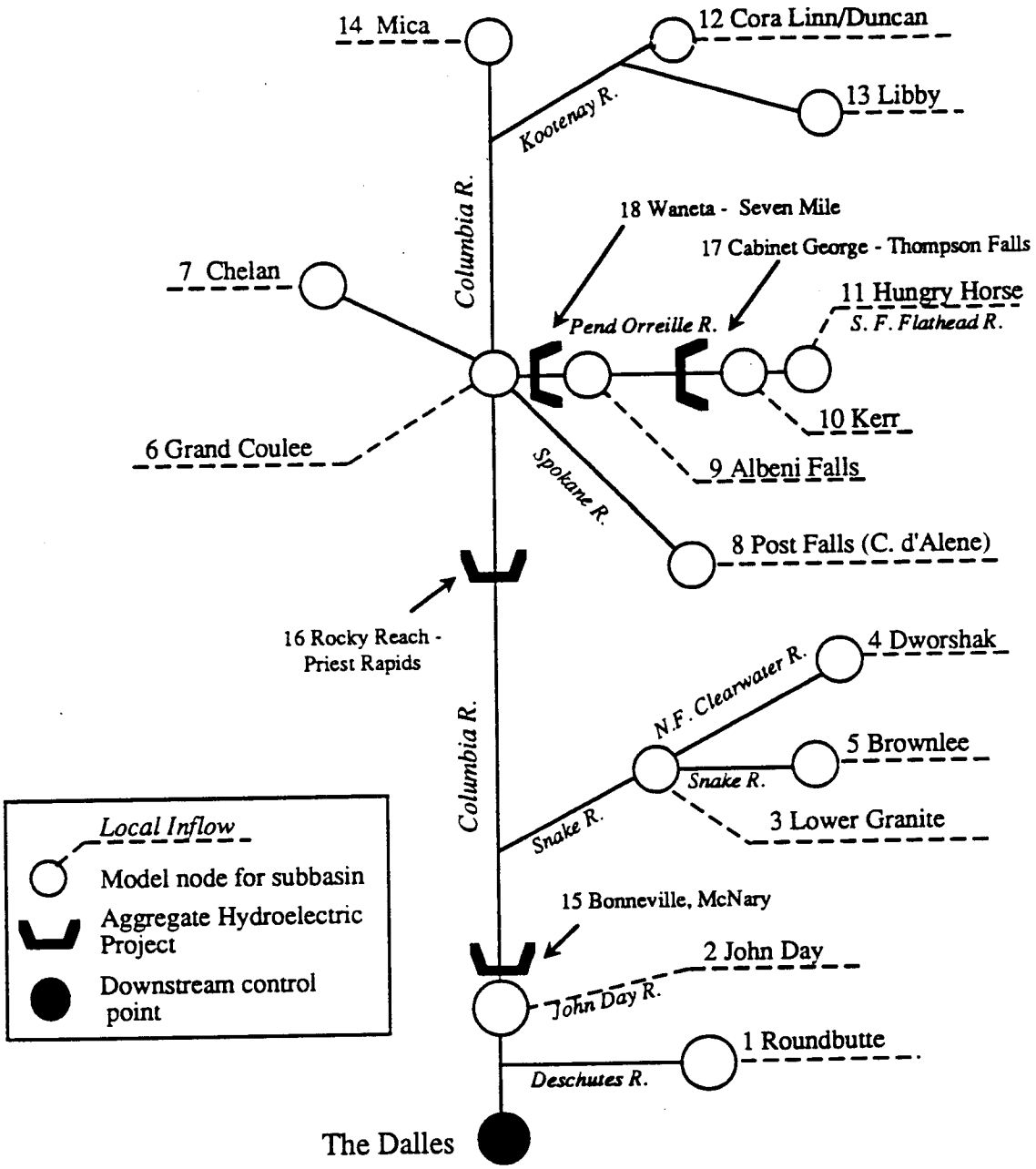

Figure 3.9 Water resources screening model routing

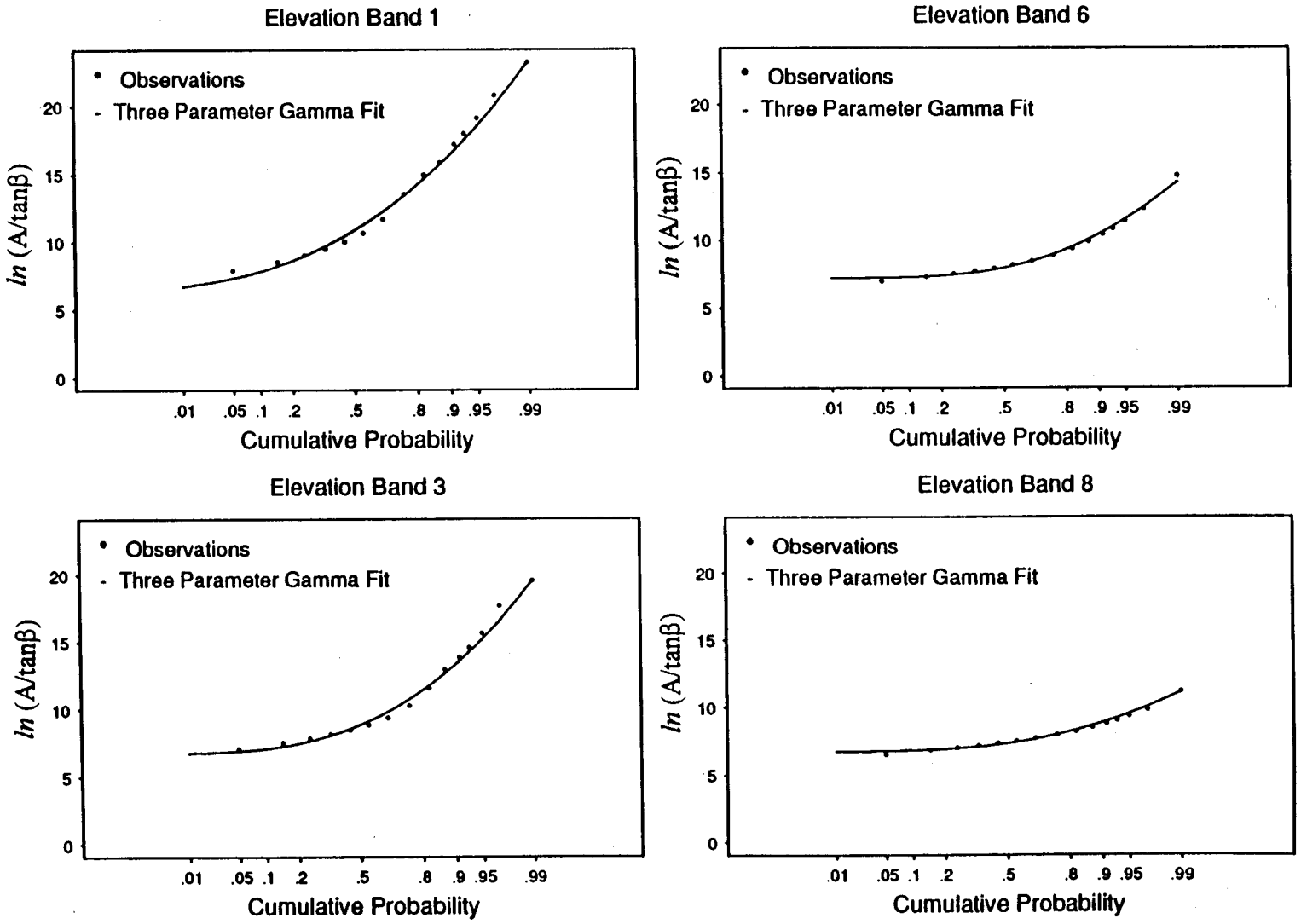

Figure 3.10 Fitted and empirical *ln* (A/tanβ) distribution for the Middle Fork Flathead River basin, bands 1, 3, 6 and 8.

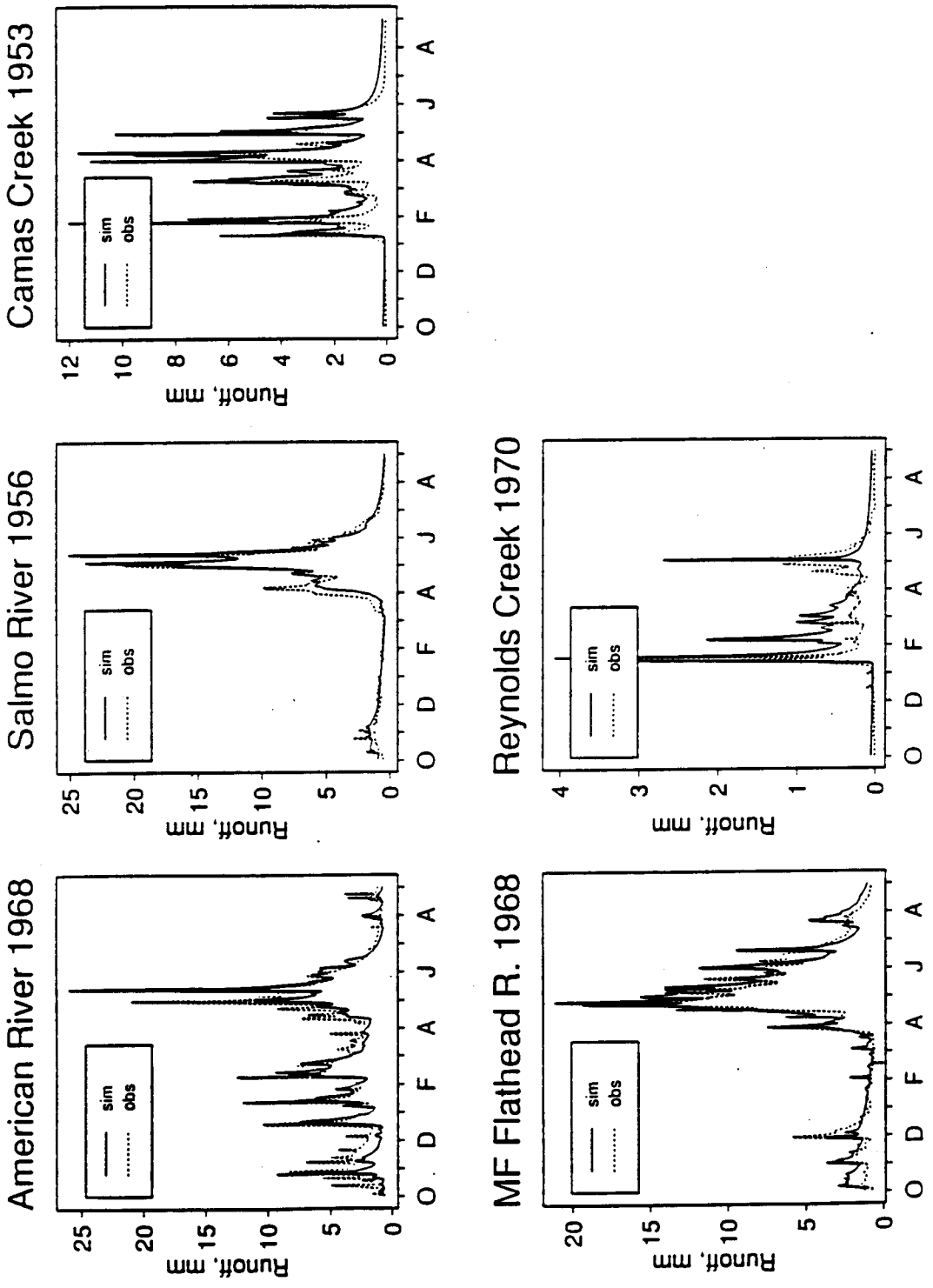

Figure 3.11 Typical daily simulations for each index catchment (one year)

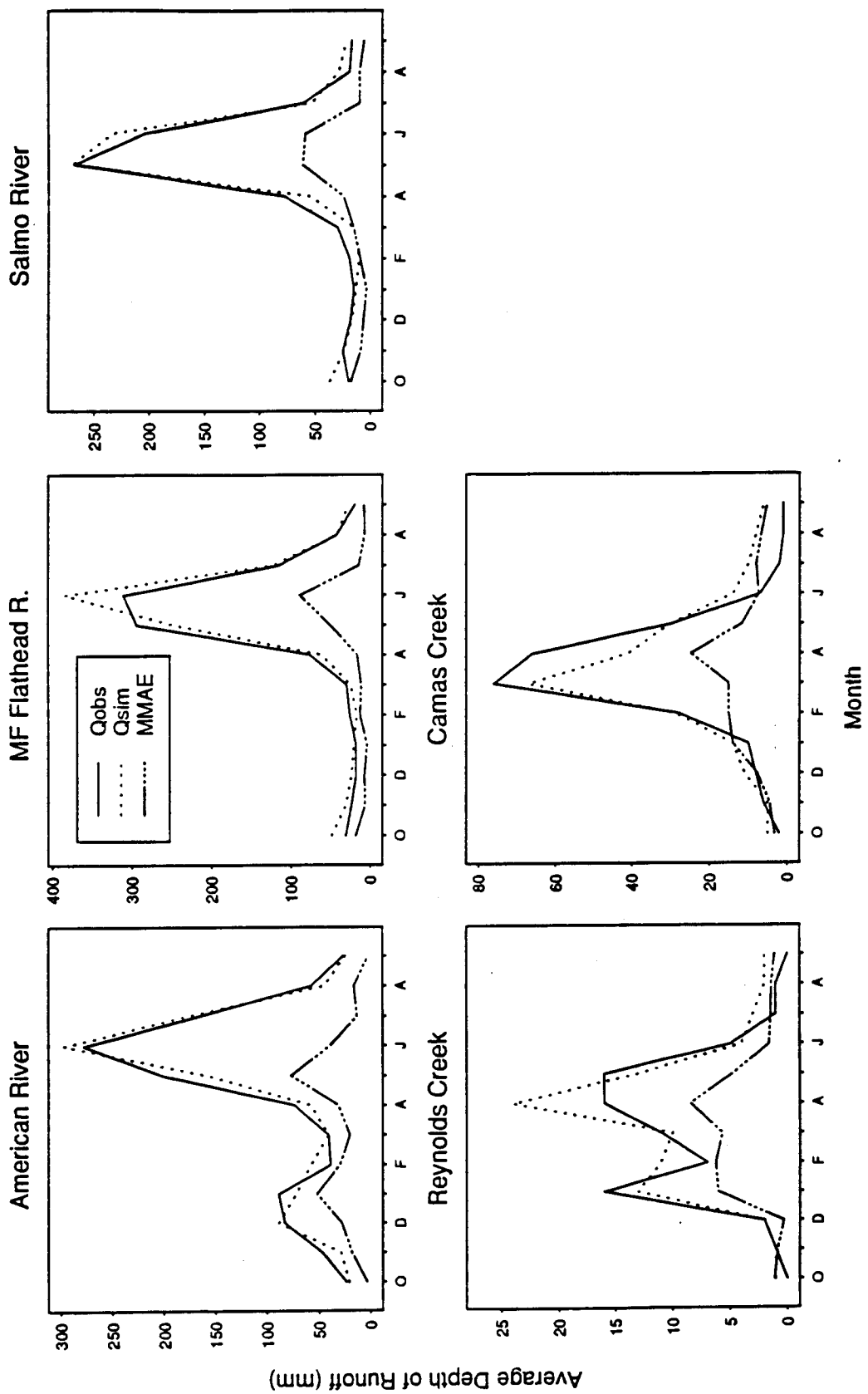

Figure 3.12 Calibration period results. Qsim: simulated streamflow, Qobs: observed streamflow; MMAE: mean monthly absolute error.

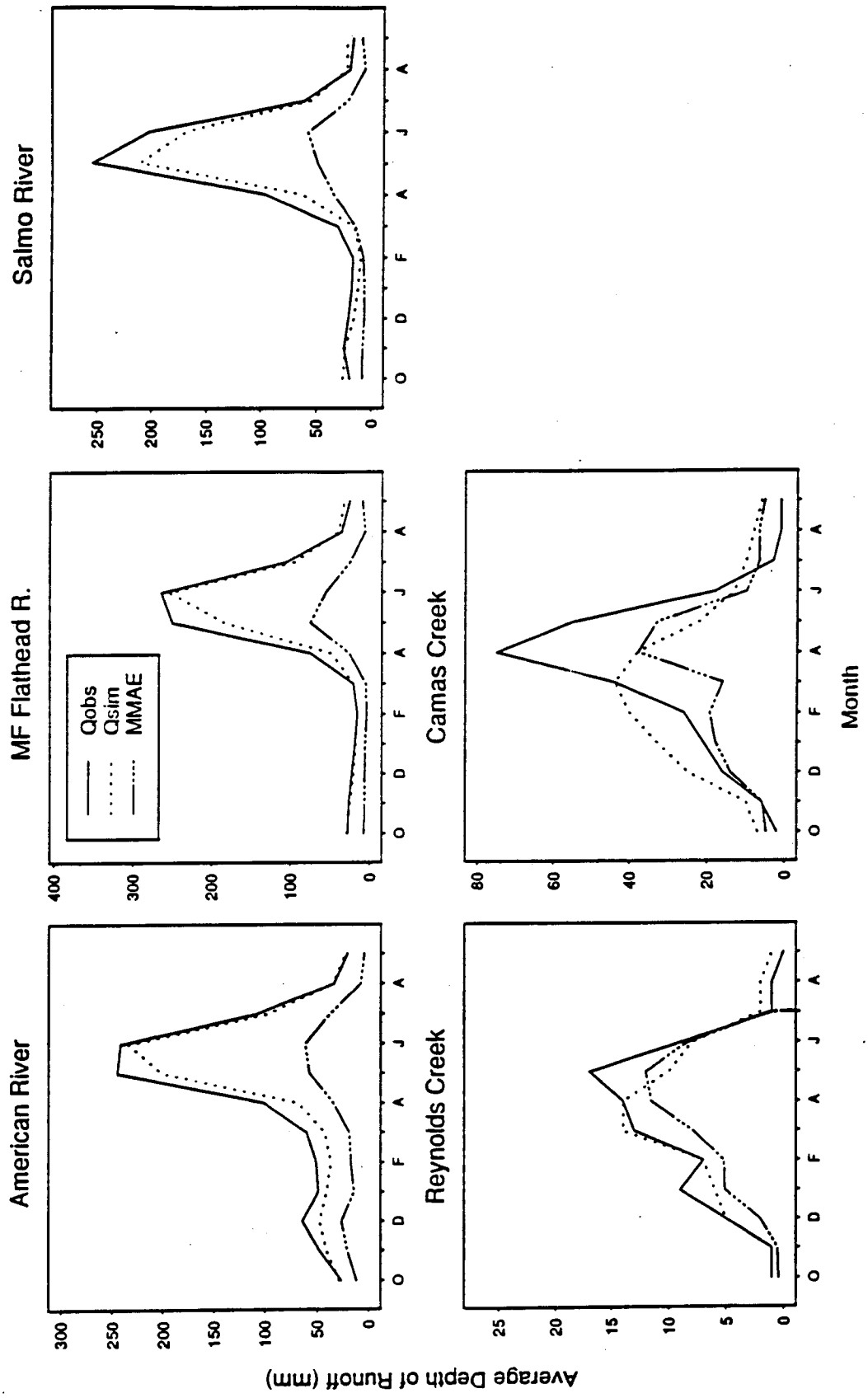

Figure 3.13 Validation period results. Qsim: simulated streamflow, Qobs: observed streamflow; MMAE: mean monthly absolute error.

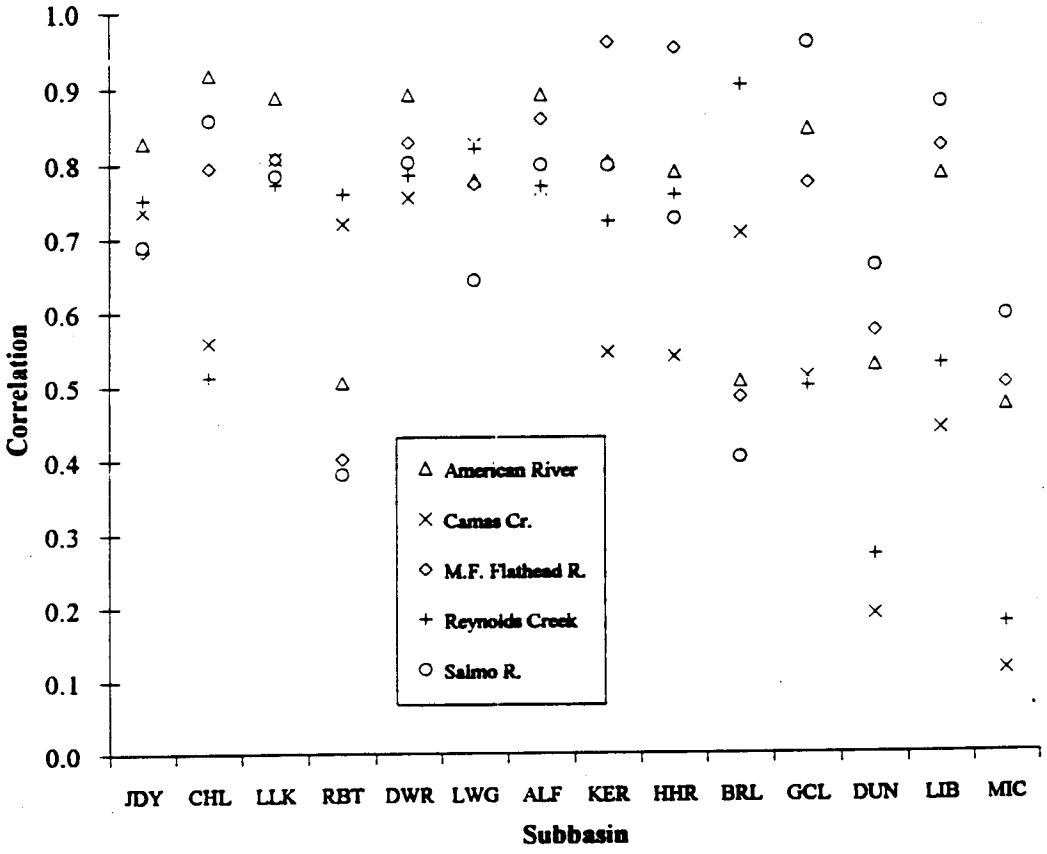

Figure 3.14 Annual cross-correlations of observed index catchment and large subbasin historical local inflows

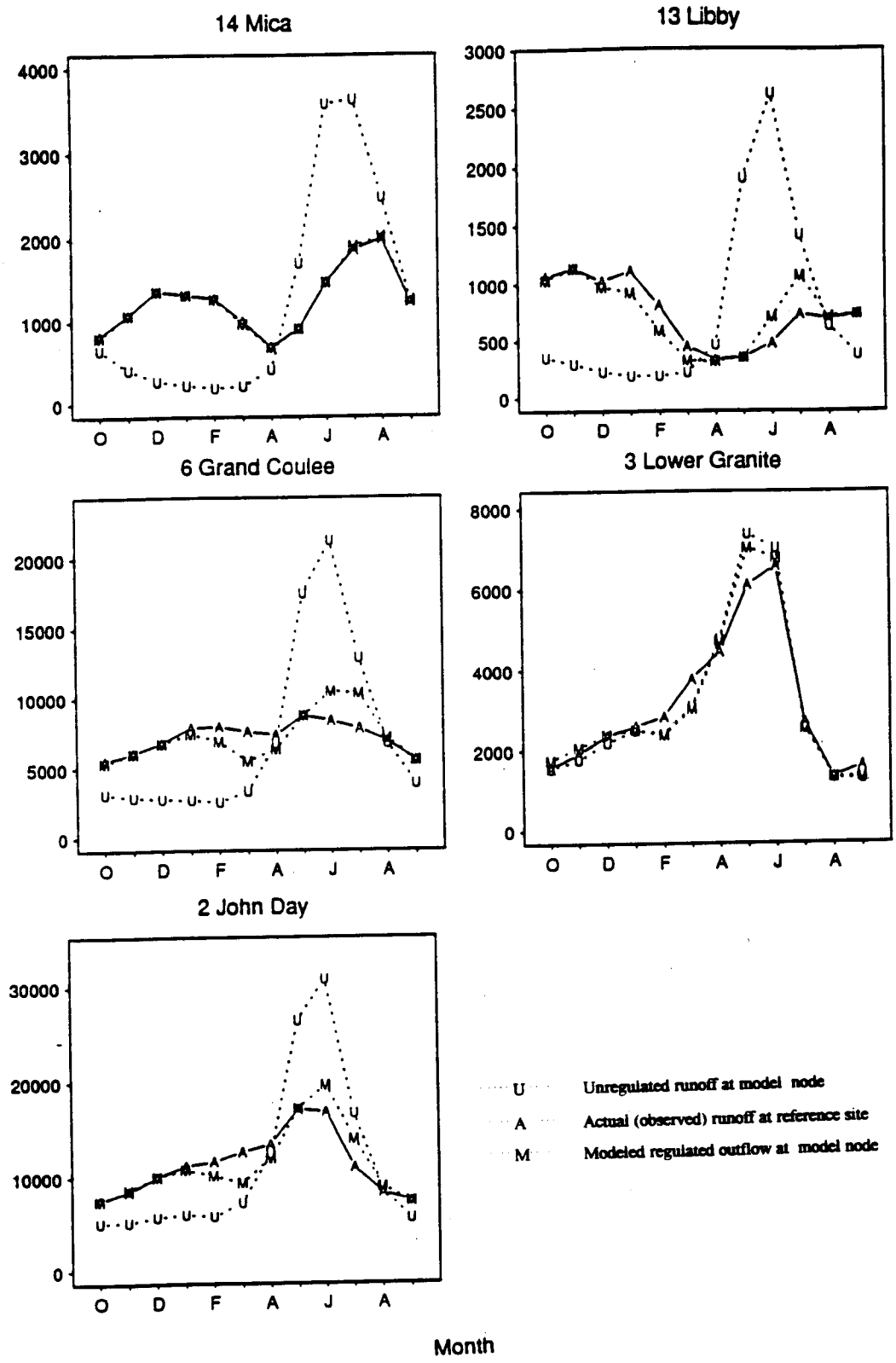

Figure 3.15 Comparison of historical and modeled discharge at major nodes

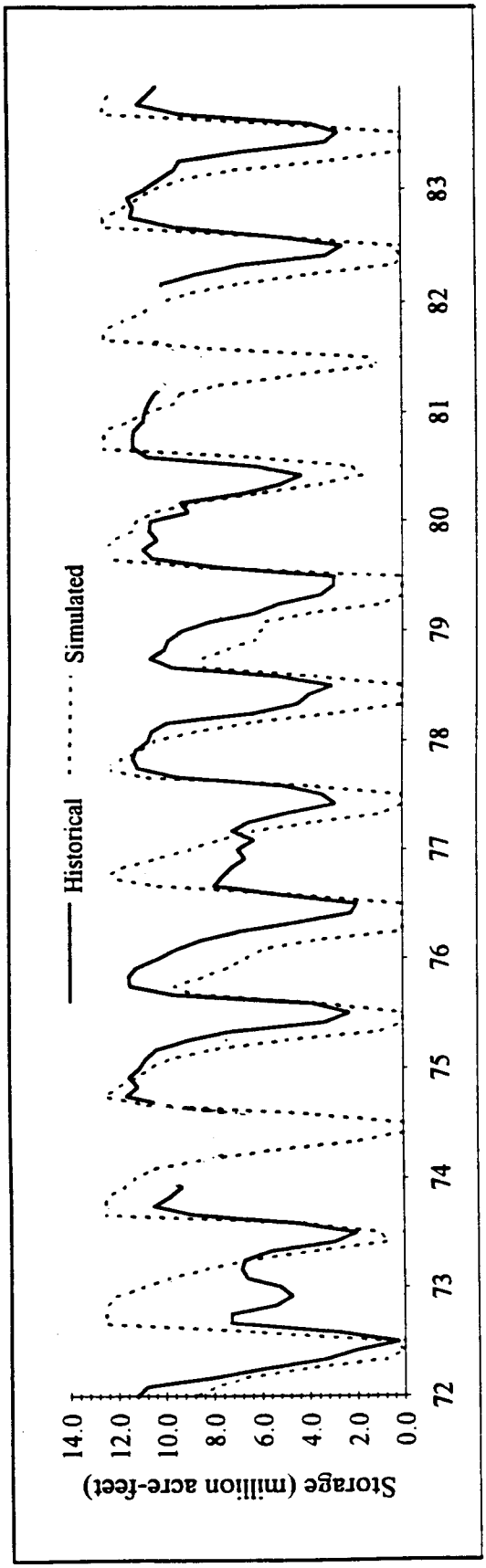

Figure 3.16 Comparison of historical and modeled Grand Coulee/Arrow aggregate reservoir monthly storage, water years 1972-1983

Chapter 4 Results and Discussion

4.0 Introduction

The results of the alternative climate simulations and the routing of generated local inflows through the water resources system model are presented. Changes in local runoff characteristics for the index catchments and the subbasins are summarized first, followed by the integrated response of the system. The remainder of this chapter emphasizes results for water supply for the Mid and Lower Columbia and for the Snake River. Water supply changes are summarized as changes in mean annual runoff, maximum mean monthly runoff, and shifts in seasonality. The effects upon reservoir storage behavior and system-wide power generation are also evaluated. Finally, normal reservoir operation is described, in the context of the use of the target discharge to simulate operation of the reservoir system for the alternative climate scenarios.

4.1 Hydrologic model results for alternative climate scenarios: Index catchment simulations

Figure 4.1 gives the mean monthly runoff for each index catchment and each alternative climate scenario (ACS), including the base case scenario. Consistent with other studies (see Chapter 2) the simulations indicate that climatic warming would result in partial or complete conversion from snowmelt-dominated to rainfall-dominated runoff for all the catchments. Overall the Middle Fork Flathead River and Salmo River are least sensitive to warming. For these two sites under the +2C scenario there is a slight change in the timing of runoff, a slight decrease in maximum monthly flow, but very little increase in winter runoff. Even with a +4C warming, the hydrographs at Middle Fork Flathead River and Salmo River are still

almost completely dominated by spring snowmelt, although the maximum monthly discharge is significantly reduced. In contrast, for the American River, the +4C scenario causes nearly complete conversion to a winter peaking, rainfall-dominated runoff pattern. The +2C scenario produces partial conversion.

The percent change in annual runoff volume for each ACS, relative to the base case, is given in Table 4.1. All three index catchments experience a decrease in mean annual flow (MAF) for both ACS's. The largest decrease is 7.3 percent in the +4C climate for the M. F. Flathead River. Changes in mean annual runoff are due to changes in actual evapotranspiration (AET), since the scenarios assume constant precipitation. Whether AET (and mean annual runoff) increases or decreases in a particular catchment depends on whether the warming scenario is sufficient to cause a large enough shift in timing of peak runoff such that peak runoff (and soil moisture) coincides with a period of low PET. The timing of snowmelt-associated runoff for the Middle Fork Flathead River and Salmo River is less sensitive to both increments of temperature increase than is the American River, so that even under the +4C scenario the timing of snowmelt coincides with periods of increased PET demand. With respect to mean annual runoff, they are more sensitive to changes in temperature and precipitation than is the American River, again because of smaller shift in timing of runoff.

4.2 Modification of adjustment procedure

The predicted effect of the ACS's on the local inflows in each subbasin will be discussed before considering the water resources screening model results. It was found that the two adjustment procedures described in Section 3.3 and Appendix A resulted in hydrographs for the ACS's at several sites that were unrealistic, and particularly for those in semi-arid regions. For example the total annual runoff in the +4C ACS for the Snake River basin (measured at Lower Granite) was predicted to increase by 53 percent over the base case result, and the total runoff at John Day by 21 percent. The additional assumption was adopted that the change in the mean

annual flow for the LSB's will be equal to that at the index catchment. For each subbasin a single factor was found to make this additional adjustment to the natural adjusted time series. The monthly and annual coefficients of variation are not affected, but both the mean monthly runoff and the monthly standard deviation are increased or decreased by this factor.

4.3 Sensitivity of local inflow to warming

As noted in Section 3.2, synthetic local inflows were generated for each of two adjustment procedures; also, two sets of flows were generated for the first adjustment procedure in order to evaluate sensitivity to the random number generator seed. The mean monthly results for the local inflows are not sensitive to the adjustment procedure (Section 3.4), nor to the seed. The results presented in Figures 4.6 through 4.8 (local inflows, model regulated outflow) pertain to both procedures. Because the variance, but not the mean, of the generated flows is dependent upon the adjustment procedure (see Appendix A), it was anticipated that the two adjustment procedures would lead to differences in storage behavior. However, there was almost no difference in the water resources screening model results obtained for the two procedures.

4.3.1 Comparison of local inflow hydrographs for each climate scenario.

The mean monthly local inflow hydrograph for each subbasin is presented in Figure 4.2. Table 4.2 gives several results for each subbasin that summarizes the sensitivity of local inflow to the +2C and +4C climates, relative to the base case result. The measures of sensitivity include the percent change in the largest of the twelve mean monthly inflows (e.g. the change in the John Day subbasin maximum runoff for the +2C case compares the +0C mean June runoff and the +2C mean February runoff), the shift in timing of the maximum monthly flow, and the fraction of total runoff that appears in the first six months of the water year. This segmentation of the water year was chosen because, in the base case climate, there is

relatively little runoff until April at most sites. Table 4.2 also gives the change in the mean annual local inflow for each subbasin (which is necessarily equal to the change at the corresponding index catchment, due to application of the adjustment procedure).

The sites listed in Table 4.2 are placed into five groups according to similarity in the pattern of sensitivity and hydrograph appearance (Figure 4.2). The order of the sites loosely follows the degree of climate sensitivity, with the Group 5 sites being least sensitive to warming. Group 1 includes John Day, Roundbutte, and Brownlee. These three are the most sensitive of all the subbasins, and all three are located in the semi-arid sub-region. These subbasins historically are less than completely snowmelt-dominated, and have substantial runoff throughout winter, which through the multiplicative adjustment procedure, become highly amplified in the +2C and +4C scenarios. The Group 2 sites (Long Lake, Albeni Falls, Lower Granite, and Dworshak) are all similar in that the snowmelt peak remains prominent in the +2C scenario (little or no decrease in peak magnitude), if not also in the +4C scenario. These sites also have a shift in timing to one month earlier.

The Group 3 and 4 sites are quite sensitive to warming. These sites retain a snowmelt peak, but one which is substantially diminished in magnitude. Within Group 3 the timing of peak flow moves forward by two to three months in the +4C scenario, and these subbasins develop more winter runoff than do Group 4 subbasins in response to warming.

Group 4 subbasins (Mica, Duncan) have late snowmelt in the base case climate, and the maximum monthly runoff actually shifts forward in time under the adjustment procedure. This is an artifact of the adjustment procedure, and stems from the fact that the timing of the maximum monthly flow for these three subbasins is later than at the index catchment (Salmo River). The Group 4 sites have decreased peak flow. The Group 5 subbasins - Hungry Horse and Kerr - have the coldest climate and show little change in the runoff in autumn and winter.

4.3.2 Comparison of results with and without the mean annual runoff correction

The additional correction for mean annual flow (see Section 4.2) has the greatest impact on the local inflows for the Group 1 and 2 subbasins (as identified in Table 4.2), all of which have significant winter runoff historically, (winter/annual runoff ratio of 0.29 or greater) whereas the index catchments at most have a ratio of 0.27 in the base case simulation. The MAF correction factor is fairly close to 1.0 for other sites. Without the mean annual flow correction, the sensitivity in mean annual runoff ranged from +20% to +78% (+4C scenario), and the change in the maximum monthly flow was as high as 300 percent. With the mean annual flow correction, the maximum monthly flows for these subbasins increased by not more than 98 percent (Roundbutte).

4.4 Water resources model results

The results from routing these local inflows through the channel network will now be described. At each time step, the model uses any available reservoir storage to attempt to make the target discharge release at each node. In many cases it will be seen that the model is able to meet the target discharge under all three climate scenarios, even when the inflow hydrograph is highly sensitive to the climate scenario, but that mean monthly storage at all of the major reservoirs is profoundly affected. The results will be interpreted within the context of network structure, emphasizing the major measurement points within the basin: Upper, Middle and Lower Columbia (Mica, Grand Coulee/Arrow, John Day nodes), Snake River (Lower Granite) and Pend Oreille/Clark Fork (Albeni Falls). All of these are validation nodes, as indicated in Section 3.7.3. Sensitivity of storage behavior will be addressed first, since the model's ability to meet the target discharge is dependent on available storage capacity.

4.4.1 Reservoir behavior and seasonal pool levels

In Figures 4.3 through 4.5, the modeled storage behavior of the three largest reservoirs - Grand Coulee/Arrow (12.5 maf capacity) and Mica (12.0 maf capacity) - are presented. In most cases seasonal fluctuations in the storage are dampened for the warmer climates, i.e. the average high pool (maximum average monthly storage volume) decreases with warming, and the average low pool (minimum average monthly storage volume) increases. At Grand Coulee, for example, the volume difference between the average high pool and average low pool is 12.5 maf in the base case climate (storage bound condition), but decreases to about 4 maf in the +4C scenario. The corresponding +0C and +4C ranges for Mica are 3.5 maf and 2.5 maf, respectively. The result that the storage profiles flatten out has indirect implications for power generation in warmer climates, and for flood control operation. This will be discussed further in Section 4.5.

The explanation for decreasing amplitude in the average seasonal storage cycle is related to the correspondence between the inflow hydrograph and the target discharge. It is generally the case that the inflow hydrograph looks increasingly similar to the target discharge as the climate warms, and therefore, the target discharge is matched through smaller changes in reservoir storage. To illustrate this point, the inflow, outflow, and target discharge hydrographs are shown for Grand Coulee and Mica in Figure 4.6. The inflow hydrograph at Mica is simply the local inflow, which is moderately sensitive to warming. The inflow hydrograph at Grand Coulee is the sum of all the regulated outflows from six upstream nodes, and the local inflow, which is moderately sensitive to warming. At both nodes, the inflow and target hydrographs become more similar as the climate warms; consequently smaller changes in storage are required to meet the target discharge.

The effects of warming on the frequency of spills, storage failures, and release failures (all defined in Section 3.4.2) follow from the effect on storage volume For example, if the average low pool is higher under an alternative climate scenario, then

it follows that the frequency and severity of storage failures should also decrease in the ACS. At least for the late winter drawdown and spring refill period, all three types of failures (spills, storage failures, release failures) tend to decrease in frequency and severity under the alternative climate scenarios, and the month of maximum failure tends to shift to earlier in the year. At Grand Coulee, the timing of both maximum monthly storage and maximum spills shifts from August (base case) to May (+4C scenario). The results for each reservoir vary slightly from this general pattern. At Libby Reservoir (Figure 4.6), the timing of the average high pool and maximum spills is not affected by warming, but the frequency and average severity of all three types of failures decreases with warming. Only at Grand Coulee does the number of storage failures increase during the summer, as a result of non-refill in the spring. This could be regarded as an artifact of the model, since presumably the system would continue to be operated with a high priority on complete refill of reservoirs at the end of the snowmelt season (see Section 4.6.1)

These results contrast with other studies of heavily snowmelt-affected water resources systems, such as Lettenmaier *et al.* (1993); Lettenmaier and Sheer (1991); Dracup and Kendall (1990). In these studies warming led to a decrease in reliable yield during the summer. A key difference between this study and other studies is that the others modeled systems in which, historically, the summer water supply demand approaches capacity. This is the situation for the Middle and Upper Snake River and the Yakima River (also a tributary of the Columbia) (Scott *et al.*, 1993). Apart from these subregions, the releases required for irrigation diversions and instream flow needs within the Columbia River basin above The Dalles, relative to the mean flow during the low flow season are smaller than those of most other western U.S. rivers (Scott *et al.*, 1993). (That this is the case could be inferred from Figures 4.3 - 4.5, insofar as the target discharge at major storage reservoirs represents releases sufficient to meet average water supply demand).

4.4.2 Power generation in each climate scenario

Figure 4.7 shows the mean monthly power production for all hydroelectric projects, as aggregated to 5 nodes. The data shown in Figure 4.7 for Grand Coulee/Arrow for example, include Lake Chelan, Spokane River, Grand Coulee Dam, and six downstream run-of-the-river projects (node 16 in Figure 3.9 and Table 3.2). Average annual power generation for the whole system is 193,650 MW in the base case scenario. System average power generation decreases slightly with warming, relative to base case: 2.4% in the +2C scenario, and 4.6% in the +4C scenario (Table 4.3). The mean monthly total power production for the system (Figure 4.7, lower right panel) closely resembles the hydrograph at John Day. Power production decreases somewhat in the spring, and increases in the winter, a pattern which would be likely to increase hydropower revenues, since demand and per unit cost historically has been highest in the winter.

Most of the projects are operating throughout the simulation period in the linear part of the power-storage-discharge curves, and in most look-up tables power is not a strong function of storage. Therefore power production changes with climate scenario in a way that closely resembles the changes in the outflow hydrographs (e.g. compare Figures 4.7 and 4.8), in all but the months of peak flow (at some of the individual nodes, mean runoff in the spring exceeds the effective discharge capacity). Thus the system wide power production, as modeled, peaks earlier in the year under the warmer climate scenarios, and the mean maximum monthly power decreases somewhat.

4.4.3 Sensitivity of total discharge and power generation from a system-wide perspective

Figure 4.8 shows the regulated discharge at each of the 14 nodes (aggregate run-of-the-river nodes 16 through 18 are not shown). The sensitivity of routed flows are evaluated with respect to target discharge at validation nodes. For this reason the base climate target discharges are given in Figure 4.8 as solid lines for reference

(the target discharge differs little for each scenario). Three validation nodes are those with significant storage (Mica, Libby, Grand Coulee/Arrow). At Mica and Libby the model meets the target discharge under all climate scenarios. At Grand Coulee the model is least able to meet the target discharge in the base case scenario. These results will be discussed in more detail below. Table 4.4 summarizes the effect of warming on routed flows, specifically, on change in mean annual flow, maximum mean monthly flow, and change in the winter/annual runoff ratio.

Figure 4.9 integrates the information in Figures 4.2 (local inflows) and 4.8 (regulated discharge) in a way that emphasizes the network structure, by showing qualitatively for each node the relative importance and climate sensitivity of each local inflow with respect to total regulated discharge. Each arrow converging upon a single node represents either a local inflow or a regulated outflow from an upstream node. Grand Coulee/Arrow, for example, has six upstream nodes and one local inflow (Mica, Libby, Duncan, Albeni Falls, Long Lake, Chelan, and Middle Columbia subbasin local inflow). The outflows of Upper Columbia are lumped together in the figure; therefore there are five arrows converging upon the triangle representing the combined Grand Coulee and Arrow Reservoirs. The two largest inflows are the highly sensitive (Middle Columbia subbasin) local inflow, and the outflow from Mica, Libby, and Duncan Reservoirs, which show little sensitivity to warming. The single arrow departing from the Grand Coulee/Arrow Reservoir represents the total discharge from that node, and is indicated as being slightly sensitive to warming. The thickness of the arrow departing from the Grand Coulee/Arrow node indicates that the mainstem Columbia inflow to John Day is much greater than the Snake River contribution. The figure is descriptive of both warming scenarios, and to serve as an aid for conceptualizing the climate sensitivity of the water resources system as a whole.

Upper Columbia

The inflows to Mica, Libby, and Duncan could all be described as moderately sensitive to the +4C scenario. The storage ratios (at-site storage capacity/mean annual runoff) for these three nodes are all in excess of 0.55. Consequently the model has no difficulty meeting the base case climate target discharge under any of the climate scenarios. This is shown in Figure 4.9 by characterization of the project inflows as moderately sensitive ('++") and the outflows as insensitive ('-'). The discharge hydrographs for Libby and the two Canadian projects are preserved, even with a +4C warming, consequently, hydropower generation is the same under the +2C and +4C scenarios as under the base case scenario. On an average monthly basis, storage behavior changes considerably for all three of the Upper Columbia reservoirs, as discussed in Section 4.4.1.

Pend Oreille/Clark Fork

The inflows to Albeni Falls (the downstream node on the Pend Oreille River) consist of the Albeni local inflow, which is slightly sensitive to warming, for both climate scenarios, and the regulated outflow from Kerr, which is insensitive to warming. The hydrograph at Albeni Falls (Figure 4.8) is slightly sensitive to warming. The peak discharge for the regulated outflow shifts and there is some increase of runoff throughout the winter, but particularly late winter and early spring. The magnitude of the maximum outflow hydrograph changes little under the +2C scenario, and decreases by about 20% in the +4C scenario. The timing of peak runoff shifts by one (two) months for the +2C (+4C) scenario. The slight sensitivity of the outflow hydrograph for the Pend Oreille has little effect on the downstream node, Grand Coulee/Arrow, since this inflow to Grand Coulee/Arrow comprises only 20 percent of the total inflow to that node.

Middle Columbia (at Grand Coulee)

The regulation at Grand Coulee is such that the target discharge is better preserved in the +2C and +4C climates scenarios than in the base case climate (Figure 4.8). The model is most successful in meeting the target discharge in the

warmest climate scenario (+4C). The ability of the model to meet the target discharge most successfully in the +4C case climate case is due to the increasing similarity of the inflow hydrographs and target discharge as the climate warms (as discussed in Section 4.5.1). The storage behavior for the Grand Coulee/Arrow aggregate reservoir shows some sensitivity to warming (Figure 4.3). There is a phase shift in the refill and drawdown curves to earlier in the year, dampening of the seasonal storage fluctuation, and decreased numbers of failures of all three types. Power generation, which averages 6,125 MW annually, decreases by 3.2% and 4.7% for the +2C and +4C scenarios, respectively.

Snake River (at Lower Granite)

Lower Granite is a validation node (with reference discharge formed from the record at Ice Harbor). Due to sensitive local inflows and limited storage capacity, the Snake River basin runoff (outflow at Lower Granite) is somewhat sensitive to warming, by comparison to the reference discharge. The hydrograph at Lower Granite has a strong snowmelt signal in all three scenarios, with a maximum mean monthly discharge that is unaffected by warming (Figure 4.8). There is however, a shift in timing of the peak runoff, from June in the base case climate, to April in the +4C climate. Storage at Dworshak and Brownlee is ineffective, insofar as the routed outflow hydrograph at Lower Granite closely resembles the sum of the local inflow to the three nodes (compare Figures 4.2 and 4.8).

The Snake River basin, which accounts for 25 percent of the runoff at John Day, has an important influence on the hydrograph at John Day. In Figure 4.9, the regulated outflow for the Snake River basin is indicated as slightly sensitive to warming. The general effect of warming would tend to reduce the late spring flood risk on the Lower Columbia (see Section 4.5), but the Snake River hydrograph tends to reinforce the snowmelt signal at John Day. Flood risk at John Day is closely linked to the hydrographs at Grand Coulee and Lower Granite, since there is little storage capacity downstream of the Snake River - Columbia River confluence. Shift

of runoff to earlier in the year could interfere with irrigation diversion and pumping in the Middle and Upper Snake basin.

With respect to hydropower, the four run-of-the-river projects in the Lower Granite aggregate node (Lower Granite through Ice Harbor) and Brownlee account for most of the Snake River generation (2300 average MW in the base case climate), and for 12.4 percent of total system generation. Winter hydropower production is sharply increased in the +4C climate (Figure 4.6), and total annual production decreases by 2.3% and 6.9%, respectively, for the +2C and +4C scenarios.

Lower Columbia (John Day)

Overall the hydrograph at John Day is moderately well preserved (Figure 4.8). The sensitivity of John Day to +4C warming is attributed mostly to the Snake River, and to a lesser extent to the local inflows to John Day and Roundbutte, which are highly sensitive to warming, but not at all to the Middle and Upper Columbia, since the outflow at Grand Coulee/Arrow is regulated to the historic level in the +4C climate scenario. Winter hydropower generation in the Lower Columbia is sharply increased, particularly in January through April. Average annual hydropower decreases only slightly from 4184 MW in the base case scenario, to 4013 MW in the +4C scenario, a 3.7 percent reduction.

4.5 Summary

Figure 4.10 presents the modeled mean monthly hydrographs for the three mainstem nodes: Mica, Grand Coulee, and The Dalles; as well as the hydrographs for the downstream node of the three major tributaries of the Columbia River: the Kootenay, Pend Oreille, and Snake Rivers. All are shown on the same ordinate scale, to emphasize relative magnitudes. Comparison of Figures 4.10 and 4.7 shows that the changes in the mean seasonal distribution of power generation follow the changes in the mean monthly hydrograph.

The largest reduction in annual runoff was 7.0 percent in the +4C scenario (Hungry Horse), and 4.0 percent in the +2C scenario (Brownlee, Albeni Falls, Kerr, and Hungry Horse). Total runoff at The Dalles decreases by 2.3 percent and 4.3 percent in the +2C and +4C scenarios, respectively.

The Snake River and Lower Columbia hydrographs (Lower Granite and The Dalles, respectively) peak two months earlier in the +4C scenario than in the base case climate (Figure 4.10). At other major nodes the peak shifts only one month earlier in the +4C scenario. Maximum peak runoff decreases substantially for three of the five nodes - 24 percent for the Pend Oreille/Flathead (at Albeni Falls), 18 percent at Grand Coulee, and 16 percent at The Dalles -, but is not much affected at Lower Granite (Snake River Basin) and Mica (Upper Columbia). The hydrographs for Canadian nodes (Mica and Duncan) do not change in the warmer climate, and probably also in a warmer and wetter climate, due to changes in storage. The same is true for the Upper Kootenay River (at Libby), the South Fork Flathead River (at Hungry Horse), and Grand Coulee/Arrow.

As modeled, the Snake River basin showed only a weak response to warming, detected mostly as a shift in timing of spring melt, but with little change in the mean maximum runoff and the abruptness of the snowmelt peak. As modeled (i.e. no storage upstream of Brownlee accounted for explicitly), the Snake River basin likely will be sensitive to any change in the seasonality and volume of precipitation, because of the limited storage on that tributary.

The results for Grand Coulee are ambiguous, since the Grand Coulee +0C hydrograph is (apparently) anomalous, as discussed in Section 3.7.3. Assuming that the Grand Coulee target discharge accurately represents the historical runoff (which may not be true), the +4C hydrograph shows no climate sensitivity (i.e. conforms to the target discharge), and the +2C hydrograph shows only a slight sensitivity.

At The Dalles, it is appropriate to focus on the target hydrograph (solid line) as the reference for classifying the response to the +4C climate; the +0C hydrograph

has a somewhat higher maximum monthly runoff than was observed historically in the regulated hydrograph (Figure 4.8C). This is due to a deficiency of the model at Grand Coulee. Given this consideration, the +2C hydrograph shows no climate sensitivity and the +4C hydrograph at John Day shows a slight climate sensitivity. The large increase in runoff in January through April (a difference of about 2,000 kaf/month with a +4C warming, with respect to the +2C scenario) has the appearance of an earlier occurring snowmelt signal. The sensitivity of the Snake River basin runoff contributes more heavily toward this climate sensitivity than does the local inflow from the John Day River subbasin (compare Figures 4.2 and 4.10). At The Dalles, the peak runoff diminishes considerably, from 20,000 kaf in July (+0C case; 330 average cfs) to 17,000 kaf (260 cfs) in March.

These results seem to demonstrate that the system of storage projects in the Columbia River basin has a large capacity for buffering changes in the seasonal distribution of surface runoff that may result from a warmer climate. Virtually all of this buffering capacity, as indicated by the model results, is provided by Mica, Libby, and Grand Coulee. Hungry Horse has a fairly significant storage capacity of 3.2 maf, but the annual volume of runoff subject to regulation at this project is relatively minor compared to the total runoff at The Dalles.

Application of the target discharge rule results, at all the storage projects, in an average monthly storage cycle with a smaller amplitude, which is associated with decreased number of failures (spills, release failures, storage failures). This is interpreted as underutilization of the reservoirs, in the sense that minimum benefits from a within-year storage system (as is the Columbia River water resources system) are derived when the storage is constant throughout the year.

4.6 Discussion

One of the difficulties with interpretations of the results is that the base case target discharge was used in the alternative climate scenario, which may or may not

reflect a reasonable operational strategy for a warmer climate. The results presented should be evaluated in consideration of this issue.

It was seen that at several sites (Mica, Libby, Duncan most notably) the model was able to enforce a discharge hydrograph that looked fairly similar to the base case climate hydrograph. It is probable that in a warmer climate, with earlier snowmelt runoff, and in some areas, transition to rainfall-dominated winter runoff (i.e. John Day and Deschutes River basins), the historical release pattern will not resemble the release pattern that would obtain from application of rational operational principles. Therefore, in order to understand how the results might be best interpreted, the general aspects of the historical operation of Columbia River storage reservoirs are explained briefly in Section 4.6.1, and the results of a study that investigated the potential effects of climate warming on hydropower demand are reviewed in Section 4.6.2. This background information is then used to evaluate the relevance of the results obtained through the use of the historically-referenced target discharge.

4.6.1 Normal reservoir operation

The Columbia River basin projects are multi-purpose. The highest priority functions are for irrigation, flood control, and hydroelectric power generation, and to provide firm energy in winter. Additional uses include recreation, and navigation. In the base case climate in most years the primary objectives - irrigation, flood control, and power production - are compatible. The operation of the system is based on volumetric forecasts of seasonal runoff, and a set of somewhat flexible operating rules which are applicable under even periods of extreme high or low runoff.

Flood control operation at the important flood control storage projects (Mica, Libby, Hungry Horse, Grand Coulee, Arrow) is contingent upon forecasts of runoff at The Dalles, Oregon. The flood control rules are designed to limit flooding at The Dalles, since adequate regulation at The Dalles will provide adequate flood protection at upstream flood prone areas as well. A Canada-US treaty grants the US

authority to use a portion of Canadian storage in Mica and Libby on an on-call basis for downstream flood control in the United States, when US storage is inadequate.

The control period begins 20 days prior to the date on which unregulated runoff is forecasted to exceed flood stage at The Dalles (450,000 cfs). In most years the control period does not begin before April 1. At the beginning of a control period, a controlled flow objective is established for The Dalles. This is the degree of regulation that is desired during the control period, and depends upon the forecasted runoff and available system-wide reserved flood control storage at the beginning of the control period. Rule curves for refill of each flood control project specify storage as a function of the controlled flow objective. Actual storage may deviate from the rule curve during a control period if minimum or maximum discharge limits for a project would be violated. The controlled flow objective at The Dalles, and the refill rate at each flood control storage project are revised if necessary as new forecasts become available.

Volumetric forecasts of unregulated runoff (i.e. in absence of any changes of storage) through August 1 at The Dalles are prepared the first of each month. The earliest forecasts are usually available in January or February of each year. These forecasts are the basis for deciding how much storage must be reserved for flood control purposes. During winter drawdown and spring refill, operation follows either the critical rule curve or the variable energy content curve (VECC). The critical rule curve draft schedule corresponds to the project outflow that meets firm energy load requirements. The VECC dictates the rate at which reservoirs must be drafted in order to provide storage for flood control by April 1 of each year, and is designed to assure 95% probability of refill at the end of flood control refill period. In the event that discharge required for flood storage reservation is less than that required for firm energy load, then the critical rule curve supersedes, and a greater risk of non-refill is incurred. Figure 4.11 gives an example of a Flood Storage Reservation

Diagram, from which the VECC is selected, depending on the seasonal volumetric runoff forecasts.

4.6.2 Possible effects of warming on hydropower and consumptive water use demands.

Under the present climate hydropower demand peaks in winter. A study of the potential effects of climatic warming and growth on hydropower and water supply by Scott *et al.* (1993) indicates that in a warmer climate (the scenario used for the study was roughly equivalent to a uniform +4C scenario), average annual energy consumption could decline (neglecting growth), but that the demand pattern could have both a summer and winter peak (Figure 4.12). Presently hydropower demand is highest in winter, and lowest in summer. Irrigation demand for water and power may increase, and energy demand for space heating would decline, possibly even to the extent that summer demand could surpass winter demand. The effects of growth on hydropower demand were also assessed. Based on growth projections to the year 2010, it was concluded that growth alone will likely present a much greater burden on the water resources of the Columbia River basin (energy and water supply) than any effect due to climatic warming on the scale of +4C. The analysis by Scott *et al.* (1993) shows a reduction in total annual hydroelectric power demand, for the case of warming with no growth.

4.6.3 Evaluation of the model results in view of historical operation strategy

Three conclusions may be drawn regarding how the pattern of project outflows at a typical storage reservoir might change if the basic principles outlined above were observed to the extent required under the altered flow regime, and if the hydropower and water supply pattern were to change as suggested by Scott *et al.* (1993).

(1) To be consistent with the historical operating rationale, flood storage reservation should be available prior to the beginning of the snowmelt season, which

under the warmer climate scenarios would be earlier in the year than April 1 at most projects. For example, at Grand Coulee the beginning of the snowmelt season shifts from April in the base case climate, to March in the +2C scenario and to perhaps February in the +4C scenario (see Figure 4.6). The target discharge resulted in an average minimum reservoir content corresponding to these months for these scenarios (Figure 4.3, upper left panel), even though it reflects the historical policy of completing evacuation by April 1.

(2) An implication of the study by Scott *et al.* (1993) is that in a warmer climate the releases in summer may need to be elevated above what they had been in the historical climate. This and the previous two considerations would tend to sustain the model result of an average pool level that is lowered in the summer, compared to the base case scenario. This may represent one of the negative impacts of a warmer climate on water resources in the Columbia River basin.

(3) In the past, flood control operation has required that releases in high runoff years be higher in the spring than would otherwise be beneficial. The model prediction that the mean maximum monthly runoff at The Dalles would decline suggests that storage reservation for flood control could be diminished in favor of storing water for future use.

The points made in this discussion support the view that the behavior of the system might indeed be modeled somewhat differently if the actual system operational rules were implemented within the model in some fashion, or if the time series of releases were optimized for each climate scenario. However this discussion does not contradict the general conclusions drawn from the results, and presented in Section 4.5.

4.6.4 Conclusion

It appears likely that with or without climate change, alternative sources of energy may need to be developed (Scott *et al.*, 1993) to meet increasing demand for

resources associated with growth, and that the impact of growth on demand may have far more implications for planning than does the potential effects of warming on both supply and demand. On the other hand, the possibility that a warmer climate could permit an increase in the total energy deliveries annually, and that warming may change the seasonal distribution of both demand and supply, as well as the average annual MW that can be generated by the system, could influence decisions about how to meet growth-related increases in demand for energy and water resources.

Table 4.1 Comparison of base case and alternative climate scenario results for index catchment simulations

Characteristic	Site	+0C	+2C	+4C
Mean Annual Runoff [a]		Result in mm	Percent Change [d]	
	American R.	1057	0.1	-0.2
	M. F. Flathead R.	909	-4.0	-7.3
	Salmo River	771	-2.3	-3.9
Timing of Peak Runoff [b]		Month	Shift of timing (# months) [d]	
	American R.	June	-1	-6
	M. F. Flathead R.	June	-1	-1
	Salmo River	May	-1	-1
Peak Runoff [b]		Result in mm	Percent Change [d]	
	American R.	275	-20.3	-50.2
	M. F. Flathead R.	292	-9.6	-32.5
	Salmo River	255	-14.1	-37.7
Ratio of Winter to Annual runoff [c]		Ratio	Ratio	
	American R.	0.27	0.49	0.65
	M. F. Flathead R.	0.16	0.24	0.37
	Salmo River	0.16	0.26	0.42

[a] Period of Record simulation

[b] maximum mean monthly runoff

[c] Ratio of October through April average runoff to average annual runoff

[d] with respect to base-case (+0C) simulation

Table 4.2: Effect of warming on local inflows to each subbasin

Subbasin	Local Inflow, kaf			Peak Mean Monthly Flow					Timing of Peak Flow			Winter Runoff (Oct- Mar) as Fraction of Annual		
		% Change		kaf			% Change			Shift, # mo's				
	kaf B/C	+2C	+4C	B/C	+2C	+4C	+2C	+4C	B/C	+2C	+4C	B/C	+2C	+4C
Group 1														
BRL	13526	-4.0	-7.2	1692	1937	2255	14.5	33.3	April	0	-2	0.51	0.60	0.70
RBT	3269	0.3	-0.2	333	481	637	44.4	91.3	Jan	0	0	0.54	0.70	0.81
JDA	11103	0.3	-0.2	2508	1417	2037	-43.5	-18.8	June	-4	-4	0.36	0.56	0.74
Group 2														
ALF	10605	-4.0	-7.3	2450	2453	2049	0.1	-16.4	May	0	-1	0.29	0.39	0.52
DWR	4405	0.2	-0.3	1146	1001	996	-12.7	-13.1	May	-1	-1	0.28	0.43	0.60
LWG	19846	-4.0	-7.2	4806	4683	3887	-2.6	-19.1	June	-1	-2	0.27	0.37	0.51
LLK	5725	0.3	-0.2	1256	1265	1128	0.7	-10.2	May	-1	-1	0.40	0.54	0.70
Group 3														
LIB	8924	-2.4	-4.1	2625	1714	1017	-34.7	-61.3	June	-1	-3	0.17	0.29	0.47
CHL	1468	0.2	-0.4	412	329	236	-20.2	-42.7	June	-1	-2	0.17	0.32	0.52
GCL	33339	-2.4	-4.1	8522	5978	4938	-29.9	-42.1	June	-1	-3	0.19	0.32	0.51
Group 4														
DUN	2658	-2.3	-4.1	683	514	451	-24.7	-34.0	June	+1	+1	0.14	0.24	0.38
MIC	15051	-2.4	-4.1	3632	3078	2714	-15.3	-25.3	July	0	0	0.13	0.23	0.36
Group 5														
HHR	2603	-4.1	-7.3	788	845	604	7.2	-23.4	June	-1	-1	0.17	0.24	0.37
KER	5932	-4.0	-7.2	1667	1689	1177	1.3	-29.4	June	-1	-1	0.19	0.28	0.41

Table 4.3 Sensitivity of mean annual power generation to warming

	Power Generated[a]		
		Percent Change	
Subregion	B/C	+2C	+4C
Upper Columbia[b]	1958	-1.9	-2.3
Pend Oreille[c]	1570	-3.2	-6.5
Grand Coulee/Arrow[d]	6125	-3.2	-4.7
Snake River[e]	2300	-2.3	-7.0
Lower Columbia[f]	4184	-1.0	-3.7

[a]Average annual MW

[b]Mica/Revelstoke, Libby, Duncan through Brilliant (nodes 12,13,14)

[c]Hungry Horse through Box Canyon (nodes 11,10,17,9)

[d]Grand Coulee (node 6), six downstream projects (node 16), Long Lake and Chelan (nodes 7 and 8)

[e]Box Canyon through Ice Harbor (nodes 3,4,5)

[f]Projects on the Lower Columbia and Deschutes River (nodes 1,2,15)

Table 4.4: Effect of warming on regulated outflow at each water resources model node

Node	Total discharge, kaf			Peak Mean Monthly Flow			Timing of Peak Flow			Winter Runoff (Oct- Mar) as Fraction of Annual		
	kaf	% Change		kaf	% Change		Mo.	Shift, # mo's				
	B/C	+2C	+4C	B/C	+2C	+4C	B/C	+2C	+4C	B/C	+2C	+4C
Lower Columbia												
The Dalles	138596	-2.3	-4.3	19946	-9.90	-15.80	June	-1	-2	0.42	0.46	0.52
John Day	135322	-2.4	-4.4	19645	-10.6	-16.2	June	-1	-2	0.42	0.46	0.51
Roundbutte	3274	0.3	-0.3	391	20.5	60.1	Jun	-3	-4	0.50	0.62	0.73
Snake River												
Lower Granite	37807	-3.5	-6.4	7027	-0.2	-1.2	May	0	-1	0.37	0.44	0.54
Dworshak	4405	0.4	0.0	730	4.5	12.1	May	0	-1	0.40	0.45	0.53
Brownlee	13577	-4.0	-7.2	1692	314.3	310.2	April	0	0	0.51	0.54	0.57
Middle Columbia												
Grand Coulee	86401	-2.2	-4.1	10487	-11.8	-18.1	June	0	-1	0.44	0.46	0.47
Long Lake	5725	0.2	-0.3	197	-4.1	-12.2	May	-1	-1	0.38	0.50	0.64
Chelan	1476	2.0	0.0	197	-4.1	-12.2	July	-1	-2	0.42	0.43	0.49
Pend Oreille/ Flathead												
Albeni Falls	19221	-4.0	-0.6	4265	-5.4	-24.3	June	-1	-1	0.33	0.34	0.36
Kerr	8607	-4.0	-7.2	1667	-7.9	-16.4	June	-1	-1	0.28	0.29	0.30
Hungry Horse	2656	-3.9	-7.0	788	-6.5	-13.0	June	-1	-1	0.29	0.29	0.30
Kootenay and Upper Columbia												
Duncan	2658	-2.4	-3.9	322	-2.5	-4.0	June	+1	+1	0.44	0.44	0.44
Libby	8892	2.0	-0.4	1137	-2.9	-6.2	Nov	0	0	0.56	0.59	0.61
Mica	15077	-2.2	-4.1	2019	-2.8	-4.7	Aug	0	0	0.45	0.46	0.46

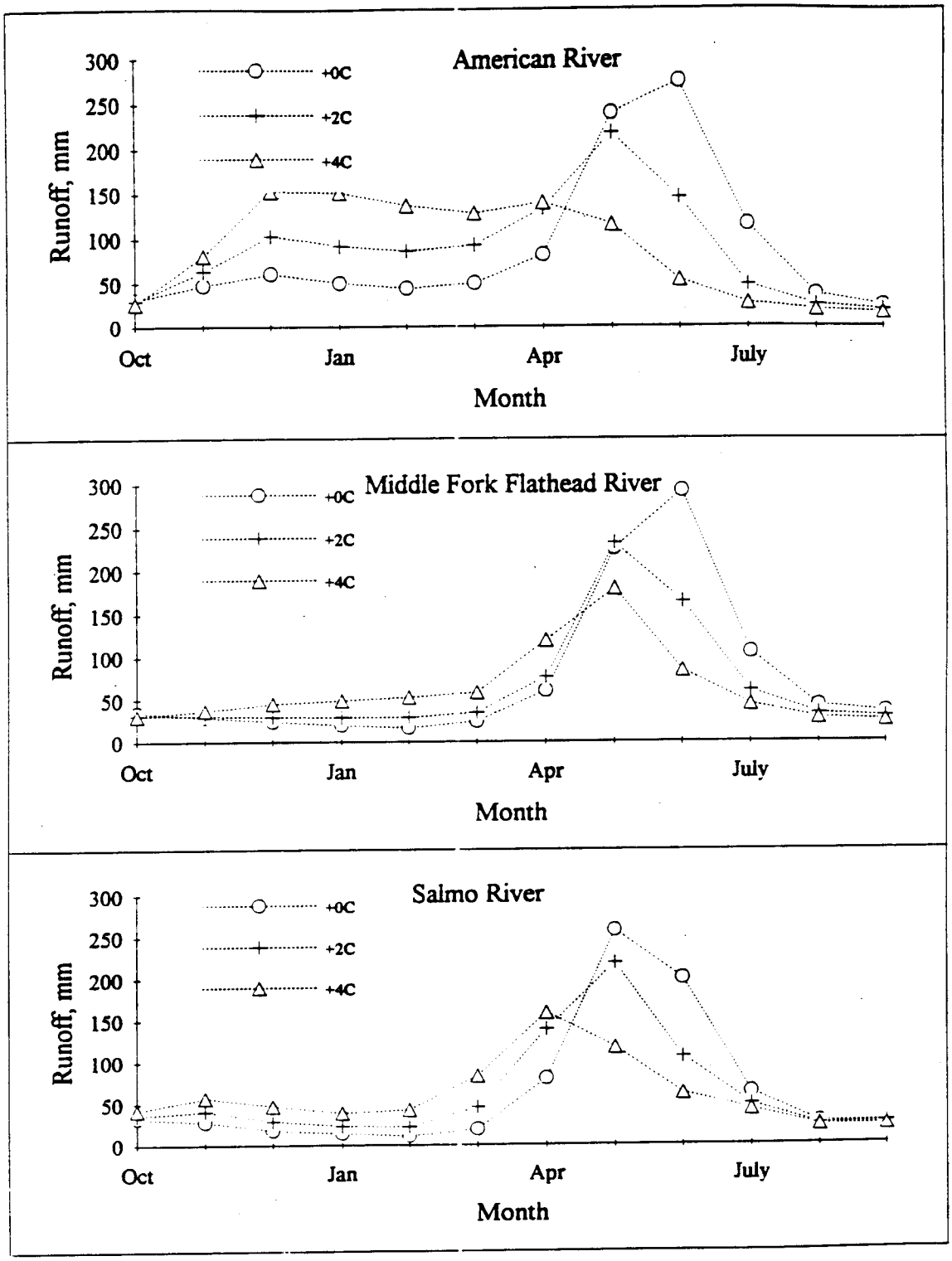

Figure 4.1 Index catchment base case and alternative climate simulated runoff

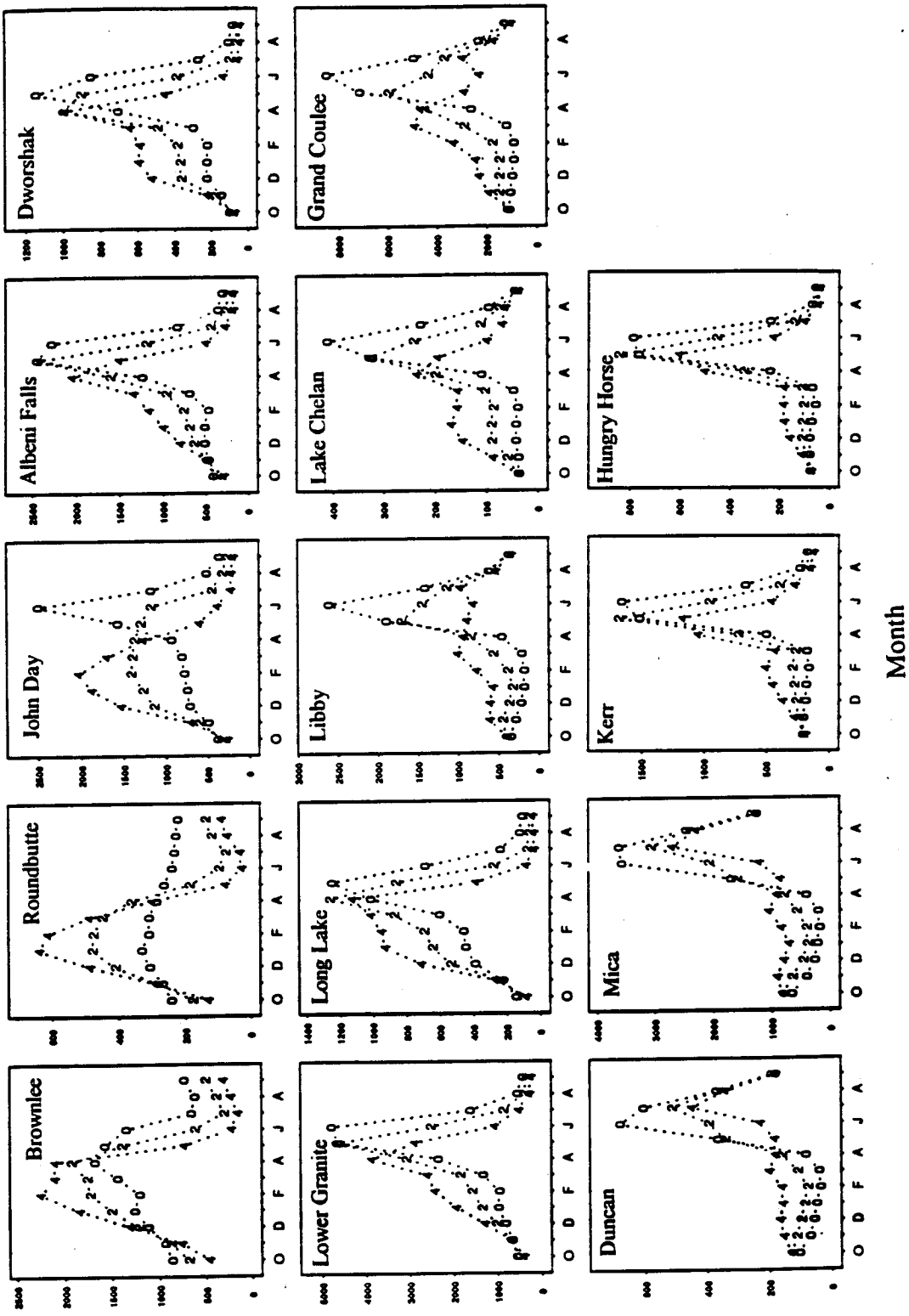

Figure 4.2 Mean monthly subbasin local inflow for each climate scenario

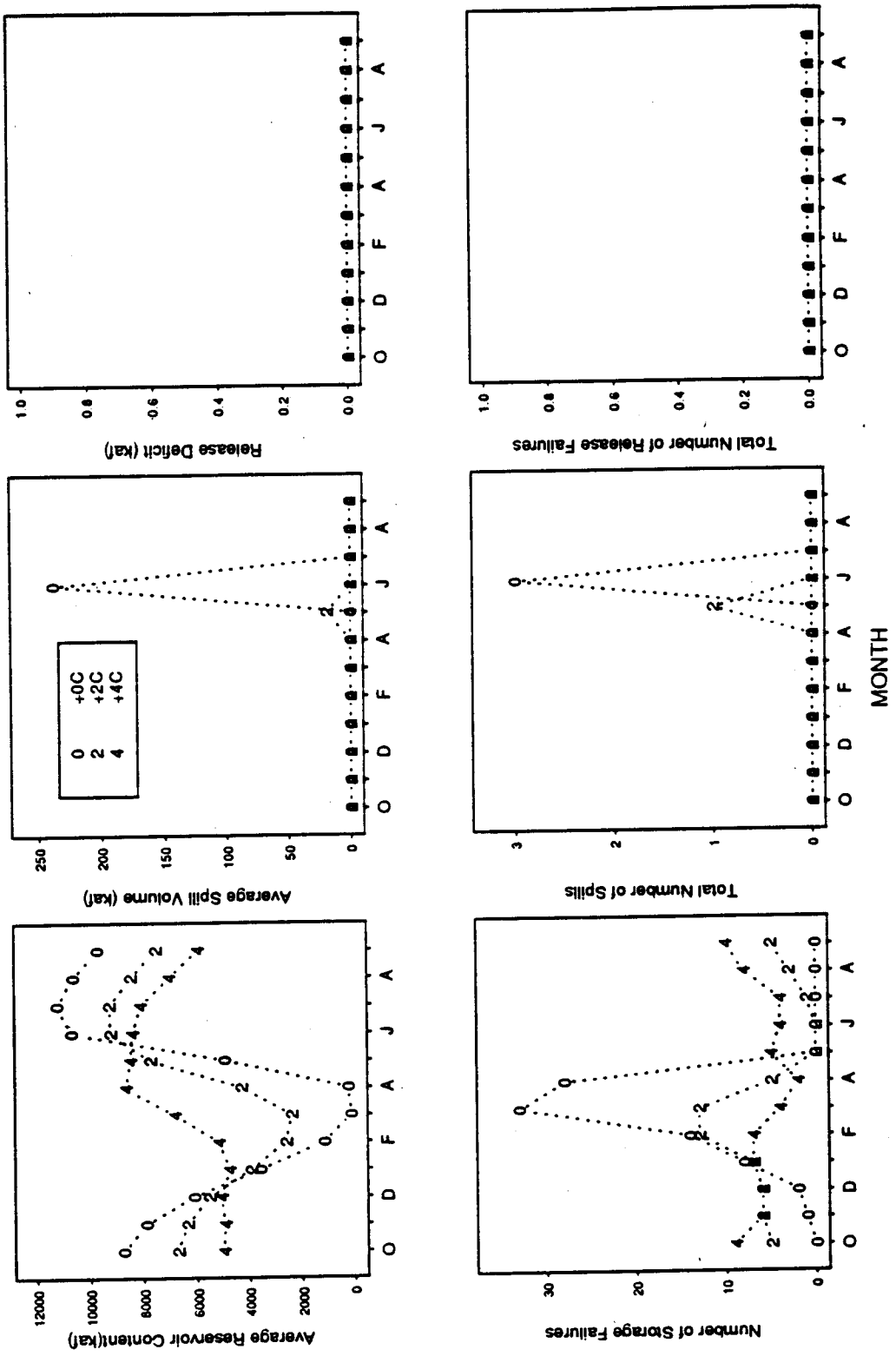

Figure 4.3 Grand Coulee/Arrow aggregate reservoir storage behavior

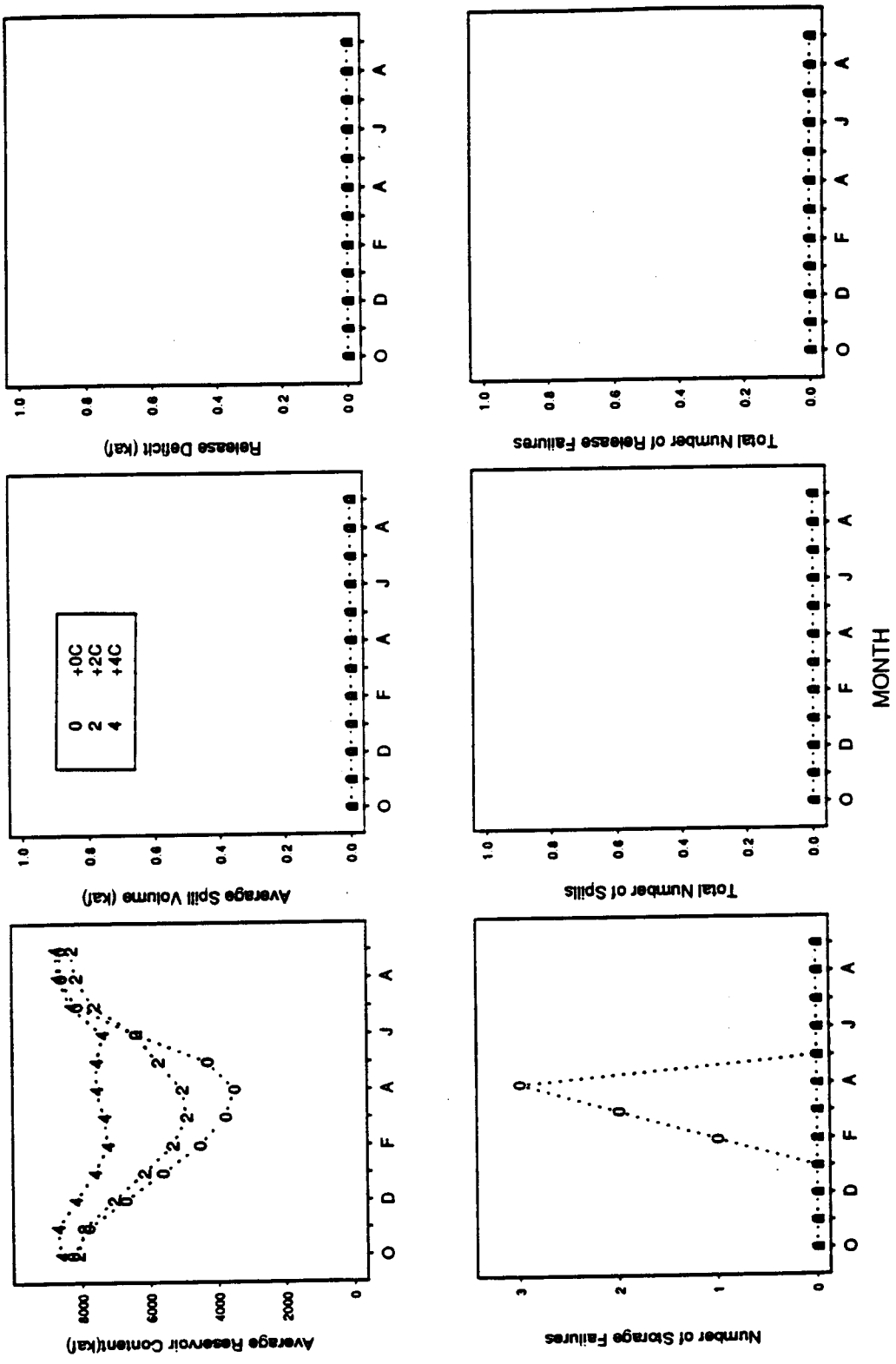

Figure 4.4 Mica Reservoir storage behavior for each climate scenario

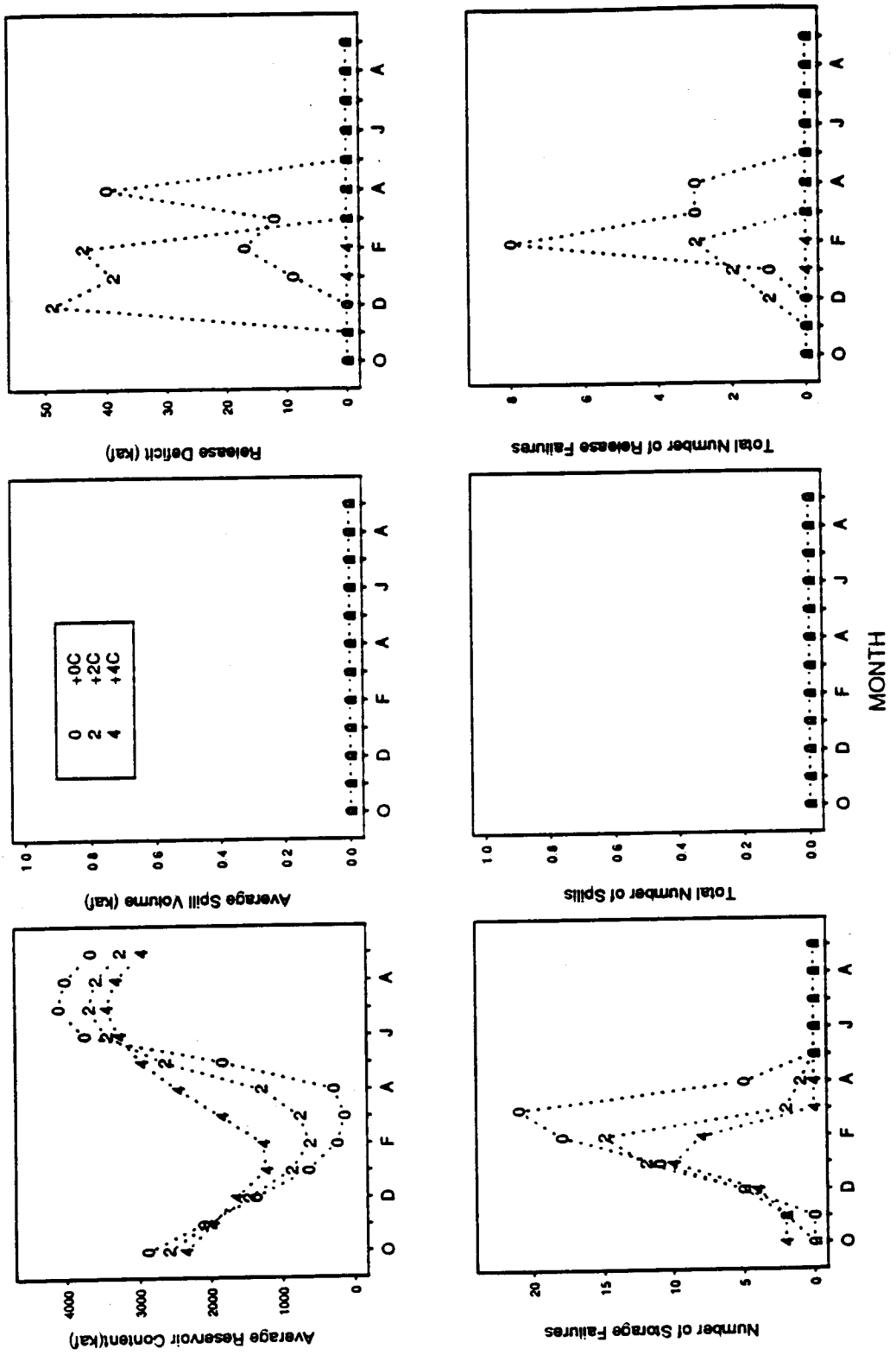

Figure 4.5 Libby Reservoir storage behavior for each climate scenario

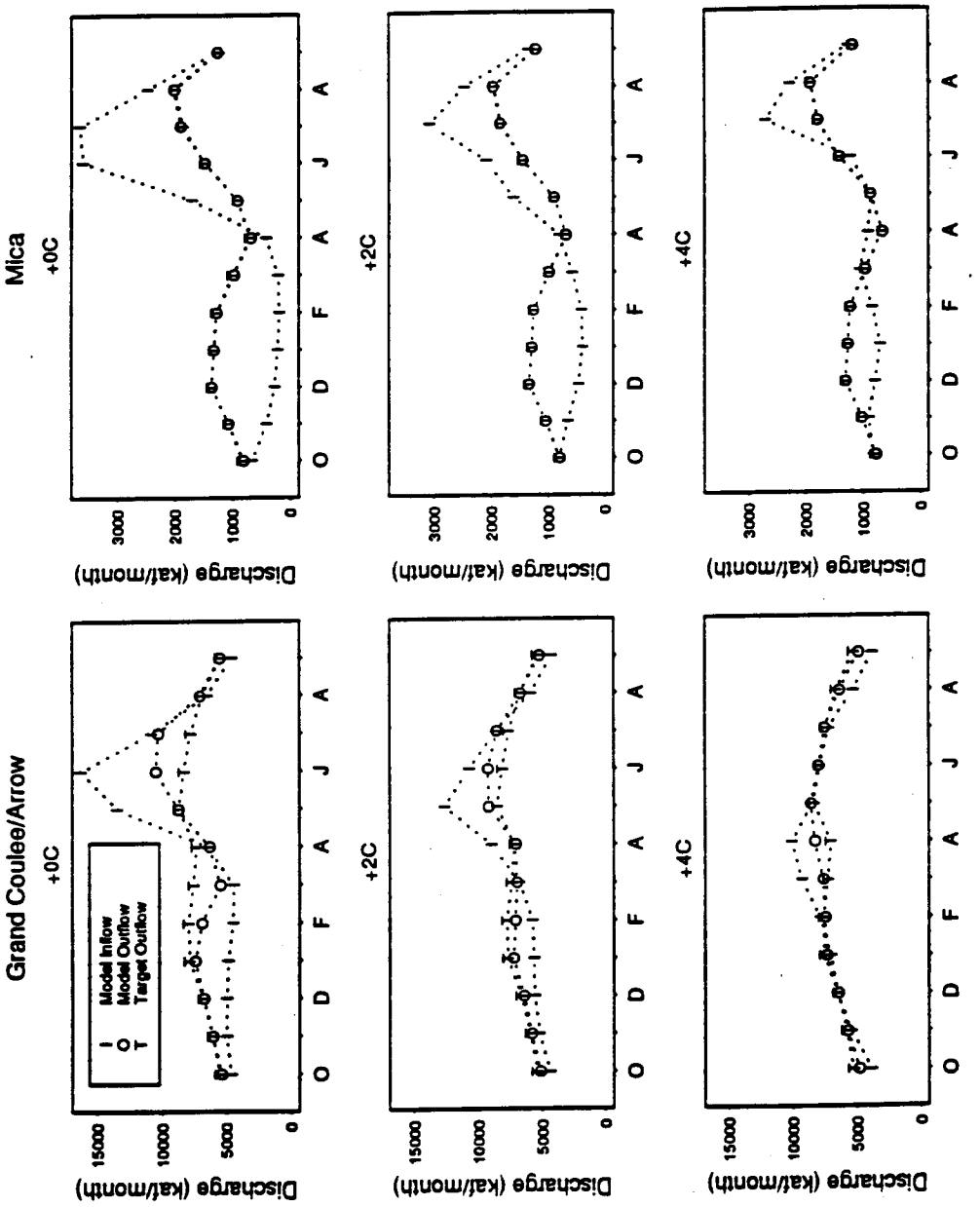

Figure 4.6 Modeled regulated inflow, outflow and target discharge for each climate scenario: Grand Coulee/Arrow and Mica Reservoirs.

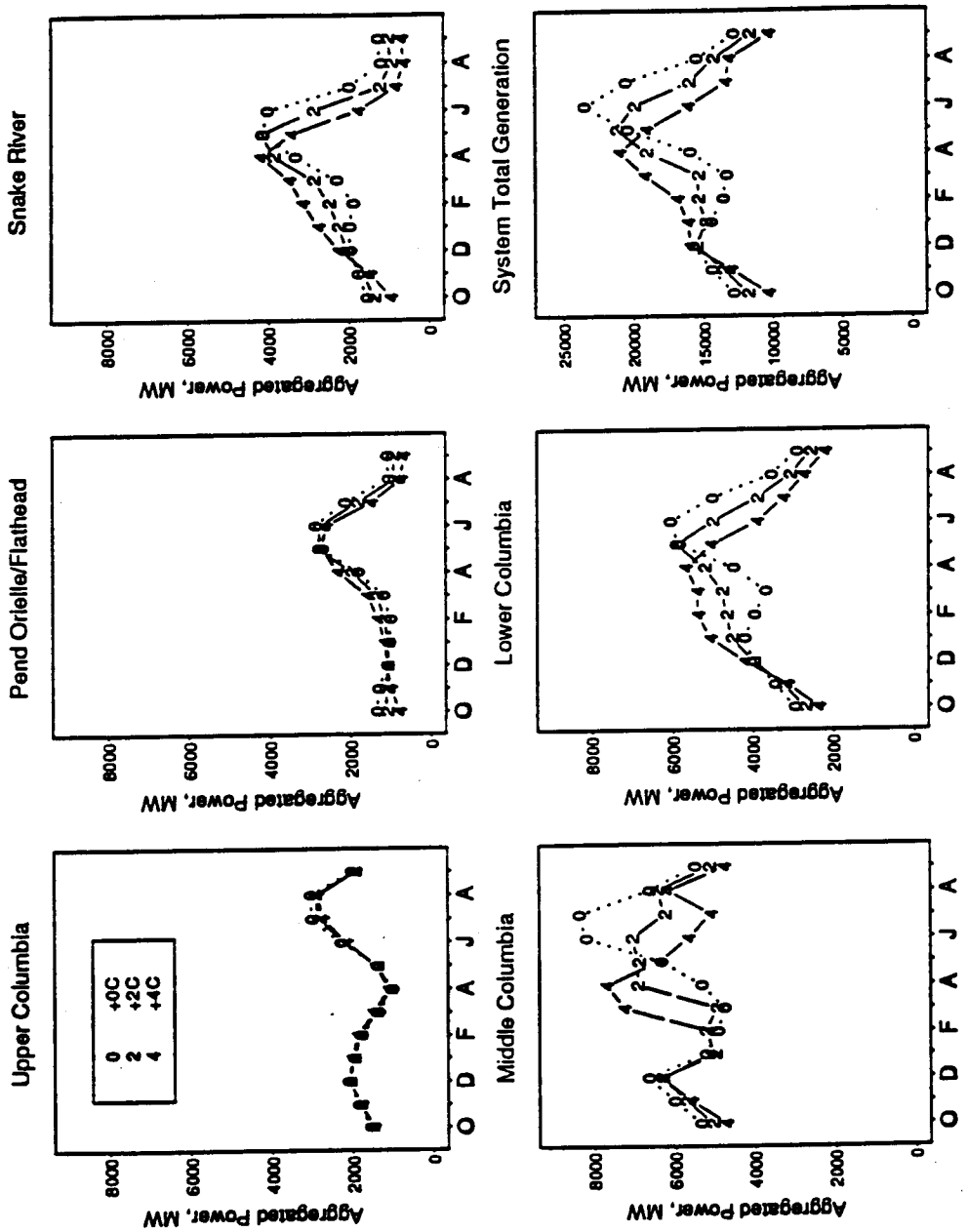

Figure 4.7 Aggregated hydroelectric power generation for each climate scenario. Table 4.3 identifies which nodes are grouped to form the five subregions represented.

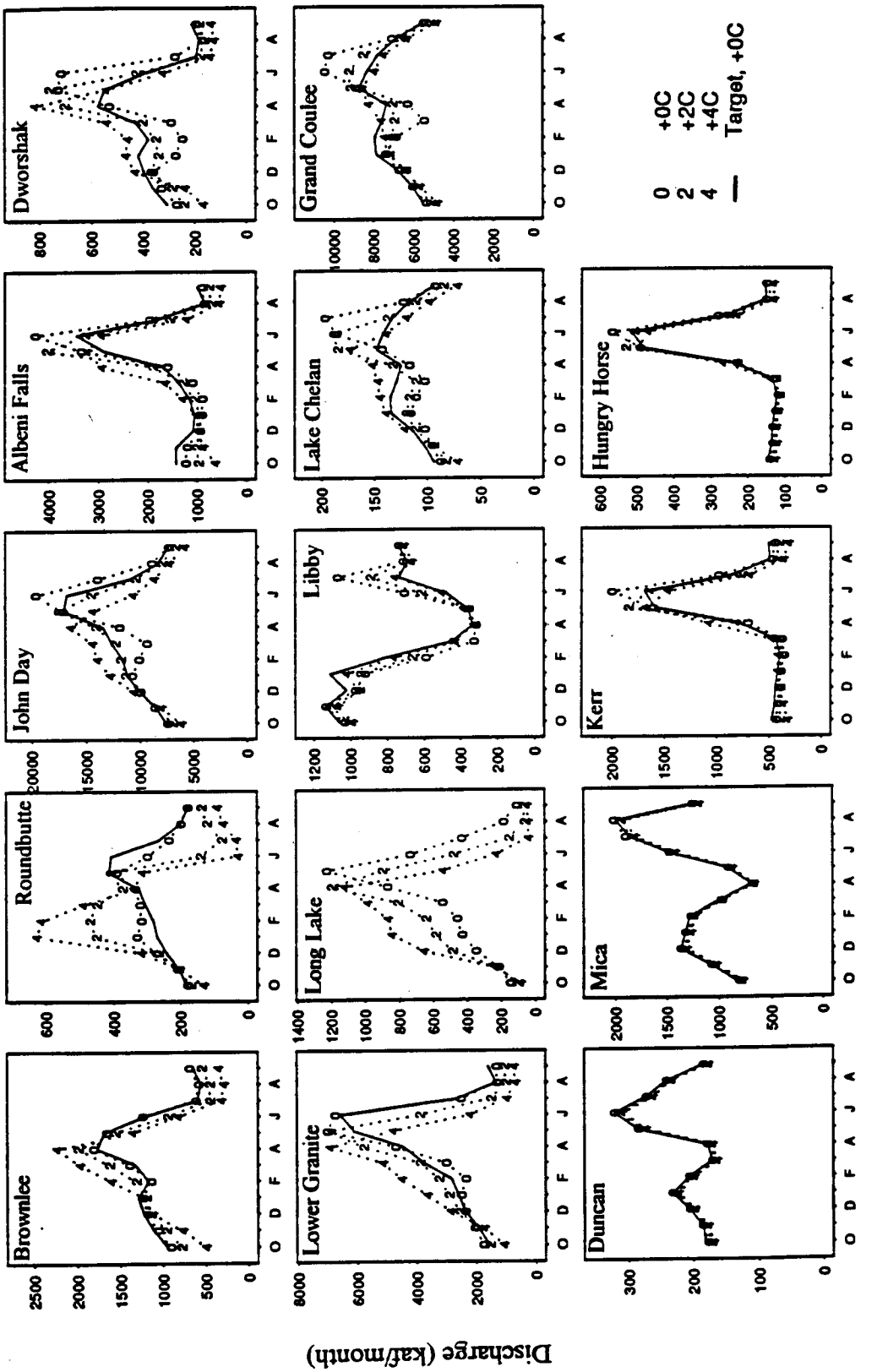

Figure 4.8 Modeled regulated discharge at major nodes for each climate scenario

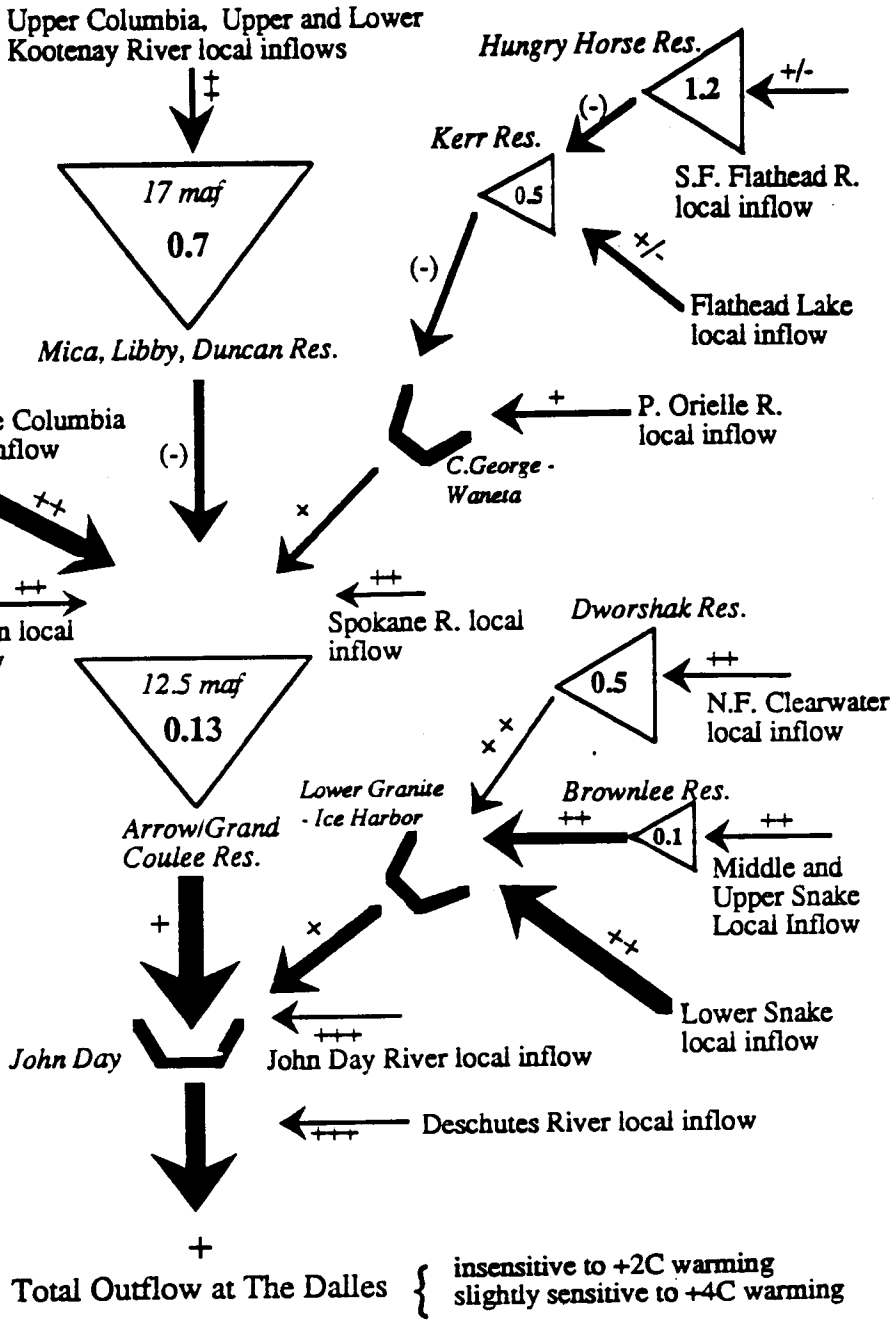

Figure 4.9 Schematic representation of the sensitivity of regulated inflow and outflow throughout the network to climatic warming scenarios. Triangles (◁) represent major storage projects; numbers within indicate storage capacity (italic) and at-site storage ratio[a] (bold). Brackets (" [") indicate nodes without any significant storage (i.e. Albeni Falls, Lower Granite, John Day, and associated projects). Relative thickness of arrows converging to a common point is roughly indicative of the relative contribution of each inflow to total discharge. Plus and minus signs indicate sensitivity of local inflow or outflow to warming ('+++' - highly sensitive, '+' slightly sensitive, '-' no sensitivity).

[a] (active storage / mean annual total discharge)

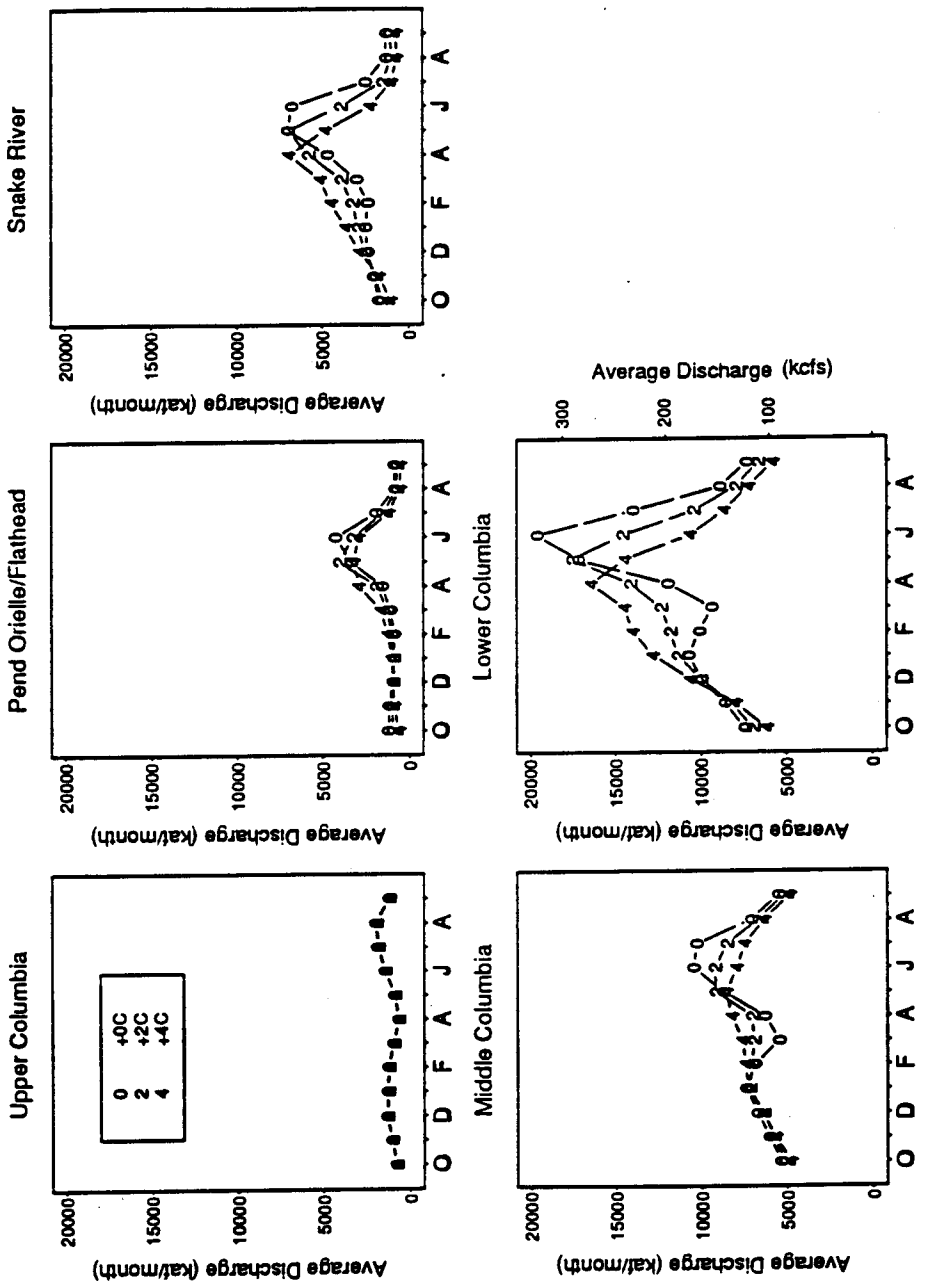

Figure 4.10 Modeled outflow for each climate scenario at major nodes. Upper Columbia: Mica; Pend Orielle: Albeni Falls; Snake River: Lower Granite; Middle Columbia: Grand Coulee; Lower Columbia: The Dalles.

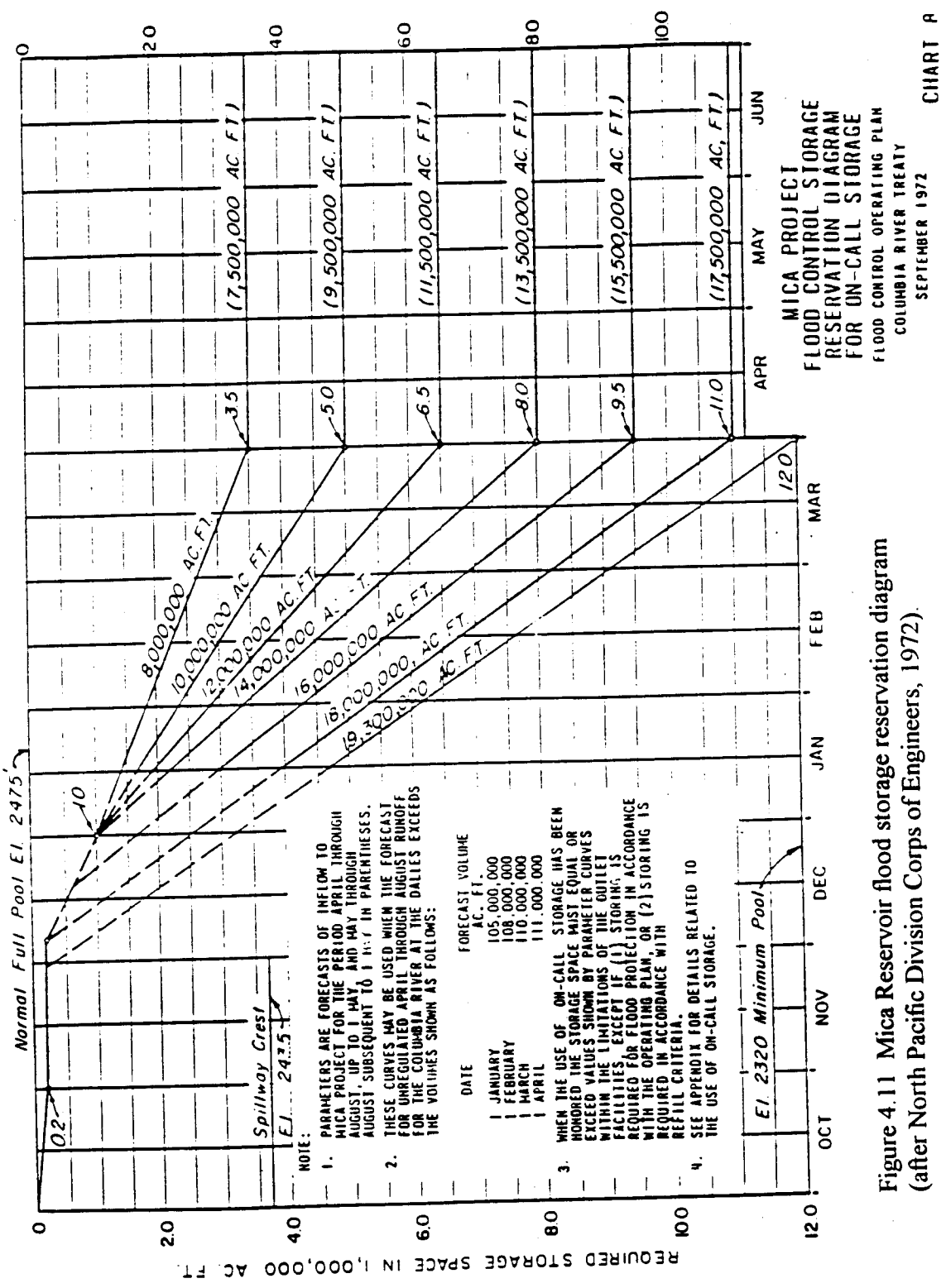

Figure 4.11 Mica Reservoir flood storage reservation diagram (after North Pacific Division Corps of Engineers, 1972).

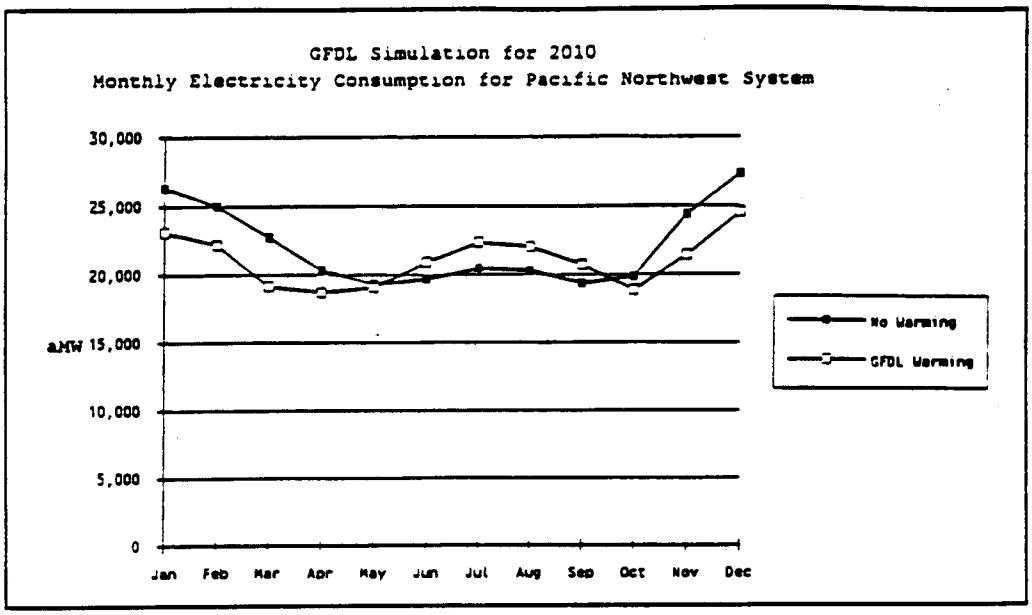

Effects of Climate Change in the GFDL Case on Pacific Northwest Electricity Demand in the Year 2010 (by month)

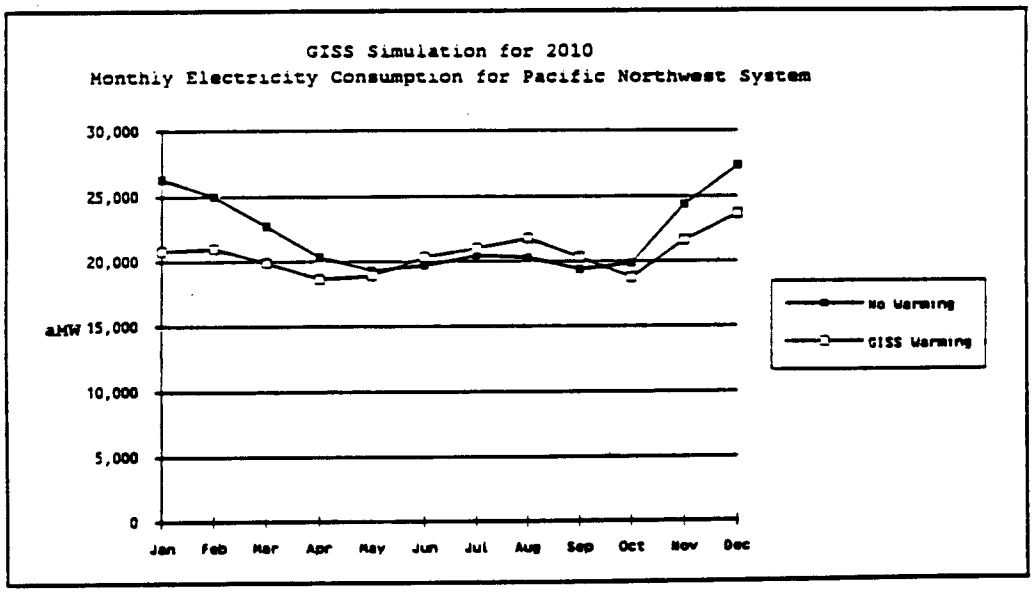

Effects of Climate Change in the GISS Case on Pacific Northwest Electric Energy Demand in the Year 2010 (by month)

Figure 4.12 Projected hydropower demand in 2010 for two GCM scenarios, compared to base case scenario (after Scott, et al., 1993)

Chapter 5

Conclusions and Recommendations for Further Research

5.1 Summary

The possible implications of climate change on the Columbia River basin water resources system were assessed through simulation of 38 years of daily streamflow for three small index catchments (drainage areas ranging from 204 to 2925 km^2) and subsequent aggregation to a monthly time step. The monthly (and annual) simulated streamflows were then disaggregated using a space-time stochastic streamflow disaggregation model to produce monthly incremental streamflow for fourteen large subbasins, which comprise the total area of the Columbia River basin above The Dalles, OR.

The streamflow simulation and disaggregation procedures were performed for each of three climate scenarios: base-case climate (historical temperature), historical temperature plus two degrees, and historical temperature plus four degrees; historical precipitation was used in all three scenarios. Two streamflow series of length 38 years were generated for each subbasin, for each climate scenario. The monthly streamflows were routed through a simple water resources system model, which represented the reservoir system (which consists of about 100 storage and run of the river reservoirs) as eighteen aggregate projects. The water resources system model operating rules were based on historical average monthly releases from each of the aggregate projects; that is, the model attempted to release from each of the storage reservoirs a target discharge equal to the historical mean release.

The disaggregation procedure was pseudo-deterministic in that the generated flows were conditioned on the simulated runoff sequences for the index catchments.

Two different procedures were used to adjust the subbasin flows produced by the stochastic disaggregation model to reflect the simulated changes at the index catchments. Both procedures assumed constant monthly means ratio (that is, that the ratio of the monthly means of the altered climate to the base climate for each subbasin was equal to the ratio for the corresponding index catchment. The first procedure assumed that the coefficients of variation were also equal; the second procedure assumed that the ratio of the coefficient of variation for alternate climate to the base climate for each subbasin was equal to the ratio for the corresponding index catchment. A second stage adjustment was then applied to rescale the adjusted sequences so that the fractional change in annual runoff for the subbasin was equal to the fractional change in annual runoff for the corresponding index catchment.

5.2 Conclusions

The major conclusions are the following:

1. The stochastic model was not very successful in reproducing the cross-correlations of subbasin flows indexed to different catchments. This is a consequence of the fact that the hydrologic model was not able to preserve the fairly strong correlations of historical index-catchment annual runoff cross-correlations. The hydrologic model produces simulations which are highly correlated to precipitation records, whereas the precipitation records of different index catchments are only weakly cross-correlated.

The weak cross-correlations probably reduce the frequency of storage and release failures at Grand Coulee, as well as affecting the frequency of high and low seasonal runoff events at John Day, but only at these two sites would water supply be affected by weak between-group cross correlations, since at all other nodes the total runoff is associated with only one index catchment.

2. The stochastic transfer scheme seems to work best if the index catchment and subbasin historical runoff hydrograph have a similar appearance. The additional

adjustment, whereby the monthly subbasin flows were rescaled such that the change in subbasin mean annual runoff was equal to that of the index catchment, seemed to compensate for the original problem.

3. The Snake River basin, Hungry Horse, and Kerr local inflows are only slightly sensitive to warming. All other local inflows were moderately to highly sensitive.

4. The results of the water resources routing were not sensitive to random number generator seed, nor to the adjustment procedure. This is because the differences between individual local inflow sequences were not so great that differences could not be obscured through month-to-month changes in storage.

5. The results suggest that the Upper and Middle Columbia basin, as currently operated, is fairly robust to changes in the streamflow hydrograph that would accompany climatic warming, in that the model was able to achieve the target discharge at major reservoirs, in spite of moderately sensitive local inflows to these nodes. In general, the greater the transition from a snowmelt-dominated regime to a winter rainfall or transitional regime, the smaller were the changes in storage required to meet the target discharge. At Grand Coulee/Arrow aggregate reservoir, for example, the model came closer to meeting the target discharge in the +4C scenario than in the +2C scenario.

6. The decrease in the maximum mean monthly inflow and the decreased amplitude of storage fluctuations imply that less storage may be needed to be reserved for flood control operation, if climatic warming occurs. An alternative interpretation is that should warming be accompanied by increased annual runoff, the system will be better able to mitigate flood flows than would be possible if annual runoff were to increase without any change in mean seasonal temperature.

7. Partial or complete transition to winter rainfall dominated runoff is beneficial both for flood control, as mentioned above, but also for hydropower

generation. However this conclusion is based on the present hydropower demand pattern; warm temperatures could be expected to alter the power demand pattern, reducing the winter peak to some extent, and elevating demand in the summer. It seems likely that the release pattern (or the operational strategy) could be modified to obtain a hydrograph and hydropower generation pattern that peaks in both winter and summer, one that would be consistent with the seasonality of demand expected in a warmer climate.

8. Although a warmer climate appears to be beneficial for hydropower and flood control, it could well interfere with efforts to restore wild runs of migratory fish, salmonids in particular.

5.3 Limitations

The methodology used to prepare local inflows, and the water resources model through which they were routed has certain important limitations which affect the interpretation of the results.

The regionalization procedure is not physically based, and only seems to give plausible results if the index catchment and subbasin have similar hydrographs. In this respect, there was not adequate indicator index-catchment for the semi-arid and for glaciated subbasins (John Day, Long Lake, Roundbutte, Brownlee, Mica, Duncan). The streamflow disaggregation model was not able to preserve within-group cross-correlations in these cases.

The inability of the model to preserve subbasin within-group and between group cross-correlations means that any analysis of the water resources model results that depends on these cross-correlations is not warranted. For this reason, only mean monthly and mean annual results in the water resources model is emphasized.

The use of the historical mean monthly release as the operating rule in the water resources model does not account for year to year variation in total runoff, and leads to larger excursion in reservoir contents. (Nevertheless, the model was able to

reproduce the mean monthly outflows.) This same rule was applied in the alternative climate scenarios, even though it is likely that the system would be operated differently in a warmer climate. As for the modeling of hydropower, the water resources model includes no consideration of hydropower revenue and avoidance costs. Finally, no attempt was made to evaluate the impacts that the altered hydrologic regime may have on fisheries and salmonid survival.

5.4 Recommendations for further research

1. TOPMODEL did not perform as well as was hoped, particularly for the semi-arid catchments. The ratio of mean monthly absolute error to mean monthly runoff was 0.29 for the humid catchments and 0.59 for the two semi-arid catchments. Because the snowmelt model was calibrated for snowmelt-dominated conditions, it is questionable whether the model is applicable to warmer climates, where for long periods the hydrologic conditions are outside the range found in the calibration period (Nemec and Schaake, 1982). Testing the model on similar catchments with better precipitation data, which of the forcing and calibration variables (temperature and precipitation, and streamflow) is most difficult to measure accurately, might help to isolate model versus data problems.

Another possibility is to emphasize minimization of error during calibration to those periods which are hydrologically similar to conditions which are more typical of warmer climate scenarios, i.e. periods of less snow accumulation and ablation; more rainfall-associated winter runoff production as opposed to snowmelt and rain plus snow associated runoff production.

2. The means ratio-stochastic disaggregation method of regionalizing index catchment simulations can produce what seem to be unrealistic results when the index catchment and subbasin historical runoff is dissimilar. One weakness of this method of obtaining the subbasin runoff is that it does not take into consideration differences in area-elevation relationships between the index catchments and the subbasins, which could have an important effect on the seasonal hydrograph of two

catchments which otherwise experience a similar climate and storm exposure. The means ratio assumption is probably most justifiable when the range of elevation of the subbasin and the index catchment are similar, and both are located in the same region of fairly homogenous climate. Even in the ideal case where the index catchment is located within the subbasin, the much larger subbasin potentially could still have a different pattern of sensitivity than the index catchment, because of differences in elevation range and the vertical distribution and form of precipitation.

This issue could be addressed by incorporating area-elevation relationships into the regionalization scheme, perhaps circumventing the use of the means ratio/stochastic disaggregation scheme, for which there is no clear physical justification.

3. This study has not adequately answered the question of how the system would perform if optimized for hydropower revenue and storage reliability, or if the existing operating rules were applied, in conjunction with simulated seasonal volume of runoff forecasts. This is recommended as a direction for research. It would be appropriate to modify the historical operating rules to take into account the earlier onset of snowmelt, by requiring an earlier completion of reservoir evacuation for flood control. This research could be useful for assessing whether the target discharge approach, which is relatively easy to implement, gives results that are consistent and sufficiently informative to warrant the simpler approach in other studies.

References

Ambroise, B., J.L. Perrin, and D. Reutenauer, Multi-criterion validation of a semi-distributed conceptual modeling of the water cycle in the Fecht Catchment (Vosges Moutains, France) 1. Physically-based catchment discretization and model parameterization, submitted for publication, in *Water Resources Research*, December 14, 1993.

Anderson, E.A., National Weather Service River Forecast System-Snow Accumulation and Ablation Model, *NOAA Technical Memorandum NWS Hydro-17*, November, 1973.

Balling, R.C., Jr., Impact of desertification on regional and global warming, *Bulletin American Meteorological Society*, 72, 232-234, 1991.

Balling, R.C., The global temperature data, *Research and Exploration*, 9(2), 203, 1993.

Beven, K.J., and M.J. Kirkby, A physically based, variable contributing area model of basin hydrology, *Hydrological Sciences Bulletin*, 24(1), 43-69, 1979.

Beven, K..J, M.J. Kirby, N. Schoffield,and A.F. Tagg, Testing a physically-based flood forecasting model (TOPMODEL) for three UK catchments, *Journal of Hydrology*, 69, 119-143, 1984.

Bras, R, L., *Hydrology, An Introduction to Hydrologic Science*, Addison, Weseley, MA, 1990.

Brettmann, Kenneth L., An Investigation of the Hydrologic sensitivities to climate: A case study for the American River, Washington, M.S. thesis, Dept. Civil Eng., Univ. of Washington, 1991.

Bristow, K.L., and G.S. Campbell, On the relationship between incoming solar radiation and daily maximum and minimum temperature, *Agric. For. Meteorol.*, 31, 159-166, 1984.

Bultot, F., A. Coppens, G.L. Dupriez, D. Gellens, F. Meulenberghs, Repercussions of a CO_2 doubling on the water cycle and on the water balance: a case study for Belgium, *Journal of hydrology*, 99, 319-347, 1991.

Burnash, R.J.C., R.L. Ferral, and R.A. McQuire, A generalized streamflow simulation system, in *Conceptual Modeling for Digital Computers*, US National Weather Service, Sacramento, CA, 1973.

Chahine, M.T., The hydrologic cycle and its influence on climate, *Nature* 359, 373 - 380, 1992.

Charlson, R.J., J.E. Lovelock, M.O. Andreae, and S.G. Warren, Oceanic phytoplankton, atmospheric sulfur, cloud albedo and climate, *Nature* 326, 655-651, 1987.

Croley, T. E. II., Laurentian Great Lakes double-CO_2 climate change hydrological impacts, *Climatic Change*, 17, 24-47, 1990.

Dean, L., *Variable Energy Content Curves*, unpublished manuscript, 1992.

Depletions Task Force, Columbia River Water Management Group, *1980-Level Modified Streamflow, 1928 - 1978*, U.S. Army Corps Eng., Portland, OR, 1983.

Dickinson, R. E., Uncertainties of estimates of climatic change: A review, *Climatic Change*, 15, 5-13, 1989.

Dracup, J.A., Impact on the Colorado River Basin and Southwest, in *Studies in Geophysics: Climate, Climatic Change, and Water supply*, National Research Council Panel on Water and Climate, National Academy of Sciences, Washington D.C., 1977.

Dracup, J.A. and D.R. Kendall, Floods and Droughts, in *Climate change and U.S. Water Resources*, P. Waggoner, ed., John Wiley & Sons, 243-267, 1990.

Eagleson, P.S., The emergence of global-scale hydrology, *Water Resources Research*, 22(9), 6S-14S, 1986.

Emiliani, C., Quaternary paleotemperatures and the duration of the high temperature intervals, *Science*, 178, 398, 1972.

Fiering, M.B., and P. Rogers, *Climate Change and Water resources planning under uncertainty*, Draft Report to the US Army Engineer Institute for Water Resources, Fort Belvoir, VA, 1989.

Giorgi, F., and Means L.O., Approaches to the simulation of regional climate change: A review, *Reviews of Geophysics*, 29(2), 191-216, 1991.

Gleick, P.H., The development and testing of a water balance model for climate impact assessment: Modeling the Sacramento Basin, *Water Resources Research*, 23(6), 1049-1061, 1987.

Gleick, P.H., Methods for evaluating the regional hydrologic impacts of global climatic changes, *Journal of Hydrology*, 88, 97-116, 1986.

Grygier, J.C., and J.R. Stedinger, Condensed disaggregation procedures and conservation corrections for stochastic hydrology, *Water Resources Research*, 24(10), 1574-1584, 1988.

Harshvardhan, Atmospheric Radiation, *Reviews of Geophysics*, Supplement S56-S68, 1991.

Henderson-Sellers, A. and K. McGuffie, *A Climate Modeling Primer*, Wiley and Sons, Chichester, New York, 1987.

Hirsch, R.M., A comparison of four streamflow record extension techniques, *Water Resources Research*, 18(4), 1081-1088, 1982.

Hornberger, G.M., K.J. Beven, B.M. Cosby, and D.E. Sappington, Shenandoah watershed study: Calibration of a topography-based, variable contributing area hydrological model to a small forested catchment, *Water Resources Research*, 21(12), 1841-1850, 1985.

Hurst, H.E., Long-term storage capacity of reservoirs, *Proceedings of the American Society of Civil Engineers*, 76(11),1950.

Idso, S.B., and A.J. Brazel, Rising atmospheric carbon dioxide concentrations may increase streamflow, *Nature*, 312, 51-53, 1984.

Intergovernmental Panel on Climate Change, *Climate* Change: *The IPCC Scientific Assessment*, I.J. Houghton, G. Jenkins, and J. Ephraums, eds., Cambridge Univ. Press, Cambridge, MA, 1990.

Intergovernmental Panel on Climate Change, *Climate Change 1992: The Supplementary Report to The IPCC Scientific Assessment*, I.J. Houghton, B.A. Callander, and S.K. Varney., eds., Cambridge Univ. Press, Cambridge, MA, 1992.

Kaczmarek, J. and D. Krasuski, *Sensitivity of Water Balance to Climate Change and Variability*, IIASA Working Paper, 1991.

Karl, T.R., and Riebsame, W. E., The impact of decadal fluctuations in mean precipitation and temperature on runoff: A sensitivity study over the United States, *Climatic Change*, 15, 423-447, 1989.

Kite, G.W., Application of a land class hydrological model to climatic change, *Water Resources Research*, 29(7), 2377-2384, 1993.

Klemes, V., R. Srikanthan, T.A. McMahon, Long-memory flow models in reservoir analysis: What is their practical value? *Water Resources Research*, 17(3), 737-751, 1981.

Kuhl, S.C. and J.R. Miller, Seasonal river runoff calculated from a global atmospheric model, *Water Resources Research*, 28(8), 2029-2039, 1992.

Langbein, W.B. *et al.*, *Annual runoff in the United States*, US Geol. Surv. Circ. no 5, US Department of the Interior, WA DC, 1949.

Lettenmaier, D.P., K. Brettmann, L.W. Vail, S.B. Yabusaki, and M.J. Scott, Sensitivity of Pacific Northwest water resources to global warming, *The Northwest Environmental Journal*, 8(2), 265-283, 1993.

Lettenmaier, D.P. and S.J. Burges, Climate change: Detection and its impact on hydrologic design, *Water Resources Research*, 14(4), 679 -687, 1978.

Lettenmaier, D.P., and T.Y. Gan, Hydrologic sensitivities of the Sacramento-San Joaquin River basin, California, to global warming, *Water Resources Research*, 26(1), 69-86, 1990.

Lettenmaier, D.P., G. McCabe, and E.Z. Stakhiv, Global climate change and effect on the hydrologic cycle, in *Handbook of Water Resources*, L. W. Mays, ed., (to be published), 1994.

Lettenmaier, D.P., and D.P. Sheer, Climatic sensitivity of California water resources, *Journal of Water Resources Planning and Management*, 117, 108-125, 1991.

Matthews, W.H., W.W. Kellogg, and G. D. Robinson, eds., *Inadvertent Climate Modification, Study of Man's Impact on Climate* (SMIC), MIT Press, Cambridge, MA. 1971.

McCabe, G.J., and M.A. Ayers, Hydrologic effects of climate change in the Delaware River basin, *Water Resources Bulletin*, 25(6), 1231-1242, 1989.

Miller, B.A., and W.G. Brock, Potential impacts of climate change on the Tennessee Valley Authority Reservoir System, in *The Potential Impacts of Global Climate Change on the United States, Appendix A: Water Resources*, US Environmental Protection Agency, Washington, D.C., 1989.

Miller, J. R., and G. L. Russell, The impact of global warming on river runoff, *Journal of Geophysical Research*, 97(D3), 2757 - 2764, 1992.

Mitchell, John F.B., The "greenhouse effect" and climate change, *Reviews of Geophysics*, 27(1), 115-140,1989.

Nash, L.L., and P.H. Gleick, Sensitivity of streamflow in the Colorado basin to climatic changes, *Journal of Hydrology*, 125, 221-241, 1991.

National Research Council, *Studies in Geophysics: Climate, Climatic Change, and Water Supply*, Panel on Water and Climate, National Academy of Sciences, Washington, D.C., 1977.

Nelder, J.A., and R. Mead, A simplex method for function minimization, *Computer Journal*, 7, 308-313, 1965.

Némec, J., and J. Schaake, Sensitivity of water resource systems to climate variation, *Hydrological Sciences Journal*, 27(3), 327-343, 1982.

North Pacific Division Corps of Engineers, *Columbia River Treaty Flood Control Operating Plan*, October, 1972.

O'Callaghan, J.F., and D.M. Mark, The extraction of drainage networks from digital elevation data, *Computer Vision Graphics Image Processing*, 28, 323-324,1984.

Office of Technology Assessment, *Preparing for an Uncertain Climate* (Vol. I and II), US Congress, 1993.

Quinn, P., K. Beven, P.Chevallier, and O.Planchon, The prediction of hillslope flow paths for distributed hydrological modeling using digital terrain models, *Hydrological Processes*, 5, 59-79, 1991.

Revelle, R.R. and P.E. Waggoner, Effects of a carbon dioxide-induced climatic change on water supplies in the Western United States, in *Changing Climate*, 419-431, National Academy Press, Washington. DC, 1983.

Rogers, P., What manager and planners need to know about climate change and water resources management, in *Climate Change and Water Resources Management*, T. Ballentine, and E.Z. Stakhiv, eds., Proc. U.S. Interagency Conference on Climate Change and Water Resources Management, US Army Institute for Water Resources, 1991.

Roger, H.H., J.F. Thomas, G.E. Bingham, Response of agronomic and forest species to elevated atmospheric carbon dioxide, *Science*, 220, 428-429, 1983.

Saelthun, N.R., *et al.*, *Climate change: Impact on Norwegian Water Resources*, Norwegian Water Resources and Energy Administration, Volume 42, 41 pp., 1990.

Sagan, C., O.G.Toon, and J.B. Pollack, Anthropogenic albedo changes and the Earth's climate, *Science*, 206, 1363-1368, 1979.

Schneider, S.H., P.H. Gleick, and L.O. Mearns, Prospects for Climate Change, in *Climate Change and U.S. Water Resources*, P. E. Wagonner, ed., John Wiley & Sons, N.Y., pp. 41-73, 1990.

Schwarz, H. E., Climatic change and Water Supply: How sensitive is the Northeast?, in *Studies in Geophysics: Climate, Climatic Change, and Water Supply*, National Research Council Panel on Water and Climate, National Academy of Sciences, Washington, D.C., pp. 111-120,1977.

Scott, M.J., R.D. Sands, L.W. Vail, J.C. Chatter, D.A. Neitzel, S.A. Shankle, *Effects of Climate Change on Pacific Northwest Water-Related Resources: Summary of Preliminary Findings*, Pacific Northwest Laboratory, Richland WA, 1993.

Sellers, P., Modeling and observing land-surface-atmosphere interactions on large scales, *Surveys in Geophysics*, 12, 84-114 (1991).

Shilkomanov, I.A., and H. Lins, Climate change impact on hydrology and water management, *Meteorologia and Gidrologia*, 4, 55-66, 1991.

Shukla, J., C. Nobre, and P. Sellers, Amazon deforestation and climate change, *Science*, 247, 1322-1335, 1990.

Shuttleworth, W.J., Evaporation, in *Handbook of Hydrology*, D.R. Maidment, ed., McGraw-Hill, Inc., New York, 1993.

Sivapalan, M., K. Beven, and E.F.Wood, On Hydrologic similarity 2. A scaled model of storm runoff production, *Water Resources Research*, 23(12), 2266-2278, 1987.

Stakhiv, E.Z., Managing water resources for adaptation to climate change, in *Engineering Risk and Reliability in a Changing Physical Environment*, Proc. NATO Advanced Studies Institute, Deaville, France, May 24 - June 3, 1993.

Stakhiv, E.Z., H.Lins, and I. Shiklomanov, Hydrology and water resources, in *Climate Change 1992, The Supplementary Report to the IPCC Impacts Assessment*, W. J. McGTegart and G.W. Sheldon, eds., pp. 72-83, Australian Government Publishing Services, Canberra, Australia, 1992.

Stedinger, J.R., and J.C. Grygier, *SPIGOT, A Synthetic Streamflow Generation Software Package, Technical Description Version 2.6*, School of Civil and Environ. Eng., Cornell Univ., Ithaca, New York, 1990.

Stedinger, J.R., D. Pei, and T.Cohn, A condensed disaggregation model for incorporating parameter uncertainty into monthly reservoir simulations, Water Resources Research, 21(5), 665-675, 1985.

Stockton, C. W., Interpretation of past climatic variability from paleoenvironmental indicators, in *Studies in Geophysics: Climate, Climatic Change, and Water Supply*, National Research Council Panel on Water and Climate, National Academy of Sciences, Washington, D.C., 1977.

Stockton, C. W. and Bogess, W. R., *Geohydrological implications of climate change on water resource development*, U.S. Army Coastal Engineering Research Center, Fort Belvoir, VA, 1979.

Tennessee Valley Authority, *Sensitivity of the TVA reservoir and power supply systems to extreme meteorology*, TVA Resource Group, Engineering Services Hydraulic Engineering, Report No WR28-1-68-111, 1993.

Tsuang, F.J., and J.A. Dracup, Effect of global warming on Sierra Nevada mountain snow storage, in *Proceedings 59th Western Snow Conference*, 17-28, Colorado State Univ. Fort Collins, CO, 1991.

US.Army Construction Engineering Research Laboratory, GRASS 4.0 software, Champaign, IL, 1991.

Urbiztondo, B.I., W.R. Rose, and P. Restrepo, *Potential Climate Change impacts in the Middle Zambezi River Basin Report*, prepared for US EPA, University of Colorado, Boulder, CO, 33 pp., 1991.

Wallis, J.R., and P.E. O'Connell, Firm reservoir yield - how reliable are historic hydrologic records, *Hydrological Sciences Bulletin*, 18(3), 347-365, 1973.

Wigley, T.M.G. and P. D. Jones, Influences of precipitation changes and direct CO_2 effects on streamflow, *Nature*, 314, 150-152, 1985.

Wigley, J.M.L., P.D. Jones, P.M. Kelly, S.C.B. Raper, Statistical sign of global warming, in *Proceedings of the Thirteenth Annual Climate Biosystem Workshop*, WA DC, National Oceanographic and Atmospheric Administration, A1 - A8, 1989.

Wolock, D.M., *Topographic and soil hydraulic control of flow paths and soil contact time; effects on surface water acidification*, PhD dissertation, Department of Environmental Science, University of Virginia, Charlottesville, VA, May 1988.

Wood, E.F., Global scale hydrology: Advances in land surface modeling, *Reviews of Geophysics*, S, 193-201, April, 1992.

APPENDIX A ADJUSTMENT PROCEDURE

The time series of seasonal flows are typically not normally distributed. For this derivation it is assumed that the seasonal distributions are lognormal. The relationship between the moments of natural and transformed flows for 2-parameter lognormal distributed flows is as follows:

$$\mu_x = exp\left[\mu_y + \frac{1}{2}\sigma^2_y\right] \qquad \text{A.1}$$

$$\sigma^2_y = ln\left[1 + C_v{}^2_x\right] \qquad \text{A.2}$$

The variables 'x' and 'y' denote natural and transformed flows respectively. Rearranging Equation A.1, the following expression is obtained.

$$\mu_y = ln\left[\mu_x\right] - \frac{1}{2}\sigma^2_y \qquad \text{A.3}$$

Equation A.2 is used to estimate the variance of the transformed flows. The mean of the normal distribution fitted to the transformed index catchment flows is estimated by Equation A.3.

In general, a normally distributed random variable $Y_1 \in N(\mu_1, \sigma_1)$ is adjusted to $Y_2 \in N(\mu_2, \sigma_2)$ thus:

$$y_2 = (y_1 - \mu_{y_1}) \left[\frac{\sigma_{y_2}}{\sigma_{y_1}} \right] + \mu_{y_2}$$

As applied to the adjustment of the generated LSB sequence from base case statistics (o), to the assumed alternative climate statistics (+), the adjustment of the normal transformed flows is

$$y^+ = \left(y^o - \mu_y^o \right) \left[\frac{\sigma_y^+}{\sigma_y^o} \right] + \mu_y^+ \qquad \text{A.4}$$

and the unknowns are $(\mu^+)_y$ and $(\sigma^+)_y$. Two assumptions regarding the mean $(\mu^+)_x$ and coefficient of variation $(Cv^+)_x$ of the natural LSB flows are adopted in order to obtain these two unknowns. The first assumption is the constant means ratio, and the second is an assumption about the coefficient of variation. Two different assumptions were taken for coefficient of variation, resulting in two different, alternative adjustment procedures. Equations A.1 and A.2 must be applied to the assumptions in order to find the expressions for the unknown mean and variances of the transformed flows.

Under the constant means ratio assumption, the ratio of the mean of the natural flow of an LSB for the alternative climate scenario to the mean flow in the base case is taken to be equal to that of the simulated flows at the associated index catchment:

$$\mu^+_{x_{LSB}} = \mu^\circ_{x_{LSB}} \left[\frac{\mu_x^+}{\mu_x^\circ} \right]_{IC} \qquad \text{A.5}$$

The two alternative assumptions about the coefficient of variation for the LSB are 1) that it is unaffected by climate change,

$$Cv^{+}_{x_{LSB}} = Cv^{\circ}_{x_{LSB}} \qquad \text{A.6}$$

and (2) constant Cv ratio, which is analogous to the constant means ratio:

$$Cv^{+}_{x_{LSB}} = Cv^{\circ}_{x_{LSB}} \left(\frac{Cv_{x}^{\cdot}}{Cv_{x}^{\circ}} \right)_{IC} \qquad \text{A.7}$$

The unknown $(\mu^{+})_{y}$ for the LSB is found by substituting the expanded form of Equation A.1 into Equation A.4. Equation A.1, expressed for the base case climate at the LSB and expanded, is:

$$\mu^{\circ}_{x_{LSB}} = \left\{ exp\left[\mu_{y}^{\circ}\right] exp\left[\frac{1}{2}\sigma_{y}^{\circ 2}\right] \right\}_{LSB}$$

Substituting the above into Equation A.5 yields

$$\left\{ exp\left[\mu_{y}^{+}\right] exp\left[\frac{1}{2}\sigma_{y}^{+2}\right] \right\}_{LSB} = \left\{ exp\left[\mu_{y}^{\circ}\right] exp\left[\frac{1}{2}\sigma_{y}^{\circ 2}\right] \right\}_{LSB} \left[\frac{\mu_{x}^{+}}{\mu_{x}^{\circ}} \right]_{IC} \qquad \text{A.8}$$

Comparison of Equation A.6 and A.2 shows that, for the first adjustment procedure (assumptions of Equations A.5 and A.6) the unknown LSB variance $(\sigma^{+})_{y}$ is unchanged from the base case, and therefore the only unknown in Equation A.4 is the mean $(\mu^{+})_{y}$. Furthermore, the terms involving the variance of the LSB transformed flows drop out of Equation A.8

$$exp\left[\mu_{y}^{+}\right]_{LSB} = exp\left[\mu_{y}^{\circ}\right]_{LSB} \left[\frac{\mu_{x}^{+}}{\mu_{x}^{\circ}} \right]_{IC},$$

so that after taking logs of both sides, the result is

$$\mu^{+}_{y_{LSB}} = \mu^{\circ}_{y_{LSB}} + ln\left[\frac{\mu^{+}_{x}}{\mu^{\circ}_{x}}\right]_{IC} \qquad \text{A.9}$$

Due to the assumption of the constant coefficient of variation, the ratio of variances in Equation A.4 is equal to one (see above). Therefore, substituting Equation A.9 into Equation A.4 gives the adjustment equation for the transformed flows under the first procedure:

$$y^{+}_{LSB} = y^{o}_{LSB} + ln\left[\frac{\mu^{+}_{x}}{\mu^{\circ}_{x}}\right]_{IC}.$$

Exponeniating both sides give the first adjustment procedure as applied directly to the natural flows, noting that the series y° is just the natural logarithm of the generated, natural flow series.

$$x^{+}_{LSB} = x^{o}_{LSB}\left[\frac{\mu^{+}_{x}}{\mu^{\circ}_{x}}\right]_{IC} \qquad \text{A.10}$$

Under the second adjustment procedures (assumptions of Equation A.5 and A.7) the ratio of variances in Equation A.4 does not drop out. Instead, according to Equation A.2,

$$\left(\frac{\sigma^{+}}{\sigma^{\circ}}\right)_{y_{LSB}} = \left(\sqrt{\frac{ln\left(1 + C_v{}^{+2}_{x}\right)}{ln\left(1 + C_v{}^{\circ 2}_{x}\right)}}\right)_{LSB} \qquad \text{A.11}$$

where Cv in the numerator is given by Equation A.7. The expression for the mean $(\mu^{+})_{y}$ is obtained from Equation A.8, but retaining the terms involving the variance. Equation A.2 is substituted for $(\sigma^{+})_{y}$ so that Equation A.8 can be written as (in simplified notation):

$$exp\left[\mu_{y}^{+}\right]_{LSB} = \mu_{x_{LSB}}^{\circ} exp\left(- \frac{1}{2} ln\left[1+Cv_{x_{LSB}}^{+\,2}\right]\right)\left[\frac{\mu_{x}^{+}}{\mu_{x}^{\circ}}\right]_{IC}$$

Taking the logs of both sides gives the expression for $(\mu^{+})_{y}$ for the second adjustment procedure:

$$\mu_{y_{LSB}}^{+} = \left\{ ln\mu_{x}^{\circ} - \frac{1}{2} ln\left[1+Cv_{x}^{+\,2}\right]\right\}_{LSB} + ln\left[\frac{\mu_{x}^{+}}{\mu_{x}^{\circ}}\right]_{IC} \qquad \text{A.12}$$

where $(Cv^{+})_{y}$ is given by Equation A.9.

To summarize, the adjustment equation for the first procedure is obtained by substituting Equation A.9 into the general equation A.4 (observing that the ratio $[(\sigma^{+})_{y} / (\sigma^{\circ})_{y}]$ equals one). The second procedure is obtained by substituting Equations A.10 and A.11 into Equation A.4.

Appendix B Statistics of historical and generated subbasin flows.

This appendix gives several tables. Table B.1 and B.2 give monthly and annual mean and standard deviations of subbasin local inflows. Table B.1 pertains the historical (reconstructed) local inflows. Table B.2 gives these statistics for the generated local inflows, after the adjustment procedure was applied (Section 3.3), and after rescaling each monthly flow to preserve the change in mean annual runoff at the corresponding index catchment (Section 4.2). Table B.3 gives the monthly and historical annual runoff cross-correlations for every subbasin-index catchment pair. It is on the basis of data in Table B.3 that the index catchment-subbasin groups were formed.

Table B.1 Means and standard deviations of reconstructed historical local inflows to each subbasin streamflow measurement point

MEANS OF HISTORICAL FLOWS

Site	Annual	OCT	NOV	DEC	JAN	FEB	MAR	APR	MAY	JUN	JUL	AUG	SEP
A John Day	11214	426	547	762	751	782	882	1033	1570	2317	1216	552	374
B Roundbutte	3290	249	267	298	319	310	324	296	270	251	240	236	230
C Chelan	1594	48	57	55	47	46	54	114	341	422	255	106	49
D Long Lake	6057	156	241	385	464	539	653	1077	1334	718	246	131	114
E Dworshak	4497	116	163	214	226	247	329	705	1174	863	269	109	84
A Lower Granite	21000	595	681	859	959	1104	1411	2429	4924	5182	1792	608	456
B Brownlee	14144	894	972	1103	1246	1357	1590	1789	1662	1422	697	646	767
C Albeni Falls	11291	416	473	521	495	537	709	1310	2626	2534	958	393	317
E Hungry Horse	2791	76	82	80	70	65	75	249	809	872	283	75	57
D Kerr	6386	208	205	188	178	177	193	527	1655	1853	771	256	176
A Grand Coulee	33512	1233	1107	1010	933	925	1197	2712	7143	8431	5054	2361	1407
B Duncan	2704	115	74	57	47	36	40	87	368	680	628	382	189
C Libby	8910	368	295	231	193	191	216	482	1809	2614	1461	637	414
D Mica	15219	695	419	279	227	196	211	407	1733	3598	3691	2503	1260

STANDARD DEVIATIONS OF HISTORICAL FLOWS

Site	Annual	OCT	NOV	DEC	JAN	FEB	MAR	APR	MAY	JUN	JUL	AUG	SEP
A John Day	3804	209	316	435	391	352	516	440	828	1104	648	380	249
B Roundbutte	343	23	22	52	57	62	72	63	42	29	19	17	15
C Chelan	382	27	38	37	20	25	31	42	115	126	101	42	18
D Long Lake	1580	44	111	267	311	277	299	392	396	312	87	30	20
E Dworshak	1170	62	92	158	141	129	168	246	341	389	117	32	27
A Lower Granite	4845	211	235	424	490	418	593	857	1389	1747	745	166	127
B Brownlee	3858	85	168	215	502	506	691	876	739	578	199	68	69
C Albeni Falls	2533	145	139	196	236	202	274	507	740	858	374	120	110
D Kerr	1281	124	87	86	71	64	81	236	392	576	307	93	82
E Hungry Horse	552	54	45	40	33	39	37	111	182	297	132	25	34
A Grand Coulee	5411	346	299	290	344	277	402	993	1753	1706	1586	733	496
B Duncan	272	25	18	12	13	7	12	32	106	120	134	69	51
C Libby	1527	111	70	63	43	45	50	205	518	691	436	154	123
D Mica	1472	97	103	50	35	30	36	119	541	707	653	369	274

Table B.2 Means and standard deviations of base case climate generated local inflows to each subbasin streamflow measurement point

MEANS OF GENERATED FLOWS (BASE-CASE CLIMATE)

Site	Annual	OCT	NOV	DEC	JAN	FEB	MAR	APR	MAY	JUN	JUL	AUG	SEP
1A John Day	11110	406	501	728	756	793	822	942	1577	2508	1189	521	368
1B Roundbutte	3275	250	271	308	333	311	312	289	267	243	235	231	225
1C Chelan	1468	38	39	43	43	40	48	110	323	412	230	96	46
1D Long Lake	5729	151	226	392	448	460	608	1020	1256	692	241	124	110
1E Dworshak	4405	104	148	227	226	223	302	709	1146	858	274	107	83
3A Lower Granite	19862	594	672	832	996	971	1345	2368	4635	4806	1634	567	443
3B Brownlee	13547	894	943	1122	1267	1213	1445	1692	1587	1355	661	625	744
3C Albeni Falls	10613	430	471	518	520	475	696	1243	2450	2289	845	364	312
3D Kerr	5936	215	208	191	187	167	180	507	1525	1667	673	239	177
3E Hungry Horse	2605	81	81	80	73	58	72	241	766	788	238	70	57
5A Grand Coulee	33379	1159	1079	996	953	938	1235	2658	7165	8522	4987	2362	1325
5B Duncan	2661	108	71	58	49	37	41	84	367	683	608	372	183
5C Libby	8932	366	298	229	193	190	223	466	1907	2625	1424	630	380
5D Mica	15066	674	408	273	221	190	214	417	1706	3582	3632	2477	1271

STANDARD DEVIATIONS OF GENERATED FLOWS (BASE-CASE CLIMATE)

Site	Annual	OCT	NOV	DEC	JAN	FEB	MAR	APR	MAY	JUN	JUL	AUG	SEP
1A John Day	3336	187	270	517	392	322	382	350	842	1484	592	305	203
1B Roundbutte	255	25	22	46	60	53	48	62	41	24	20	17	14
1C Chelan	375	16	23	30	17	19	26	43	130	135	98	36	14
1D Long Lake	1588	44	106	342	282	236	293	450	475	336	95	29	17
1E Dworshak	1257	59	84	239	168	124	154	258	375	397	134	33	25
3A Lower Granite	4885	164	228	339	505	431	663	774	1379	1797	722	176	158
3B Brownlee	3271	73	149	171	400	381	556	905	751	570	173	66	68
3C Albeni Falls	2371	131	117	153	205	204	264	453	746	805	341	128	126
3D Kerr	1228	134	88	87	66	62	83	242	433	493	259	98	88
3E Hungry Horse	522	66	44	33	26	36	37	111	187	273	100	24	30
5A Grand Coulee	5929	302	242	249	279	268	364	882	2075	1952	1722	690	290
5B Duncan	256	22	16	10	12	5	8	33	122	115	133	60	33
5C Libby	1580	85	69	49	33	32	48	192	672	729	438	129	59
5D Mica	1245	95	104	48	30	26	30	155	603	640	704	332	207

Table B.3 Monthly and annual subbasin-index catchment cross-correlations (historical index catchment runoff; reconstructed historical local inflows)

	Month												
	Oct	Nov	Dec	Jan	Feb	Mar	Apr	May	June	July	Aug	Sep	Annual
JOHN DAY													
American R.	0.34	0.68	0.68	0.44	0.60	0.67	0.59	0.65	0.72	0.54	0.19	0.01	0.83
Camas Creek	0.34	0.25	0.58	0.66	0.71	0.77	0.54	0.48	0.22	0.13	-0.22	-0.26	0.74
MF Flathead R	0.48	0.67	0.77	0.62	0.41	0.63	0.55	0.39	0.48	0.61	0.19	0.06	0.68
Reynolds C.	-0.30	-0.02	0.52	0.63	0.72	0.83	0.69	0.55	0.72	0.14	-0.19	0.29	0.75
Salmo River	0.59	0.55	0.61	0.55	0.60	0.59	0.65	0.57	0.38	0.58	0.06	-0.02	0.69
CHELAN													
American R.	0.68	0.78	0.79	0.82	0.85	0.95	0.90	0.93	0.92	0.89	0.91	0.72	0.92
Camas Creek	0.64	0.06	0.08	0.24	0.55	0.62	0.57	0.30	0.46	0.18	0.43	0.24	0.56
MF Flathead R	0.64	0.72	0.81	0.60	0.81	0.96	0.76	0.77	0.74	0.88	0.89	0.43	0.80
Reynolds C.	0.12	0.11	-0.07	-0.12	0.36	0.66	0.67	0.40	0.71	0.49	0.21	0.02	0.51
Salmo River	0.77	0.59	0.71	0.53	0.75	0.91	0.86	0.92	0.82	0.75	0.73	0.78	0.86
LONG LAKE													
American R.	0.80	0.80	0.60	0.76	0.78	0.78	0.72	0.64	0.86	0.82	0.58	0.58	0.89
Camas Creek	0.60	0.48	0.88	0.66	0.82	0.82	0.82	0.55	0.67	0.45	0.46	0.34	0.81
MF Flathead R	0.90	0.86	0.65	0.92	0.57	0.75	0.75	0.62	0.89	0.79	0.73	0.71	0.81
Reynolds C.	0.13	-0.20	0.76	0.34	0.63	0.88	0.81	0.76	0.70	0.65	0.49	0.37	0.77
Salmo River	0.87	0.60	0.54	0.72	0.75	0.69	0.81	0.65	0.81	0.74	0.59	0.72	0.78
ROUNDBUTTE													
American R.	-0.09	-0.03	0.44	0.34	0.43	0.59	0.56	0.61	0.46	0.69	0.53	0.32	0.50
Camas Creek	0.09	0.28	0.76	0.77	0.82	0.81	0.74	0.67	0.64	0.35	0.49	-0.17	0.72
MF Flathead R	-0.01	0.10	0.39	0.42	0.21	0.51	0.54	0.43	0.22	0.50	0.58	-0.12	0.40
Reynolds C.	0.61	0.58	0.88	0.68	0.87	0.90	0.75	0.73	0.54	0.64	0.42	0.50	0.76
Salmo River	0.03	0.10	0.31	0.30	0.42	0.46	0.62	0.45	0.21	0.55	0.51	-0.01	0.38
LOWER GRANITE													
American R.	0.45	0.72	0.73	0.68	0.79	0.77	0.72	0.77	0.76	0.69	0.50	0.30	0.78
Camas Creek	0.75	0.64	0.77	0.88	0.78	0.89	0.86	0.45	0.47	0.46	0.50	0.49	0.83
MF Flathead R	0.68	0.83	0.76	0.79	0.68	0.76	0.81	0.79	0.83	0.79	0.71	0.71	0.78
Reynolds C.	0.35	-0.02	0.61	0.68	0.80	0.91	0.75	0.68	0.73	0.82	0.65	0.60	0.82
Salmo River	0.71	0.59	0.60	0.57	0.62	0.71	0.85	0.75	0.67	0.57	0.52	0.58	0.64

Table B.3 (Continued)

	Month												
	Oct	Nov	Dec	Jan	Feb	Mar	Apr	May	Junr	July	Aug	Sep	Annual
DWORSHAK													
American R.	0.65	0.74	0.76	0.73	0.89	0.91	0.83	0.74	0.86	0.87	0.71	0.46	0.89
Camas Creek	0.72	0.58	0.73	0.76	0.72	0.82	0.77	0.43	0.57	0.40	0.53	0.57	0.76
MF Flathead R	0.88	0.87	0.78	0.88	0.74	0.91	0.80	0.74	0.86	0.83	0.86	0.72	0.83
Reynolds C.	0.08	-0.03	0.70	0.50	0.56	0.85	0.77	0.64	0.68	0.71	0.36	0.20	0.79
Salmo River	0.88	0.58	0.61	0.67	0.74	0.85	0.85	0.75	0.82	0.81	0.70	0.75	0.80
ALBENI FALLS													
American R.	0.74	0.78	0.78	0.75	0.85	0.90	0.73	0.81	0.87	0.72	0.52	0.48	0.89
Camas Creek	0.67	0.52	0.61	0.59	0.67	0.78	0.71	0.40	0.55	0.54	0.51	0.29	0.77
MF Flathead R	0.89	0.91	0.89	0.95	0.86	0.92	0.80	0.81	0.89	0.87	0.82	0.79	0.86
Reynolds C.	0.36	-0.16	0.41	0.28	0.52	0.80	0.77	0.67	0.81	0.79	0.54	0.63	0.77
Salmo River	0.89	0.75	0.81	0.82	0.84	0.85	0.85	0.79	0.79	0.77	0.63	0.70	0.80
KERR													
American R.	0.70	0.80	0.81	0.67	0.69	0.92	0.76	0.75	0.77	0.74	0.70	0.44	0.80
Camas Creek	0.53	0.47	0.40	0.43	0.39	0.75	0.62	0.08	0.51	0.32	0.49	0.32	0.55
MF Flathead R	0.97	0.95	0.97	0.95	0.93	0.96	0.98	0.96	0.97	0.98	0.94	0.95	0.96
Reynolds C.	0.07	-0.14	0.24	0.23	0.32	0.76	0.67	0.54	0.74	0.56	0.52	0.21	0.72
Salmo River	0.85	0.76	0.84	0.88	0.77	0.87	0.94	0.83	0.83	0.73	0.68	0.71	0.80
HUNGRY HORSE													
American R.	0.62	0.73	0.83	0.77	0.73	0.88	0.78	0.76	0.75	0.72	0.59	0.30	0.79
Camas Creek	0.65	0.47	0.52	0.59	0.42	0.60	0.62	0.11	0.50	0.38	0.43	0.38	0.54
MF Flathead R	0.92	0.94	0.93	0.95	0.96	0.95	0.98	0.97	0.96	0.97	0.88	0.89	0.95
Reynolds C.	0.04	-0.03	0.57	0.39	0.38	0.73	0.61	0.44	0.77	0.74	0.55	0.25	0.76
Salmo River	0.86	0.66	0.72	0.77	0.74	0.87	0.92	0.78	0.83	0.70	0.53	0.54	0.73
BROWNLEE													
American R.	0.00	-0.11	0.39	0.18	0.26	0.56	0.35	0.62	0.46	0.60	0.38	0.35	0.51
Camas Creek	0.28	0.25	0.40	0.68	0.39	0.74	0.70	0.47	0.39	0.42	0.38	0.12	0.71
MF Flathead R	0.22	-0.03	0.35	0.29	0.42	0.52	0.49	0.61	0.55	0.55	0.57	0.21	0.49
Reynolds C.	0.75	0.72	0.57	0.72	0.81	0.92	0.91	0.86	0.67	0.80	0.67	0.65	0.91
Salmo River	0.23	0.08	0.30	0.16	0.28	0.46	0.56	0.59	0.27	0.38	0.39	0.25	0.40

Table B.3 (Continued)

	Month												
	Oct	Nov	Dec	Jan	Feb	Mar	Apr	May	Junr	July	Aug	Sep	Annual
GRAND COULEE													
American R.	0.68	0.68	0.65	0.76	0.61	0.82	0.68	0.82	0.82	0.74	0.72	0.56	0.85
Camas Creek	0.52	0.29	0.28	0.42	0.53	0.57	0.69	0.19	0.48	0.16	0.58	0.39	0.52
MF Flathead R	0.74	0.72	0.76	0.87	0.69	0.82	0.83	0.79	0.75	0.87	0.79	0.56	0.78
Reynolds C.	0.05	-0.03	-0.01	0.08	0.27	0.80	0.79	0.40	0.66	0.23	0.17	0.24	0.50
Salmo River	0.78	0.88	0.88	0.86	0.82	0.86	0.90	0.92	0.90	0.86	0.89	0.85	0.96
DUNCUN													
American R.	0.43	0.38	0.56	0.25	0.72	0.73	0.64	0.73	0.60	0.53	0.61	0.28	0.53
Camas Creek	0.23	-0.01	-0.03	0.47	0.32	0.27	0.50	0.07	0.18	0.05	0.53	0.17	0.19
MF Flathead R	0.45	0.45	0.51	0.17	0.35	0.74	0.80	0.76	0.43	0.78	0.73	0.25	0.57
Reynolds C.	-0.13	-0.03	0.15	0.37	0.58	0.37	0.54	0.02	0.45	0.10	0.36	-0.01	0.27
Salmo River	0.39	0.48	0.53	0.13	0.35	0.76	0.79	0.82	0.54	0.65	0.68	0.60	0.66
LIBBY													
American R.	0.70	0.59	0.71	0.55	0.63	0.75	0.75	0.81	0.76	0.61	0.71	0.50	0.79
Camas Creek	0.40	0.24	0.18	0.23	0.32	0.84	0.66	0.06	0.36	0.20	0.44	0.40	0.44
MF Flathead R	0.83	0.73	0.89	0.82	0.71	0.81	0.93	0.84	0.74	0.88	0.87	0.65	0.83
Reynolds C.	0.19	0.14	0.06	0.02	0.21	0.82	0.65	0.20	0.59	0.19	0.26	0.54	0.53
Salmo River	0.75	0.72	0.88	0.77	0.79	0.78	0.95	0.89	0.82	0.75	0.76	0.85	0.88
MICA													
American R.	0.24	0.23	0.35	0.20	0.50	0.28	0.48	0.67	0.58	0.44	0.53	0.40	0.47
Camas Creek	-0.14	0.11	-0.05	-0.11	0.12	-0.10	0.39	0.02	0.15	0.05	0.41	-0.05	0.11
MF Flathead R	0.07	0.34	0.39	0.10	0.21	0.38	0.71	0.75	0.34	0.77	0.66	0.15	0.50
Reynolds C.	-0.30	-0.12	0.02	-0.41	-0.03	-0.23	0.32	-0.06	0.44	0.05	0.36	-0.15	0.18
Salmo River	0.05	0.58	0.34	0.15	0.21	0.46	0.70	0.81	0.40	0.56	0.52	0.39	0.60